DISSERTATION

BIOMECHANICS OF RECUMBENT CYCLING:

INSTRUMENTATION, EXPERIMENTATION, AND MODELING

Submitted by

Raoul Frederick Reiser, II

Department of Mechanical Engineering

In partial fulfillment of the requirements

For the Degree of Doctor of Philosophy

Colorado State University

Fort Collins, Colorado

Spring 2000

COLORADO STATE UNIVERSITY

February 7, 2000

WE HEREBY RECOMMEND THAT THE DISSERTATION PREPARED UNDER OUR SUPERVISION BY RAOUL FREDERICK REISER, II ENTITLED BIOMECHANICS OF RECUMBENT CYCLING: INSTRUMENTATION, EXPERIMENTATION, AND MODELING BE ACCEPTED AS FULLFILING IN PART REQUIREMENTS FOR THE DEGREE OF DOCTOR OF PHILOSOPHY.

Committee on Graduate Work

Adviser

Co-Adviser

Department Head

ABSTRACT OF DISSERTATION

BIOMECHANICS OF RECUMBENT CYCLING:

INSTRUMENTATION, EXPERIMENTATION, AND MODELING

Cycling in the recumbent position has recently become popular. However, very little is known about this position, specifically in regards to the effects of body position and orientation on maximal power output and the energetics of the lower extremity. Three separate experimental investigations were completed in order gain a better understanding of this mode of cycling.

In the first investigation, the effects of altering body configuration angle (included angle between mid torso, hip joint, and crank-arm spindle) on maximal-power output were examined while recumbent cycling (hip joint 15° below crank-arm spindle). Power output declined significantly as body configuration angle was reduced from that selected by subjects in the standard, upright cycling position. However, power output in the recumbent cycling position was not reduced compared to the standard cycling position when body configuration angle was matched.

In the second investigation, body configuration angle was held constant while the effects of hip orientation angle (hip joint to crank-arm spindle relative to horizontal) on maximal-power output in three different recumbent positions were examined. Hip orientation angle had no effect on power output. Body configuration angle was matched to that selected by the subjects in the standard cycling position. No difference in power output was found between the recumbent and standard cycling positions.

In the third investigation, lower-extremity energetics were examined through inverse-dynamics modeling. In order to perform the inverse dynamics, clipless pedals were modified to measure reaction forces as well as pedal and crank-arm angles. While cycling steady state at 90 rpm and 250 W in a recumbent and standard cycling position with matched body configuration angle, simultaneous force-pedal system and lower-extremity joint kinematics were collected. While the kinematics and kinetics were extremely similar, several significant differences were found. Energy transferred across the hip joint from the upper body/pelvis was significantly reduced in the recumbent position. Additionally, work at the knee was redistributed in the recumbent position with more work done during knee flexion and less during knee extension compared to the standard cycling position. These differences may have implications on performance between the two modes of cycling.

Raoul Frederick Reiser, II
Mechanical Engineering Department
Colorado State University
Fort Collins, CO 80523
Spring 2000

ACKNOWLEDGEMENTS

I would first like to thank my adviser and friend, Dr. Mick Peterson, for his support throughout my doctoral program. His guidance and insight have been invaluable during the last three years in helping me develop the 'culture.'

I would also like to thank the rest of my committee members: Dr. Jeff Broker, for his friendship, mentoring, and great knowledge of cycling; Dr. Susan James, for her thoughts and advice as I completed my dissertation and began the search for 'what's next;' and Dr. Robert Gotshall, for stepping forward when I needed additional help and motivation towards the end of the project.

Many thanks also go to my parents and sister. They have been there all these years, serving as great role models as I matured and continued on with my academic pursuits.

Finally, I will forever be grateful to my wife, and best friend, Donna. She has waited patiently as I pursued my academic goals. Donna and 'The Boys' also deserve thanks for providing the necessary distractions, so that I could keep my sanity through the whole experience.

PREFACE

Due to the nature of this project, it was necessary to perform several tasks in a chronological order. The results from each task were necessary for proper formulation and execution of the task(s) that followed. This broke the project up into discrete sections that could be analyzed and written-up independently. This proved to be the most logical way to proceed, since each section then could be submitted for publication as I went along and serve as a chapter in the final document. **Chapter 1**, the traditional review of literature, has been published with minor changes: Reiser, R.F. and Peterson, M.L. (1998). 'Lower-extremity power output in recumbent cycling: a literature review.' *Human Power*, 13(3): 6-13. **Chapter 2**, the first round of experimentation, has been accepted for publication in the *Journal of Applied Biomechanics*. **Chapter 3**, the second round of experimentation that built on the results from the first, is in review for publication in *Ergonomics*. **Chapter 4**, describing necessary custom instrumentation, has been prepared for submission to the *IEEE/ASME Transactions on Mechatronics*. **Chapter 5**, the third round of experimentation that also included modeling, has been prepared for submission to the *Journal of Biomechanics*.

Since this dissertation is a series of journal articles, some information is replicated between chapters. Additionally, transitions between chapters are often sudden. I apologize, in advance, for any difficulties that may be incurred by this format. However, each chapter is a complete document that may be read from the manuscript independently without need for any additional material.

TABLE OF CONTENTS

Chapter 1

Lower-Extremity Power Output in Recumbent Cycling: A Literature Review

1.1 Introduction

The recumbent cycling position has become popular for high-performance human-powered land vehicles. The popularity is due mainly to its reduced frontal area, and thus reduced aerodynamic drag, as compared to the familiar upright position (Gross *et al.*, 1983). In addition to the reduced frontal area, the recumbent position has several other features that make it attractive as a cycling position when compared to other riding positions. The center of mass of the vehicle may be positioned relatively low to the ground, making the vehicle more stable and safer since there is less distance to fall if a crash were to occur. In a crash situation the head is protected in the recumbent position as compared to the upright position, where the head leads the body if thrown forward over the handlebars (Wilson *et al.*,1984). Visibility is improved in the recumbent position with the head naturally facing forward which improves the safety of the vehicle by keeping the oncoming road in the field of vision (Martin, 1984; Wilson *et al.*, 1984). The natural forward-facing position of the head may also reduce neck strain (Ice and Waite, In Preparation). For many riders the seat position is more comfortable in a recumbent position, reducing the likelihood of crotch pain and injury (Kita, 1997; Wilson

et al., 1984), and gives the rider firm support to push against while pedaling (Wilson *et al.*, 1984). This position also reduces the strain on the lower back and wrists as compared to the familiar upright position (Ice and Waite, In Preparation; Wilson *et al.*, 1984).

While the recumbent riding position has these many advantages when compared to the standard cycling position, it may have two key disadvantages. The recumbent position may not allow for peak-power production and sustained aerobic performances from the rider that are as high as those obtained in the upright cycling position. Several studies have found that the standard position is favorable to other positions (Diaz *et al.*, 1978; Kyle and Caiozzo, 1986; Metz *et al.*, 1986), while others have found just the opposite (Nadel and Bussolari, 1988; Wescott, 1991).

Regardless, the recumbent riding position has been very successful which seems to indicate that the advantages outweigh any disadvantages, at least for a high-speed sprint vehicle. Three noteworthy recumbent-position human-powered vehicles have been ridden over 96.5 km/h [60 mile/h] on flat terrain unaided by a tailwind. In contrast, the top speeds in the standard riding position is just over 80.49 km/h [50 mile/h] (82.53km/h set by Jim Glover in a fully-faired Moulton AM7). The Vector Tandem was a tricycle that reached 101 km/h [63 mile/h]. The Gold Rush, a bicycle, attained a top speed of 105.9 km/h [65.84 mile/h] and the Cheetah, another bicycle, currently holds the human-powered vehicle speed record at 110.6 km/h [68.73 mile/h]. While all three utilized the recumbent riding position, all three had slightly different positional variations relative to the other designs. The Vector Tandem utilized a hip position approximately level with the pedal crank, while the Gold Rush had the hips slightly above the cranks. The Cheetah had the rider positioned with the hips slightly below the cranks. However, the exact

riding positions are not known for these designs, as are a number of the other biomechanical parameters and design factors.

At the present time, it is unclear what the impact of slightly different riding positions is on the performance of the vehicle, and it is possible that higher speeds could have been achieved by utilizing a different riding position. However, a small body of research has emerged which addresses some of the questions surrounding the biomechanics of recumbent cycling. In particular, the optimal position for power production is of interest for these type of vehicles.

1.2 Definition of Terms

Due to the wide variety of cycling positions and variations among each position, several geometrical terms must be defined so that any cycling position may be clearly and completely described. First, hip orientation angle (HOA) will refer to the angle that is produced by the intersection of a line connecting the hip joint and the center of the crank spindle with a horizontal line through the center of the crank spindle (0° with the hips horizontal and behind the crank). For clarity, all terms are represented graphically in Figure 1.1. Second, hip-to-pedal distance will refer to the straight line distance from the hip joint to the pedal spindle when the leg is in its most extended position of the cycling motion (similar to saddle height in upright cycling nomenclature). Third, torso angle will refer to the angle that is produced by the intersection of a line connecting the shoulder joint and the hip joint with a horizontal line through the hip joint (0° with the shoulders horizontal with and behind the hips). Fourth and fifth, the horizontal and vertical foot positions will refer to distance between the pedal spindle and the ball of the foot in the

directions parallel and perpendicular to the bottom of the foot, respectively (positive distances with the ball of the foot in front of and above the pedal spindle). Additionally, the term body configuration angle (BCA), a combination of the HOA and torso angle, will refer to the angle produced by the intersection of the line connecting the shoulder joint and the hip joint with the line connecting the hip joint and the center of the crank set.

1.3 Review of Literature

When a geometrical parameter (HOA, hip-to-pedal distance, foot position on pedal, foot-to-pedal interface, torso angle, and crank-arm length) or operational parameter (pedaling cadence and load) is altered in the cycling motion, the tendency is to also produce a change in the kinematics of the lower extremity (Brown *et al.*, 1996; Too, 1994; Too, 1991b). When the kinematics are altered, the body's ability to produce a force on the pedal is also affected (Kroemer, 1972). The pedal force can be separated into a muscular component that is due directly to the net joint moments and a non-muscular component due to gravitational and inertial effects. Both of these pedal force components contribute to propulsive and non-propulsive forces on the crank-arm and may be altered by a change in one or more of the geometrical or operational parameters (Kautz and Hull, 1993).

1.3.1 Musculoskeletal Biomechanics: The net joint moments are predominantly a sum of the individual joint moments produced by each muscle that crosses a joint. In addition to the muscular contribution, passive structures such as ligaments and joint friction produce moments about the joint. In healthy joints that are not operating near the

extremes of motion, friction and passive structure contributions to the net joint moment may be ignored (Winter, 1990; Zajac and Gordon, 1989).

The moment produced by the muscle is a product of the tensile force in the musculotendon and the moment arm created by the joint geometry. Both the ability of a muscle to produce force and the moment arm vary as the joint angle varies (Hoy *et al.*, 1990; Kulig *et al.*, 1984; Winters and Stark, 1988). Some muscles cross more than one joint (biarticular) and therefore have a dependence on two joints for their ability to produce a moment at a single joint (Kulig *et al.*, 1984).

Geometrically, the ability of a musculotendinous unit to produce force is dependent on the muscle length, tendon length, arrangement of muscle fibers, and the rate of muscle shortening/lengthening (Hoy *et al.*, 1990; Winters and Stark, 1988; Zajac, 1989). Skeletal muscle is connected to bone at each end by tendon. Tendon is a passive structure which stretches under load. Since the tendon is in series with the muscle, both transmit the same load and any change in length of the tendon causes a change of length in the muscle in order to maintain tension on the bone or prevent damage to the tendon, muscle, or bone.

Muscle is comprised of individual muscle fibers. Each muscle fiber has a force-length-velocity profile which is a combination of the active and passive force-producing elements in the fiber (Figure 1.2) (Winter, 1990). The passive force-producing elements are similar to tendon in that they produce a force when stretched beyond their no-load resting length. The active force-producing elements (sarcomeres) generate force by attempting to shorten. There is an optimal length for producing peak force. Any shortening or lengthening of the fiber from this optimal length (resting length) reduces

the fiber's ability to produce force. In addition, the velocity of shortening/lengthening has an influence on the fiber's ability to produce force (Gregor and Rugg, 1986) (Figure 1.3). The faster the fiber shortens, the less force it is able to produce. Peak power from the muscle fiber occurs at approximately one-third the maximum force production level (Figure 1.3). Peak power is the product of the force and the velocity of shortening.

The individual muscle fibers can vary in resting length and orientation relative to the line of action of the entire muscle (Alexender and Ker, 1990). These variations give each muscle its own unique force-length-velocity profiles which are further altered by the type of muscle fibers, number of muscle fibers, and fatigue level of the fibers (Kulig *et al.*, 1984). The active force produced by a muscle is then altered through nervous-system control by varying the number of muscle fibers active at any one time. The net joint torque that a person can generate is further influenced by age, sex, body type, motivation, training, and exercise conditions (Kulig *et al.*, 1984). It is beyond the scope of this review to discuss these factors in more detail. However, it is important to understand that they do contribute to the force a muscle can produce as well as increase the complexity of finding the optimal position for high performance recumbent cycling.

The moment arm of a muscle is altered as the joint angle changes due to changes in the line of action of the muscle. Most muscles act directly along a line connecting the origin and insertion of the muscle. However, some muscles do not follow a straight-line path due to a bony obstruction. The obstruction may be present for all or just part of the range of motion of the joint that the muscle crosses (Hoy *et al.*, 1990; Seirig and Arvikar, 1989).

Cycling is a highly planar activity that involves the hip extensors (gluteus maximus, gluteus medius, gluteus minimus, biceps femoris (long head), semimembranosus, and semitendinosus) and flexors (iliospoas and rectus femoris), knee extensors (vastus lateralis, vastus intermedius, vastus medialis, and rectus femoris) and flexors (biceps femoris, semimembranosus, semitendinosus, and gastrocnemius), and ankle plantar flexors (gastrocnemius and soleus) and dorsi flexors (tibialis anterior) (Figure 1.4) (Gregor *et al.*, 1991; Hull and Hawkins, 1990; Hull and Jorge, 1985; Too, 1993a; Too, 1991a). Additional muscles are also involved during all movements to a smaller degree as joint stabilizers that may act synergistically or antagonistically (Zajac and Gordon, 1989). Investigations have found that the moment arms of many of these muscles change dramatically with joint angle (Hoy *et al.*, 1990; Nemeth and Ohlsen, 1985; Spoor and Leeuwen, 1992; Spoor *et al.*, 1990). For example, Nemeth and Ohlsen (1985) found that the moment arm of the gluteus maximus decreased 48 mm, the moment arm of the hamstrings decreased 20 mm, and the moment arm of the adductor magnus increased 46 mm when the hip was flexed in the sagittal plane from the anatomical position to 90°. This change could have a significant impact on the power production of this important muscle.

As mentioned, the non-muscular components are also affected by alterations in the geometrical and operational parameters. The gravitational contribution to the pedal force is altered with variations in HOA. As the HOA is changed, the horizontal distance between the pedal and seat also changes. The gravitational force contributed by each segment that is shared between the pedal and seat is therefore altered. In addition, the torque contribution of gravity on each segment will be altered with a change in HOA.

Finally, the inertial contribution is dependent on pedal cadence. The faster the pedaling cadence, the greater the inertial forces (Kautz and Hull, 1993).

Since both the muscular and non-muscular contributions to the pedal force are dependent on the geometric and operational parameters, it is hard to predict the best rider position to produce optimal joint moments from the hips, knees, and ankles. A number of investigations have been performed to examine the effects upon recumbent cycling performance by varying one or more of the biomechanical factors. A summary of the key results as they relate to the HOA and torso angle follows. While the other geometrical and operational parameters are important, they do not contribute large changes in the design of the vehicle in terms of the size and shape of the vehicle nor does space allow for adequate discussion of these parameters. However, references are provided for the reader on these parameters in the Appendix.

1.3.2 Experimental Investigations into Recumbent Cycling: Too (1991b) systematically altered the HOA from -10° to 65° in 25° increments while maintaining a 90° torso angle (Figure 1.5). Fourteen male recreational cyclists (ages 21-32 yrs) with very little to no recumbent cycling experience performed the 30-second Wingate anaerobic cycling test with a resistance of 0.83 N/kg of the subject's body mass (BM) (5.0 joules/pedal rev/kg BM) in each of these positions. Subjects were strapped to the seat and back rest by means of a lap belt and shoulder harness while pedaling with toe clips. Additionally, hip-to-pedal distance (100% of trochanteric leg length (distance from floor to greater trochanter when standing erect)) and crank-arm length (not specified) were controlled for each subject.

Kinematic analysis from static measures found that the mean ankle and knee angles stayed relatively constant, ranging from 90.1 to 92.8° and 98.2 to 103.6°, respectively, while the mean hip angle increased from 58.9 to 114.0° from the HOA of -10 to 65°. Relative peak power output (highest average power during any successive five second interval divided by body mass) varied from 10.55 ± 1.38 to 11.73 ± 1.03 W/kg BM with the 15° HOA yielding the greatest values. The 15° HOA was significantly greater than the -10 and 65° HOAs, but not significantly different from the 40° HOA (Table 1.1). Additionally, relative average power (over the entire test) and fatigue index (percentage of peak power subtracting the lowest power from the peak power and dividing by the peak power) were calculated. Relative average power values followed a similar trend to the relative peak power scores while the fatigue index was similar across all positions studied.

From this experimental design it could not be determined if the changes in power output were attributable to changes in mean hip angle (BCA), gravity effects on the lower extremity, or a combination of both. Too (1994) refined the experimental design to try to isolate the effects of gravity on peak power output. A similar set-up and test protocol was utilized while varying the torso angle along with the HOA in order to maintain a constant BCA of 105°. The 105° BCA was selected because it was the most powerful in the previous study. Sixteen male recreational cyclists (age 20-36 yrs) performed the same Wingate test against a resistance of 0.83 N/kg body mass with a HOA of -15, 15, and 45° (torso angle of 60, 90, and 120°, respectively) (Figure 1.6). Kinematic analysis from static measures confirmed that mean hip (80°), knee (100°), and ankle (83°) angles did not vary significantly between these three positions. The relative peak power was

found to be greatest in the 15° hip-orientation position, but not significantly greater than the 45° hip-orientation position (the total range of relative peak power was between 11.68 ± 1.25 and 12.29 ± 1.19 W/kg BM) (Table 1.2). Similar trends occurred for the relative average power calculations. The fatigue index was similar for all three test positions.

Too (1989 and 1990) performed experiments in similar HOAs and torso angles as in the previous two studies, but measured cycling duration and total work output to exhaustion using a pre-selected sequence of power outputs (varying both pedal cadence and work load). He found that the 15° HOA (90° torso angle) produced significantly greater cycling duration and total work output to exhaustion than any of the other positions studied from -10 to 90° (all with 90° torso angle). When torso angle was varied along with HOA (similar to Too (1994)) to maintain the same BCA, no significant differences were found in cycling duration and total work output to exhaustion between the three positions.

In order to get a sense of why peak anaerobic power output and aerobic performance might change with different HOAs, Too (1991a and 1993a) repeated the recumbent positions tested earlier and examined electromyography (EMG) levels while cycling with a resistance of 0.64 N/kg of body mass and pedaling cadence of 60 rpm. EMG gives an indication of muscle activity levels by measuring its electrical activity. EMG of the gluteus maximus, rectus femoris, biceps femoris (long head), vastus medialis, gastrocnemius (lateral head), and tibialis anterior of the lower right limb were monitored. Based on his analysis there was a forward shift in pedal position location that the muscles were active and inactive from the -10 to 90° HOA (torso angle at 90°). However, there were no significant differences in muscle activity sequence/timing or duration of activity

with changes in HOA. A similar shift in the pedal position location where the muscles were active was found when both the torso angle and HOA were altered simultaneously. No differences in cycling performance could be attributed to the differences in EMG patterns examined from these studies.

Brown *et al.* (1996) also simultaneously manipulated the HOA and torso angle while subjects (7 males and 4 females, healthy recreational cyclists, average age 27.5 yrs) pedaled at a constant power level (workload of 80 W and cadence of 60 rpm). In addition to collecting EMG from the tibialis anterior, gastrocnemius (medial head), rectus femoris, and biceps femoris, the lower-extremity kinematics and pedal forces were also measured. The kinematics and pedaling kinetics were combined to calculate the ankle-, knee-, and hip-joint moments using inverse dynamics. In this experimental protocol the HOA and torso angle were identical, with data collected at angles of zero through 80° in 10° increments (Figure 1.7).

Results showed that the changes in body position systematically altered all net joint moments. Mean hip torque showed increased flexor values as the cycling position became more vertical, while at the knee there was increased extensor values, and mean ankle torque showed increased dorsiflexor values. The EMG results supported the alterations in joint moments by adjusting muscular activity. Integrated EMG showed heightened levels of tibialis anterior, rectus femoris, and biceps femoris, and depressed levels of gastrocnemius activity as the body was tilted into a more vertical position. Slight changes in pedaling kinematics were also noted as the body orientation was altered. The authors concluded that these changes were necessitated by both alterations

in the mechanical aspects of gravitational forces and sensory consequences from the changes in cycling position.

Kyle and Caiozzo (1986) performed power-output studies with subjects in standard cycling, supine, and prone positions. Little information was given about the exact positions studied, training state of subjects, or details of the power-output tests. It was found that the greatest power outputs were achieved in the standard cycling position, followed closely by the supine position, and finally the prone position. This trend occurred for power-output tests lasting less than one minute and tests lasting one minute and longer.

In addition to the two sets of experiments performed by Too (1989 and 1990) that examined time and total work output to exhaustion, others have investigated the effects of body position on long-duration cycling performance (Bevegard *et al.*, 1966; Diaz *et al.*, 1978; Metz *et al.*, 1986; Nadel and Bussolari, 1988; Stenberg *et al.*, 1967; Wescott, 1991). The body's ability to perform sustained work was found to vary with body position due to alterations in its ability to circulate the blood and exchange gases in the lungs (Bevegard *et al.*, 1966; Stenberg *et al.*, 1967). The blood both provides nutrients to the working muscles and removes waste products of energy production. While tasks that are primarily aerobic in nature must consider these physiological adaptations that occur with changes in body position, a primarily anaerobic task, such as a performance for setting the human-powered speed record which takes approximately two minutes to complete, does not rely on optimal blood circulation and ventilation in the lungs during the task (Foster *et al.*, 1995; Too, 1994). However, since a large amount of time might be

spent training in the vehicle or in the run-up leading to the sprint, blood circulation should be considered no matter what the intended goal of the vehicle.

1.3.3 Analytical Investigations into Recumbent Cycling: The only analytical approach directed to investigate the recumbent position was by Lei *et al.* (1993). This model took into account both the geometry of the rider as well as the effects of the riding position on the aerodynamic cross-section of the vehicle. The model did not include any muscles and, therefore, the effects of different muscle lengths in different rider positions. HOA, torso angle, hip-to-pedal distance, and crank-arm length were all varied within constrained limits which included a minimum torso angle in order to maintain adequate forward visibility. Both anaerobic and aerobic performances were evaluated by means of two different cost functions. For anaerobic performance the cost function was designed to minimize the moment variations on the hip and knee joints while for aerobic performance the cost function was to minimize both the average and maximum variation of the hip- and knee-joint moments. The model was designed for a target speed of 40.0 km/h with a vehicle weight of 50.0 kg, air drag coefficient of 0.15, rolling friction of 0.01, and pedaling cadence of 60 rpm with a 50^{th} percentile male rider.

The optimal aerobic (endurance) performance was computed to occur with a HOA of -5.70° and torso angle of 26.72°. The optimal anaerobic (speed) performance was calculated with a HOA of -25.4° and torso angle of 48.1°. Both simulations found the optimal hip-to-pedal distance to be 0.751 m and crank-arm length to be 0.15 m. The model was also run without taking aerodynamic drag into account in order to compare with the results of Too (1991b). This simulation found the optimal anaerobic position to be with a HOA of 22.9° and hip-to-pedal distance of 0.662 m as compared to 15° and

0.666 m, respectively, experimentally established by Too (1991b). Since the length of muscles crossing the hips are not considered by the model and aerodynamics no longer a concern, allowable torso angles include any angle that would maintain visibility. Crank-arm length of this modified model was not reported.

Other analytical investigations have been performed to investigate the effects of HOA on steady-state cycling performance, as reviewed by Gregor *et al.* (1991). However, these studies generally constrained the HOA to stay greater than 70° in order to stay within the bounds prescribed for the standard bicycling position. The most comprehensive multivariable analysis was conducted by Hull and Gonzalez (1990). They found that changes in HOA significantly altered the results of the joint-moment-based cost function. It was also found that the optimal HOA was altered by rider size. In addition to the model being constrained to maintain an upright, standard cycling position, muscles were not included in the model. Without muscles, the effects on performance by changing their lengths and moment arms with the changes in position could not be assessed.

Additional experimental investigations have looked into various HOAs and torso angles while maintaining the upright riding position, such as Umberger *et al.* (1998). However, the majority of these studies have concentrated on the aerodynamic implications of the various positions with the assumption that time training in the most aerodynamic position will make it a viable riding position. These studies are reviewed in Gregor *et al.*, (1991).

1.4 Discussion

From the reviewed literature it is clear that varying one or more of the biomechanical parameters may alter the power-production capabilities of the cyclist. However, the optimal recumbent riding position is still not clear. Nor is it clear whether the standard cycling position is better biomechanically and physiologically than recumbent cycling, since none of the reviewed articles tested the subjects in the standard cycling position as well as the recumbent positions.

1.4.1 Effect of Gravity on Performance: Brown *et al.* (1996) showed through inverse dynamics and EMG analysis that muscle-group contributions do change as the effects of gravity are altered on the lower extremity. Too (1991a) also noted alterations in muscle activity when only the effects of gravity on the extremities were altered. However, due to the low-power output of the cyclists measured relative to their peak power in these two studies it cannot be concluded that peak-power output would be altered similarly by the effects of gravity on the lower extremities. Too (1990) showed that altering the effects of gravity on the lower extremity and blood circulation did not alter the work output and time to exhaustion in the three positions studied. In addition, two out of the three positions studied were not significantly different in peak-power output (Too, 1994). While this limited number of studies is not conclusive, it appears that the effects of gravity on performance may be small, at least in the range of positions studied.

1.4.2 Effect of Body Configuration Angle (BCA) on Performance: No studies to date have altered the BCA while maintaining a constant HOA in order to remove the effects of gravity on the cycling performance. However, assuming that gravity is a

secondary effect based on the previous discussion, BCA has a major effect on power production while cycling. Based on the work of Too (1989 and 1991b) the 105° BCA may be optimal for both peak power production and sustained aerobic performance. However, the differences in the peak power at the 130° BCA were not statistically significant. Also, with 25° increments between the BCAs tested, the optimal configuration may be a position not tested. Gravity also may play a large enough role to alter the optimal BCA at some HOAs. More research is needed into the effects of BCA as well as the effects of gravity to make any solid conclusions about the optimal riding position.

It is interesting to note that the 105° BCA falls in the range used in the standard cycling position. Cavanagh and Sanderson (1986) reported that elite pursuit cyclists rode with an average torso angle of 145°. Considering that the standard cycling position general uses a HOA (seat tube angle) from 70 to 90° (Burke and Pruitt, 1996), the cycling position for these elite pursuit riders has a BCA from 105 to 125°. The 125° BCA is within 5° of the position that Too (1991b) found to be not statistically different from the 105° BCA. This knowledge lends further support to the assumption that the musculoskeletal biomechanics at the hip may be of more concern than the effects of gravity on the lower extremity for power output. These conclusions may be a bit premature, however, since Too (1989 and 1991b) did not test his subjects in the standard cycling position and they would not be considered 'elite pursuit riders' who may have trained into their riding position. The human body is highly trainable and may be able to adapt to a seemingly non-optimal position and make it optimal, as long as the cycling position is not too drastically different from a good power producing position.

Additionally, care must be taken when implementing the results from Too and Brown *et al.* These studies are based on results from recreational cyclists with little to no recumbent cycling experience. Also, these results are based on studies where the subjects used toe-clips rather than clipless pedals which are more common for high performances. Clipless pedals may make a large difference in recumbent cycling since gravity is acting differently on the legs than in the standard cycling position.

While analytical models can provide great insight into what position may be optimal and why, the results from those reviewed in this article were not used here to justify one position over another. These models did not incorporate the effects of changing the muscle lengths and moment arms across the hips that appear to be a major determinant of performance based on the experimental results. Without the inclusion of these musculoskeletal effects the analytical results are difficult to use, even if they appear to be consistent with the experimental results.

1.5 Conclusions

Along with the power-production capabilities of the rider and the aerodynamics of the vehicle, additional performance factors and practical constraints must be considered when designing a successful human-powered vehicle. Performance factors include the power-train efficiency, vehicle dynamics, and road friction for a land vehicle. The fairing must also be designed to allow adequate air flow in order to keep the rider cooled. Practical constraints include the visibility, controllability, structural stability, safety, and comfort of the vehicle. Many of these factors are not independent. For example, the rider position, in addition to affecting the rider's ability to produce power and the

aerodynamic design of the vehicle, may also affect the drive-train construction and thus its ability to transfer the energy from the pedals to the wheels efficiently. For these reasons, the overall design may not include the optimal riding position for peak-power production/sustained performance or the design with the lowest aerodynamic cost. However, a global optimal for all design constraints should be selected.

More research is needed into the effects of BCA and gravity acting on the lower extremity, as well as the effects of training on cycling position. None-the-less, an aerodynamic position with a low hip-orientation angle (either positive or negative) combined with a BCA from 105 to 130° appears based on current literature to be justifiable for a high-performance human-powered vehicle.

1.6 References

Alexander, R.M. and Ker, R.F. (1990). The architecture of leg muscles. In *Multiple Muscle Systems: Biomechanics and Movement Organization* (Edited by Winters, J.M. and Woo, S.L.-Y.). Springer-Verlag: New York, pp. 568-577.

Bevegard, S., Freyschuss, U., and Strandell, T. (1966). Circulatory adaptation to arm and leg exercise in supine and sitting position. *J. Applied Physiology,* **21**(2), 37-46.

Broker, J.P. and Gregor, R.J. (1996). Cycling biomechanics. In *High-Tech Cycling* (Edited by Burke, E.R.). Human Kinetics Publishers: Champaign, pp. 145-166.

Brown, D.A., Kautz, S.A., and Dairaghi, C.A. (1996). Muscle activity patterns altered during pedaling at different body orientations. *J. Biomechanics,* **29**(10), 1349-1356.

Burke, E.R. and Pruitt, A.L. (1996). Body positioning for cycling. In *High-Tech Cycling* (Edited by Burke, E.R.). Human Kinetics Publishers: Champaign, pp. 79-99.

Cavanagh, P.R. and Sanderson, D.J. (1986). The biomechanics of cycling: studies of the pedaling mechanics of elite pursuit riders. In *Science of Cycling* (Edited by Burke, E.R.). Human Kinetics Publishers: Champaign, pp. 91-122.

Coast, J.R. (1996). Optimal pedaling cadence. In *High-Tech Cycling* (Edited by Burke, E.R.). Human Kinetics Publishers: Champaign, pp. 101-116.

Diaz, F.J., Hagan, R.D., Wright, J.E., and Horvath, S.M. (1978). Maximal and submaximal exercise in different positions. *Medicine & Science in Sports and Exercise*, **10**(3), 214-217.

Foster, C., Hector, L.L., McDonald, K.S., and Snyder, A.C. (1995). Measurement of Anaerobic Power and Capacity. In *Physiological Assessment of Human Fitness* (Edited by Maud, P.J. & Foster, C.). Human Kinetics Publishers: Champaign, pp. 73-85.

Gregor, R.J., Broker, J.P., and Ryan, M.M. (1991). The biomechanics of cycling. In *Exercise and Sport Sciences Reviews* (Edited by Holloszy, J.O.). Williams & Wilkens: Baltimore, Vol. 19, pp. 127-169.

Gregor, R.J. and Rugg, S.G. (1986). Effects of saddle height and pedaling cadence on power output and efficiency. In *Science of Cycling* (Edited by Burke, E.R.). Human Kinetics Publishers: Champaign, pp. 69-90.

Gross, A.C., Kyle, C.R., and Malewicki, D.J. (1983). The aerodynamics of human-powered land vehicles. *Scientific American*, **249**(6), 142-152.

Hoy, M.G., Zajac, F.E., and Gordon, M.E. (1990). A musculoskeletal model of the human lower extremity: the effect of muscle, tendon, and moment arm on the moment-angle relationship of musculotendon actuators at the hip, knee, and ankle. *J. Biomechanics*, **23**, 157-169.

Hull, M.L. and Gonzalez, H. (1990). Multivariate optimization of cycling biomechanics. In *Biomechanics of Sports VI* (Edited by Kreighbaum, E. and McNeill, A.). Montana State University: Boseman, pp. 15-41.

Hull, M.L. and Hawkins, D.A. (1990). Analysis of muscular work in multisegmental movements: application to cycling. In *Multiple Muscle Systems: Biomechanics and Movement Organization* (Edited by Winters, J.M. and Woo, S.L.-Y.). Springer-Verlag: New York, pp. 621-638.

Hull, M.L. and Jorge, M. (1985). A method for biomechanical analysis of bicycle pedaling. *J. Biomechanics*, **18**(9), 631-644.

Ice, R. and Waite, J. (In Preparation). Overuse injuries in cycling. *Int. J. Sports Medicine*.

Inbar, O., Dotan, R., Trousil, T., and Dvir, Z. (1983). The effect of bicycle crank-length variation upon power performance. *Ergonomics*, **26**(12), 1139-1146.

Kautz, S.A. and Hull, M.L. (1993). A theoretical basis for interpreting the force applied to the pedal in cycling. *J. Biomechanics*, **26**(2), 155-165.

Kita, J. (1997). The unseen danger (Special report: impotency and cycling). *Bicycling Magazine,* August, pp. 68-73.

Kroemer, K.H.E. (1972). Pedal operation by the seated operator. SAE Paper 72004. Society of Automotive Engineers: New York.

Kulig, K., Andrews, J.G., and Hay, J.G. (1984). Human Strength Curves. In *Exercise and Sport Sciences Reviews.* Williams & Wilkens: Baltimore, Vol. 12, pp. 417-466.

Kyle, C.R. and Caiozzo, V.J. (1986). Experiments in human ergometry as applied to the design of human powered vehicles. *Int. J. Sports Biomechanics,* **2**, 6-19.

Lei, Y., Trabia, M.B., and Too, D. (1993). Optimization of the seating position in a human-powered vehicle. In *Biomechanics in Sports XI* (Edited by Hamill, J., Derrick, T.R., and Elliott, E.H.). University of Massachusetts at Amherst, pp.115-119.

Martin, G. (1984). Notes on human powered practicality. In *Proceedings of the Second International Human Powered Vehicle Scientific Symposium.* Long Beach, CA: IHPVA, Box 2068, Seal Beach, CA, pp. 115-117.

Metz, L.D., Moeinzadeh, M.H., White, L.R., and Groppel, J.L. (1986). In *Biomechanics: The 1984 Olympic Scientific Congress Proceedings* (Edited by Adrian and Deutsch). Microfilm Publishers. University of Oregon: Eugene, pp. 289-295.

Moran, G.T. (1990). Biomechanics of cycling-the role of the foot pedal interface. In *Biomechanics in Sports VI* (Edited by Kreighbaum, E. and McNeill). Montana State University: Boseman, pp. 43-49.

Moran, G.T. and McGlinn G.H. (1995). The effect of variations in the foot pedal interface on the efficiency of cycling as measured by aerobic energy cost and anaerobic power. In *Biomechanics of Sports XII* (Edited by Barabis, A. and Fabian, G.). Budapest: Hungary, pp. 105-109.

Nadel, E.R. and Bussolari, S.R. (1988). The Daedalus project: physiological problems and solutions. *American Scientist,* July-August, pp. 350-360.

Nemeth, G. and Ohlsen, H. (1985). *In vivo* moment arm lengths for hip extensor muscles at different angles of hip flexion. *J. Biomechanics,* **18**(2), 129-140.

Seirig, A. and Arvikar, R.J. (1989). Modeling of the musculoskeletal system for the upper and lower extremities. In *Biomechanical Analysis of the Musculoskeletal Structure for Medicine and Sports.* Hemisphere Publishing Corp.: New York, pp. 99-154.

Spoor, C.W. and Leeuwen, J.L. van (1992). Knee muscle moment arms from MRI and from tendon travel. *J. Biomechanics,* **25**(2), 201-206.

Spoor, C.W., Leeuwen, J.L. van, Meskers, C.G.M., Titulaer, A.F., and Huson, A. (1990). Estimation of instantaneous moment arms of lower-leg muscles. *J. Biomechanics,* **23**(12), 1247-1259.

Stenberg, J., Astrand, P.-O., Ekblom, B., Royce, J., and Saltin, B. (1967). Hemodynamic response to work with different muscle groups, sitting and supine. *J. Applied Physiology,* **22**(1), 61-70.

Too, D. (1996). The effect of pedal crankarm length on power production in recumbent cycle ergometry. In *Biomechanics in Sports XIII* (Edited by Bauer, T.). Lakehead University: Thunder Bay, Ontario, pp. 350-353.

Too, D. (1994). The effect of trunk angle on power production in cycling. *Research Quarterly for Exercise and Sport,* **65**(4), 308-315.

Too, D. (1993a). The effect of hip position/configuration on EMG patterns in cycling. In *Biomechanics in Sports XI* (Edited by Hamill, J., Derrick, T.R., and Elliott, E.H.). University of Massachusetts at Amherst, pp. 126-131.

Too, D. (1993b). The effect of seat-to-pedal distance on anaerobic power and capacity in recumbent cycling (Abstract). *Medicine & Science in Sport and Exercise,* **25**(5), s68.

Too, D. (1991a). The effect of body orientation on EMG patterns in cycling. In *Biomechanics in Sports IX* (Edited by Taut, C.L., Patterson, P.E., and York, S.L.). Iowa State University: Ames, pp. 109-115.

Too, D. (1991b). The effect of hip position/configuration on anaerobic power and capacity in cycling. *Int. J. Sport Biomechanics,* **7**, 359-370.

Too, D. (1990a). The effect of body configuration on cycling performance. In *Biomechanics of Sports VI* (Edited by Kreighbaum, E. and McNeill, A.). Montana State University: Boseman, pp. 51-58.

Too, D. (1990b). Biomechanics of cycling and factors affecting performance. *Sports Medicine,* **10**(5), 286-302.

Too, D. (1989). The effect of body orientation on cycling performance. In *VII International Symposium of Biomechanics in Sports* (Edited by Morrison, W.E.). Melbourne, Australia, pp. 53-60.

Umberger, B.A., Scheuchenzuber, H. J., and Manos, T. M. (1998). Differences in power output during cycling at different seat-tube angles. *Medicine & Science in Sport and Exercise,* **30**(5), s81.

Urlocker, J.A. and Prassas, S.G. (1996). Phasic muscle activity of the lower extremity at different powers and pedaling cadences in cycle ergometry. In *Biomechanics in Sports XIII* (Edited by Bauer, T.). Lakehead University: Thunder Bay, Ontario, pp. 354-357.

Wescott, W.L. (1991). Comparison of upright and recumbent cycling exercise. *American Fitness Quarterly*, October, pp. 36-38, 46.

Wheeler, J.B., Gregor, R.J., and Broker, J.P. (1995). The effect of clipless float design on shoe/pedal interface kinetics and overuse knee injuries during cycling. *J. Applied Biomechanics*, **11**, 119-141.

Whitt, F.R. and Wilson, D.G. (1982). Human power generation. In *Bicycling Science* (Second Edition). MIT Press: Cambridge, pp. 29-70.

Wilson, D.G., Forrestall, R., and Hendon, D. (1984). Evolution of recumbent bicycles and the design of the Avatar Bluebell. In *Proceedings of the Second International Human Powered Vehicle Scientific Symposium*. Long Beach, CA: IHPVA, Box 2068, Seal Beach, CA, , pp. 92-103.

Winter, D.A. (1990). *Biomechanics and Motor Control of Human Movement* (Second Edition). John Wiley & Sons, Inc.: New York.

Winters, J.M. and Stark, L. (1988). Estimated mechanical properties of synergistic muscles involved in movements of a variety of human joints. *J. Biomechanics*, **21**(12), 1027-1041.

Zajac, F.E. (1989). Muscle and tendon: properties, models, scaling, and application to biomechanics and motor control. In *CRC Crit. Rev. Biomed. Engng* (Edited by Bourne, J.R.). CRC Press: Boca Raton, Vol. 17, pp. 359-411.

Zajac, F.E. and Gordon, M.E. (1989). Determining muscle's force and action in multi-articular movement. In *Exercise and Sport Sciences Reviews* (Edited by Pandolf, K.). Williams & Wilkens: Baltimore, Vol. 17, pp. 187-230.

1.7 Appendix: Additional Operational-Parameter Sources

The following are references that discuss geometric and operational parameters beyond HOA and torso angle. References followed by an '**R**' have information directly related to recumbent cycling.

Hip-to-pedal distance: Gregor *et al.* (1991), Too (1993b) **R**, Too (1990b) **R**

Crank-Arm Length: Gregor *et al.* (1991), Inbar *et al.* (1983), Too (1990b) **R**, Too (1996) **R**, Too (1998) **R**

Foot Position on Pedal: Burke and Pruitt (1996), Hull and Gonzalez (1990)

Foot-to-Pedal Interface: Broker and Gregor (1996), Gregor *et al.* (1991), Moran (1990), Moran and McGlinn (1995), Wheeler *et al.* (1995)

Pedaling Cadence and Power Output: Coast (1996), Gregor *et al.* (1991), Too (1990b) R, Urlocker and Prassas (1996), Whitt and Wilson (1982)

1.8 Tables

Table 1.1: Results from Too (1991b)

HOA	-10	15	40	65
Torso Angle	90	90	90	90
BCA	80	105	130	155
Peak Power	10.91	11.73	11.43	10.55
Average Power	7.84	8.29	8.14	7.53
Fatigue Index [%]	47.9	49.6	49.8	49.4

Angles reported in degrees, power in W/kg body mass

Table 1.2: Results from Too (1994)

HOA	-15	15	45
Torso Angle	60	90	120
BCA	105	105	105
Peak Power	11.68	12.29	12.14
Average Power	8.73	9.27	9.00
Fatigue Index [%]	46.1	44.3	46.0

Angles reported in degrees, power in W/kg body mass

1.9 Figures

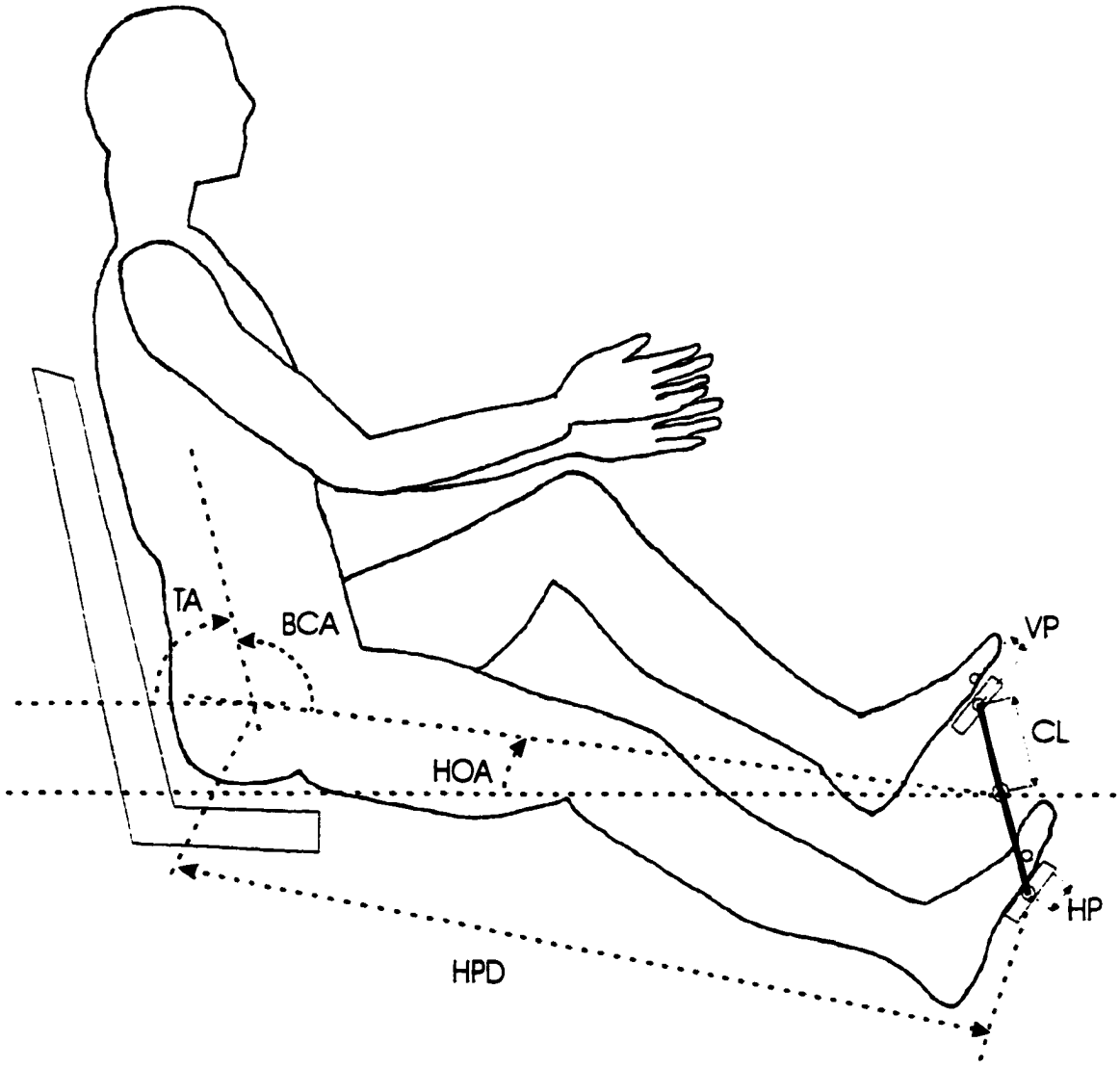

Figure 1.1: Geometrical variables which must be defined to completely describe the cycling position of the rider: hip orientation angle (HOA), torso angle (TA), hip-to-pedal distance (HPD), crank-arm length (CL), and horizontal (HP) and vertical (VP) foot position, as well as the foot-to-pedal interface (not shown). Body configuration angle (BCA), which may be deduced from TA and HOA, is also included to help describe the cycling position.

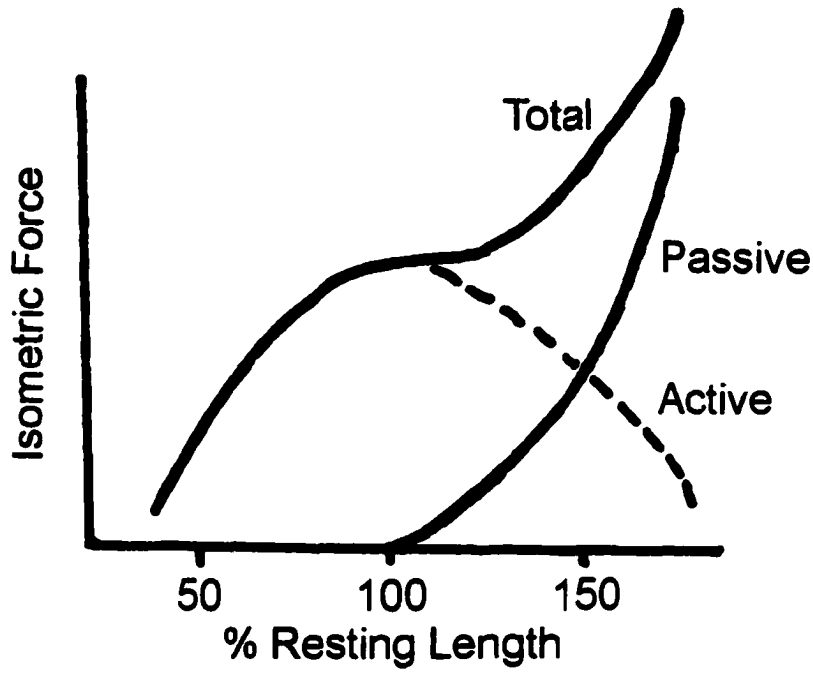

Figure 1.2: The force-length relation of a muscle/muscle fiber. Total force is the sum of the passive (solid line) and active (dotted line) components.

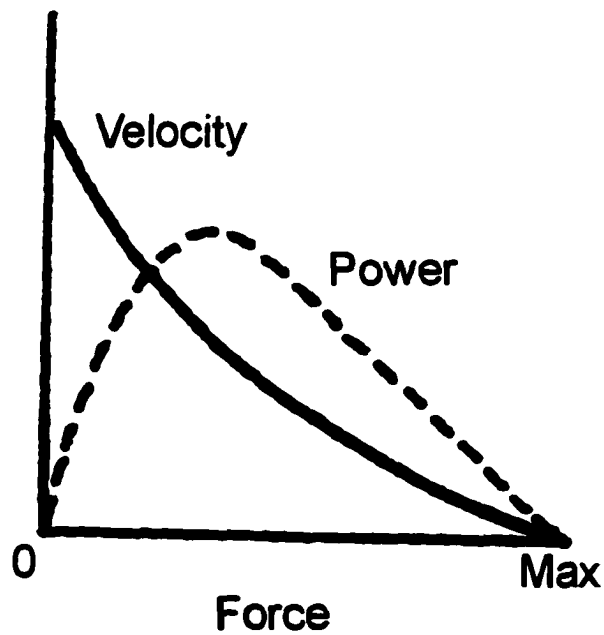

Figure 1.3: The force-velocity of shortening (solid line) and force-power (dotted line) relations of muscle.

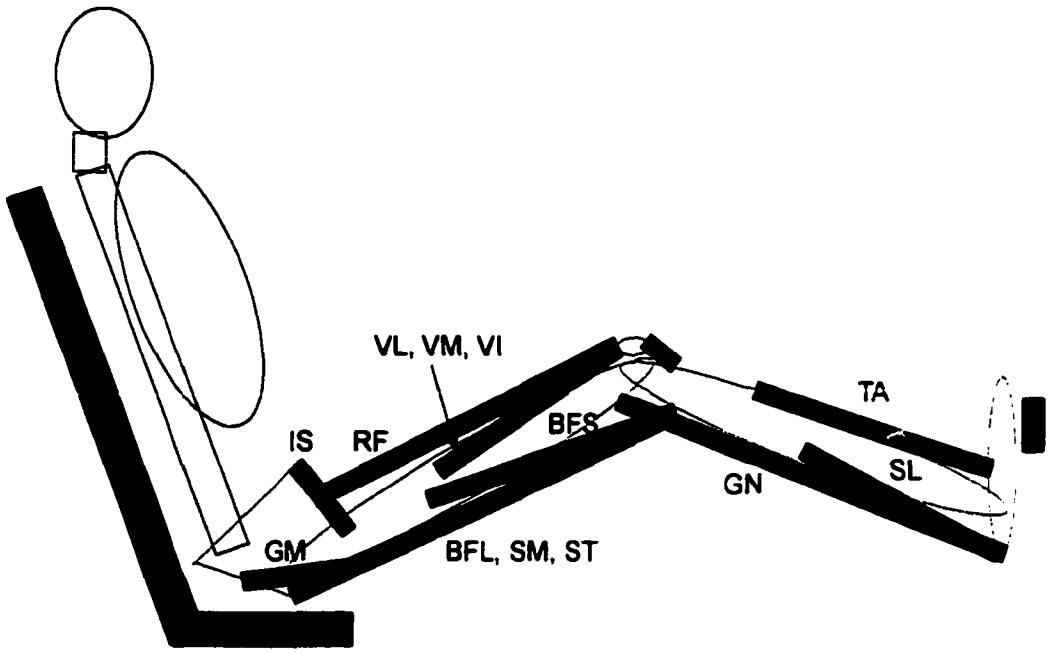

Figure 1.4: Schematic representation of the muscles of the lower extremity identified as prime movers in cycling: biceps femoris long head (BFL), biceps femoris short head (BFS), gastrocnemius (GN), gluteus maximus (GM), gluteus medius (GM), gluteus minimus (GM), iliospoas (IS), rectus femoris (RF), soleus (SL), semimembranosus (SM), semitendinosus (ST), tibialis anterior (TA), vastus intermedius (VI), vastus lateralis (VL), and vastus medialis (VM).

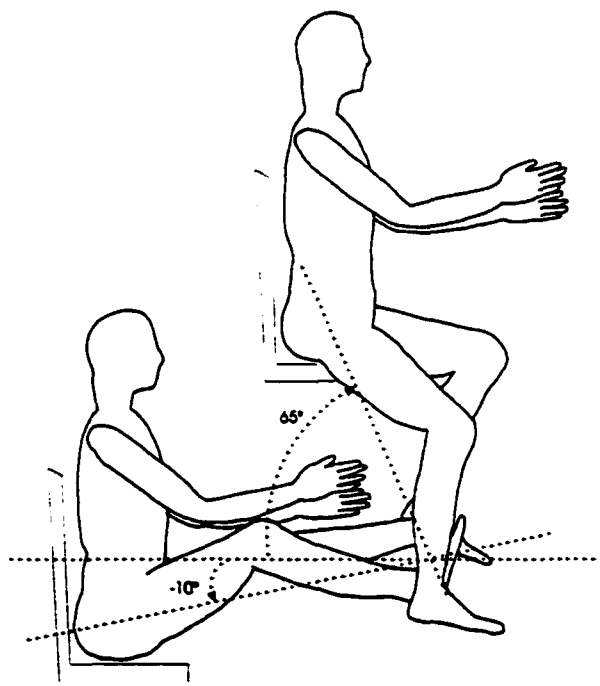

Figure 1.5: Test position range utilized by Too (1991b): HOA from -10° to 65° in 25° increments with constant 90° torso angle.

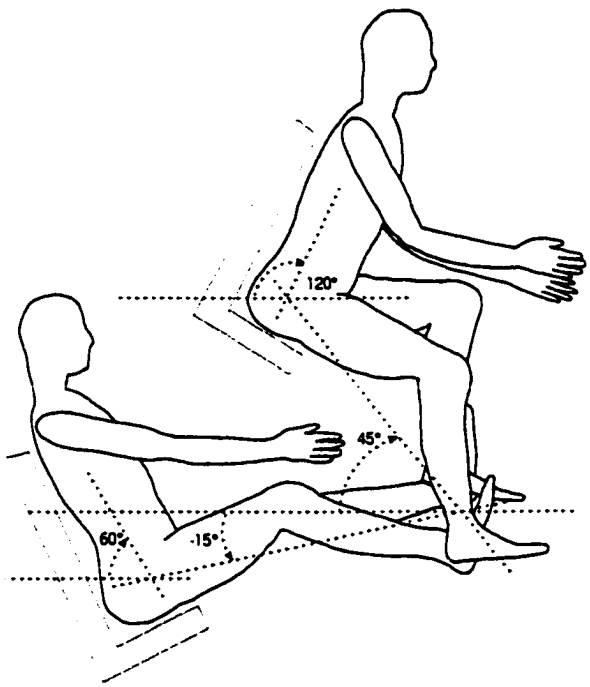

Figure 1.6: Range of test positions utilized by Too (1994): HOA of -15 to 45° in 30° increments. The torso angle was adjusted with HOA from 60 to 120° in order to maintain a 105° BCA.

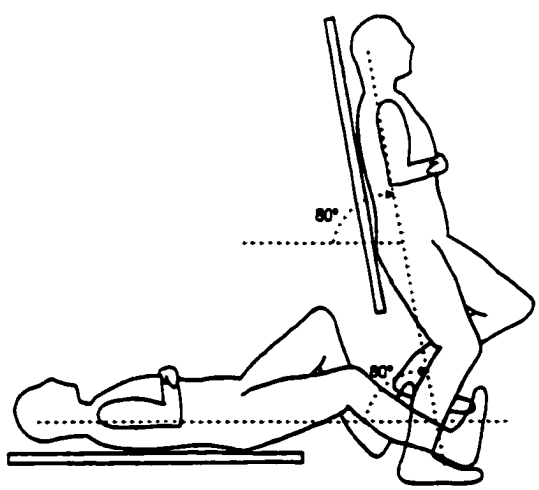

Figure 1.7: Range of test positions utilized by Brown *et al.* (1996): HOA and torso angle were varied together from zero to 80° in order to maintain a 180° BCA in 10° increments. Note: While not diagrammed, a seat was used to maintain a constant hip to pedal distance when pedaling as well as to remove the effects of the upper body mass on the cycling kinematics and kinetics.

Chapter 2

Anaerobic Cycling Power Output with Variations in Recumbent Body Configuration

2.1 Abstract

While the recumbent cycling position has become common for high-performance human-powered vehicles, questions still remain regarding what is the optimal riding position, the influence of familiarity on recumbent cycling, and how recumbent cycling positions compare to the standard cycling position (SCP). Eight recumbently familiar cyclists and 10 recreational control cyclists were compared using the 30-second Wingate test in five recumbent positions as well as the SCP. For the recumbent positions, hip position was maintained 15° below the bottom bracket while the backrest was altered to investigate body configuration angle (BCA) changes from 100 to 140° in 10° increments. BCA was defined as the included angle between the bottom bracket, hip, and a marker on the mid torso. Only slight, mainly non-significant ($p \leq 0.05$), differences were measured between the two groups. Whole group peak power (12.7 W/kg body mass) and average power (9.7 W/kg body mass) were greatest in the 130 and 140° BCA positions, with power dropping off as the BCA decreased through 100° (peak = 11.3, average = 9.0 W/kg body mass). Power output in the SCP (peak = 12.8, average = 9.6 W/kg body mass) was similar to that produced in the 130 and 140° BCA. Average hip and ankle angles

increased, 36 and 9° respectively, with BCA while knee angles remained constant. The lower-extremity kinematics of the130 and 140° BCA were most similar to those of the SCP. However, the SCP joint angles were generally significantly different from these two recumbent positions, even though the BCA of the SCP was not significantly different. These findings suggest: 1) BCA is a major determinant of power output, 2) recumbent position anaerobic power output matches that of the SCP when BCA is maintained, even though lower-extremity kinematics may be altered, and 3) the amount of recumbent familiarity in this study did not produce large changes in power output or kinematics.

2.2 Introduction

The recumbent cycling position has become popular for high-performance human-powered vehicles due to its reduced aerodynamic drag compared to a fully-crouched standard racing position (Gross *et al.*, 1983). Aerodynamic drag is often times regarded as the most critical factor for success, since it produces the greatest resistive forces against the rider/bicycle system of all resistive elements. For example, an upright riding cyclist will have to produce approximately 800 W in order to maintain a riding speed of 50 kph on a flat surface with no wind. Of the 800 W, approximately 700 W go towards overcoming air resistance and only 100 W go towards overcoming mechanical resistance (Hagberg and McCole, 1996).

The recumbent cycling position reduces aerodynamic drag compared to the standard cycling position (SCP) by reducing the effective frontal area. This is accomplished in two ways: 1) the hips are placed almost directly behind the crank, horizontally, and 2) the

torso is raised only slightly so that the rider may see forward (Figure 2.1). The location of the hip joint relative to the crank is best described by the angle these two points make with the horizontal, termed the hip orientation angle (HOA) (Figure 2.1, nomenclature also included in Appendix). The HOA is similar to the seat-tube angle often used to describe the hip position of the SCP. However, because the line of the seat tube does not pass through the hip joint in the recumbent position as it generally does in the SCP, the seat-tube angle does not describe the hip position accurately in the recumbent position. The torso position is best described by an angle made between the mid-rib cage, the hip, and the horizontal, termed the torso angle (TA) (Figure 2.1). In the recumbent position the TA is similar to the backrest angle. However, the backrest angle does not take into account any slight curvature of the back that may exist, nor is it applicable to both the recumbent and SCP.

The HOA and TA may be manipulated independently to modify the aerodynamics of the vehicle. However, together they define the overall configuration of the rider which may be critical in determining the peak-power output capacity of the rider. The included angle formed by the HOA and TA, termed body configuration angle (BCA), alters the lower-extremity kinematics of the cyclist. Increasing the BCA will mainly increase the mean hip angle while cycling with only small adjustments at the knee and ankle (Heil *et al.*, 1995; Heil *et al.*, 1997; Price and Donne, 1997; Too, 1991; Umberger *et al.*, 1998).

Altering the mean hip angle will modify the musculoskeletal dynamics of cycling. In particular, increasing the hip angle will decrease the length of the muscles crossing behind the hip, while decreasing the hip angle will have the opposite effect. Changes in hip angle will also change the moment arms of the muscles acting about the hip. Both

muscle length and moment arm changes will have an effect on each muscle's ability to produce power. The modeling effort by Yoshihuku and Herzog (1996) demonstrated that the combined effect on all muscles by varying the mean hip angle may significantly alter peak-power output, even in practical ranges for upright cycling.

2.2.1 Review of Literature: The effects on peak-power output by altering the BCA has been examined experimentally in both the recumbent (Too, 1991; Welbergen and Clijsen, 1990) and the SCP (Umberger *et al.*, 1998; Welbergen and Clijsen, 1990). However, each of these studies has limitations which reduce their applicability in determining the true effect of altering BCA on peak-power output.

Too (1991) systematically altered the HOA in 25° increments from -10° to 65° while maintaining a 90° backrest angle, relative to horizontal. This effectively manipulated the BCA from approximately 90 to 165° (when adjusting backrest and seat-tube angle each by 5° to produce TA and HOA, respectively). In the study by Too(1991), subjects unfamiliar with recumbent cycling produced the greatest power, as determined by a 30-second Wingate test, in the 115° BCA. During a Wingate test, subjects pedal with maximal effort against a set resistance for the entire duration. Peak-power output is calculated over a 5-second period near the start of the test. Additionally, average power, minimum power, and fatigue index (percentile difference between peak and minimum power output) are usually calculated. While the Wingate test has become generally accepted as a valid assessment tool for peak-power output (Bar-Or, 1987), from this experimental design it could not be determined if the changes in power output were attributable to changes in BCA, HOA, or a combination of both. Changes in HOA directly alter the gravitational contribution of the lower-extremity segments and has been

found to have a statistical affect on peak-power output (Too, 1994). Changing the HOA may also directly alter the effective forces on the pedal (Browning *et al.*, 1992; Price and Done, 1997). Additionally, due to the relatively large increments in HOA, sensitivity to the different positions could not be assessed further.

Welbergen and Clijsen (1990) assessed peak-power output on six subjects (three trained cyclists and three experienced recumbent cyclists) in two different recumbent positions as well as two different SCP. The recumbent positions utilized a 30° HOA combined with either a 75 or 105° TA, while the SCP utilized a 69° HOA combined with either a 105 or 180° TA. The TA measurements were approximate, since they were only visually monitored. Peak power was reported as an average power over the last three minutes of a nine minute test. Only the peak power in the upright SCP position was significantly greater than any others. In addition to only having a vague description of the BCA for each position, the peak power test was an average over a period of time that would require a substantial amount of aerobic energy as well as anaerobic energy. Therefore, a true peak power was not determined.

Umberger *et al.* (1998) had 12 non-cyclists perform a 15 second max test in four different SCP. The HOA was altered from 69 to 90° in relatively even increments while maintaining a similar grip on the handlebars. This effectively kept the TA (as defined by a marker on the shoulder rather than mid torso) constant at approximately 45°. Power output was found to decrease as the BCA increased. However, as with Too (1991), power output differences could be attributable to both alterations in HOA and BCA.

To date, no study has effectively isolated the effect of BCA on peak-power output. Since the tradeoffs between the aerodynamic improvements made based on BCA

adjustments and the effects on power output are not well understood, it is currently impossible to optimize the design of a human-powered vehicle for high speeds over a short period of time. Both sprint and endurance races require high speeds over short periods in order to be successful. Sprint races in open human-powered vehicle competitions may be extremely short, lasting as little as 30 seconds; requiring the rider to produce peak effort for most, if not all, of the race. Endurance events are also heavily dependent on peak-power output, since sprints are required intermittently, both for passing and breaking away from other racers as well as for finishing the race. Again, these sprints may require near maximal effort for as little as 30 seconds and are critical to success.

In addition to the lack of understanding concerning the effects of BCA on peak-power output, it is unclear how power outputs in recumbent cycling positions compare to those measured in the SCP, in terms of both peak-power output and the effects of training. This information is critical for two reasons: 1) cyclists with no recumbent cycling experience are often recruited to ride recumbent vehicles and given only a short period of time to train in the recumbent position prior to competition, and 2) recumbent vehicles are often designed with power output parameters defined based on tests performed in the SCP.

Training for athletic events has long been established as an effective means of improving performance. Generally, the more specific the training is to the competitive event, the better the results. In this case, training in the recumbent position would be most specific to the event. However, if recumbent cycling is sufficiently similar to standard cycling, it too may be considered specific training. Unfortunately, differences

between the recumbent and SCP have not been investigated well enough to determine what effect recumbent training would have on power output.

2.2.2 Purpose: The objectives of this investigation were three-fold. First, to determine the effects of changes in BCA, while keeping HOA constant, on peak-power output in recumbent cycling. Second, to determine if having a cyclist train in a recumbent position for a short period of time will produce adaptations that alter recumbent cycling peak-power output and lower-extremity kinematics, compared to a cyclist with no recumbent cycling experience. Three, to determine how peak-power output in the SCP compares to similar measurements taken while cycling recumbently.

2.3 Methods

2.3.1 Subjects: Eighteen male recreational cyclists participated in this study. Subjects were separated into two groups based on their familiarity with the recumbent cycling position from training. A familiar group consisted of eight subjects, while the remaining 10 subjects were in a control group. All familiar group subjects and approximately half of the control group subjects were members of an undergraduate team that was constructing a recumbent human-powered vehicle that they would race at the American Society of Mechanical Engineering Human-Powered Vehicle Competition held later that year.

In order to qualify for the familiar group, the subjects had to average one or more cycling sessions per week of at least 30 minutes duration on a Schwinn 205P (Schwinn Cycling & Fitness, Inc., Boulder, Colorado) stationary recumbent trainer during the eight weeks prior to the start of testing (familiar group average = 1.5 ± 0.4 sessions/week

(mean ± SD)). The control group consisted of one subject who started the recumbent training, but did not continue (recumbent cycling average = 0.5 sessions/week). All other members of the control group performed no recumbent cycling. There was no history of recumbent cycling experience for any of the 18 subjects prior to involvement with this study. No restrictions were placed on the amount of cycling in the SCP for either group during the eight weeks prior to the start of testing.

The Schwinn 205P stationary recumbent trainer was chosen because it is commercially available, utilizes a BCA (~130°) very similar to but slightly reduced from the SCP, and incorporates a HOA (~5°) that was closest of the commercially available trainers to that being tested. The training in this position would allow the familiar group to be acclimated to the altered effects of leg orientation while recumbent cycling, but not have to adjust to cycling in a drastically different BCA.

Prior to participation, subject age, mass, standing height, and lower extremity anthropometric measurements were collected (Table 2.1). All leg lengths were measured on the right side. The thigh length was measured from the greater trochanter to the knee center of rotation, the shank length from the knee center of rotation to the lateral malleolus, and the foot length from the lateral malleolus to the head of the 5^{th} metatarsal. The maximum hip-to-pedal distance (HPD) while cycling was set at the beginning of each cycling session at 105% of the standing leg length from greater trochanter to the floor for both groups.

2.3.2 Equipment: To accommodate the changes in BCA required of this study and maintain consistent HOA and HPD for different sized individuals, a four degrees-of-freedom, variable-seating device was interfaced with a Monark 824E bicycle ergometer

(Monark Exercise AB, Varberg, Sweden) (Figure 2.1). The four degrees of freedom were horizontal seat position, vertical seat position, backrest angle, and seat angle. The ergometer was equipped with 175 mm crank arms and Shimano SPD® compatible clipless pedals. Constant foot position on the pedals was achieved by requiring the subjects to maintain the same cleat positioning on their shoes during the testing period.

2.3.3 Experimental Protocol: Seven test sessions were required of each subject. The first session was used to obtain university-approved informed consent along with information on cycling experience and health status. Additionally, anthropometric measurements were made and a test was administered in a random position to familiarize subjects with the apparatus and procedures (pilot testing showed a one-test learning curve with no further improvements after the second test). Each of the remaining six sessions tested a different cycling position. Five of the cycling positions tested were recumbent with a -15° HOA and backrest angle of 30, 40, 50, 60, or 70°. TA was found to be consistently 5° less than the backrest angle, allowing for analysis of BCA from 140 to 100°. The sixth position was a SCP with 75° HOA and no backrest so that the subject could choose their own angle of torso lean (each subject was also allowed to adjust handlebar height and rotation).

The -15° HOA was selected for its practicality in a streamlined recumbent vehicle. This HOA was the highest hip position relative to the bottom bracket where the heels of the feet did not drop below the horizontal level of the buttocks during the pedal cycle. In this position the feet do not increase the frontal cross-sectional area of the vehicle. This HOA is more negative than that found on most commercially available recumbent bicycles. However, this HOA is used on at least some recumbent bicycles built for

racing. For example, the M-5 Low Racer by Lightning Cycle Dynamics (Lompoc, California) has a HOA estimated at approximately -20°.

The backrest angle range was then set once the HOA was determined. The maximum backrest angle of 70° was set based on four criterion: 1) the BCA produced was smaller than found to be optimal by Too (1991), 2) the BCA produced was smaller than that in the SCP, 3) several subjects found smaller BCAs produced interference between the thighs and torso while cycling, and 4) a higher backrest angle would produce a cross-sectional area no longer considered practical for a streamlined vehicle. The minimum backrest angle of 30° was set based on six criterion: 1) the BCA produced was greater than found to be optimal by Too (1991), 2) the BCA produced was greater than that in the SCP, 3) forward visibility was beginning to be impaired by the feet and bottom bracket, 4) heart level dropped below the working musculature at backrest angles lower than 30°, 5) subjects felt like they were pushing themselves out of the seat at backrest angles lower than 30°, and 6) proprioception may reduce one's ability to produce power in a supine position (Brown *et al.*, 1996).

All subjects were tested in each cycling position with the testing sequence randomly determined. However, the position tested in the familiarization session was repeated in the seventh session. There was a minimum of 24 hours between test sessions with each subject testing at the same time of each day with a minimum of exercise during the hours of that day prior to testing. Once testing commenced, all sessions were completed within a 14 day period. Subjects were weighed prior to every session in order to ensure consistent body mass (BM). For each recumbent position, the subject was strapped to the

seating device with both a hip and mid-torso belt. No belts were worn during the SCP testing. However, the subjects were required to remain seated during the entire SCP test.

In order to quantify body position and lower extremity joint kinematics while cycling, reflective markers were placed on each subject's right mid-torso (mid-rib cage, in line with hip/shoulder axis), hip (approximating the greater trochanter), knee (lateral femoral epicondyle), ankle (lateral malleolus), and toe (head of 5^{th} metatarsal). Markers were also placed on the ergometer at the crank and pedal-spindle centers (Figure 2.1).

The 30-second Wingate test was chosen as the measure of maximal anaerobic power output with the administered test protocol similar to that utilized by the Sport Science & Technology Division of the United States Olympic Committee (R.L. Wilber, personal communication, March 1998). The test protocol consisted of a five minute warm-up with a load of 2.0% BM in the test position of that session. During the warm-up period, two short sprints of five second duration with a load of 4.1% BM were administered at the three and four minute marks. A three minute recovery period followed the warm-up prior to the initiation of the test. The recovery period allowed the subject to continue cycling with zero load or stop and stretch. To begin the test, each subject cycled at 60 rpm against zero load until, after a five second countdown, the resistance was increased to 8.5% BM. Simultaneous with the increase in resistance, the subject began pedaling as hard and fast as possible, and continued for the next 30 seconds. After completion of the test, the subject was allowed to continue cycling against a light load for recovery.

Power output during the test was measured with the OptoSensor 2000™ (Sports Medicine Industries, Inc., St. Cloud, Minnesota). This system used an optical sensor to measure rotation of the ergometer flywheel in 22.5° intervals. Power was then calculated

at one second increments throughout the test based on drive-system properties, drive-system kinematics, and the applied load to the flywheel. Also during the test, subjects were videotaped by a camera positioned orthogonally to the plane of motion at a distance of approximately 4 m and operating at 30 Hz with a shutter speed of 0.001 second.

2.3.4 Data Analysis: From each test, peak-power (PP) and minimum-power output were calculated by averaging the largest and smallest powers computed during consecutive five second intervals, respectively. PP and minimum power were then used to calculate the fatigue index (FI). FI is the percentile difference of PP minus minimum power divided by PP. 30-second average-power (AP) output over the entire test was also calculated. Power-output results were computed by the OptoSensor 2000™ software for both a standard method and a corrected method. Standard-method power-output (P_S) results were computed using the velocity of the flywheel and the braking resistance:

$$P_S = T_{BF} \cdot \omega_F \qquad [2.1]$$

The corrected-method power (P_C) calculation used the velocity of the flywheel and braking resistance as well as the inertial contribution of both the flywheel and crank:

$$P_C = P_S + I_F \cdot \alpha_F \cdot \omega_F + I_C \cdot \alpha_C \cdot \omega_C \qquad [2.2]$$

In the calculations, T_{BF} is the belt friction torque, I_F is the flywheel moment of inertia, I_C is the crank moment of inertia, α is the angular acceleration of the flywheel (F) and crank (C), and ω is the angular velocity of the flywheel (F) and crank (C). I_F and I_C are constants equal to 0.396 kgm^2 and 0.08 kgm^2, respectively (Sports Medicine, 1998). Flywheel moments of inertia on Monark ergometers have been measured as high as 0.8 kgm^2 (G. Street, personal communication, December 1999). However, since

independent verification of flywheel inertial properties was impractical, the conservative estimate of flywheel inertia was utilized. By choosing the conservative value for the flywheel inertia, power output values might be slightly underestimated, however, trends between positions would not be compromised. All power calculations were normalized by dividing by the subject's BM to report relative-power outputs (W/kg BM).

The reflective markers were automatically digitized (Peak Motus System, Peak Performance Technologies, Inc., Englewood, Colorado) at 30 Hz for three successive pedal revolutions beginning at top-dead center (right crank arm pointing vertically upward). The three pedal revolutions that were digitized were those that crossed the 15 second point during the test. The two-dimensional coordinate data were then smoothed at 5 Hz using a recursive, low-pass Butterworth filter.

HPD, HOA, TA, and BCA, were all calculated along with maximum, average, and minimum hip, knee, ankle, and pedal angles (Figure 2.1). Hip angle was defined as the included angle between the mid-torso, hip, and knee markers. Knee angle was defined as the angle between hip, knee, and ankle markers with zero referenced at full extension and angle increasing with knee flexion. Ankle angle was defined as the included angle between the knee, ankle, and toe markers. Pedal angle was defined as the angle produced by the line connecting the toe marker with center of the pedal spindle relative to vertical. Maximum and minimum values are an average of the three maxima or minima from the digitized pedal cycles, while the remaining kinematic parameters are an average over the entire three pedal cycles.

The power output and kinematic data were tabulated for the five different recumbent positions (BCA from 100 through 140°) and the SCP for each group. Additionally, the

optimal recumbent PP output position for each subject (ORP) was selected from one of the five different recumbent positions. Average and standard deviations were calculated within groups and for all subjects combined. Between groups, the familiar and control groups were compared, position for position, using Student's t-test (two-tailed, two sample with equal variance).

The between groups analysis found no statistical differences in any of the 21 kinetic parameters, and only four differences ($p \leq 0.05$) in any of the 105 kinematic parameters (minimum hip angle in the 130° BCA position, minimum knee angle and HPD in the 120° BCA position, and HPD in the 130° BCA position). Since all trends were similar between groups and very little was significantly different, both groups were combined for comparisons across the positions. The five recumbent positions and SCP were compared using repeated measures ANOVA with post-hoc analysis using Tukey's HSD (due to the extreme differences in TA and pedal angle between the recumbent positions and the SCP, the SCP values were held out of the statistical procedures for these two parameters). Between the ORP and the SCP, Student's t-test (two-tailed with repeated measures) was used for comparison. All significance was evaluated at the $p \leq 0.05$ level.

2.4 Results

2.4.1 Controlled Parameters: HOA, TA, BCA, and maximum hip-to-pedal distance (HPD) were well controlled in the experiment (Table 2.2). The average HOA across all positions was $-15 \pm 0°$. The TA decreased approximately 10° with the backrest angle and was consistently 5 to 7° less than the backrest angle. Each TA was significantly different from one another. The BCA produced through the combined HOA

and TA were within 2° of the expected BCA. Each recumbent BCA was significantly different from each other. However, the average BCA in the SCP was not significantly different from either the 140 or 150° BCA. The BCA for the ORP was within 1° of the SCP. The HPD, expressed as a percentage of the subject's standing leg length, showed slightly greater variation than the other controlled parameters. Five out of the six positions averaged 104 or 105%. The seventh position (BCA = 110°) averaged 103%, which was significantly different from the 105% HPD.

Even though only four parameters were significantly different between the familiar and control groups, it is interesting to note that the HOA and BCA were consistently greater, and the TA and HPD were consistently lower, in the control group compared to the familiar group. The differences in TA, BCA, and HPD between the two groups were also noticeable in the SCP data.

2.4.2 Power Output: Requiring the subjects to begin the Wingate test pedaling at 60 rpm produced large flywheel accelerations during the first ten seconds with peak cadences recorded above 150 rpm. With these large flywheel accelerations, it was necessary to use power output values that were corrected for inertial effects, rather than the standard calculations (Table 2.3A). However, since the majority of the Wingate results reported in the literature use the standard method, uncorrected data is also included (Table 2.3B). Peak-power (PP) outputs were approximately 5% higher when using the corrected method. Similarly, the average-power (AP) outputs were approximately 1% greater, and fatigue index (FI) values were approximately 10% greater, compared to the standard method of power calculation.

The ORP was evenly distributed between the 130 and 140° BCA positions. The only exception to this was one member of the familiar group who produced peak power in the 120° BCA position.

PP and AP exhibited similar trends across the positions (Figure 2.2 & Table 2.3). Both PP and AP output were greatest in the 130 and 140° BCA positions, with power dropping off as the BCA decreased further. The power output of these two recumbent positions was similar to that produced in the SCP. For both PP and AP, the power output generated in the 130 and 140° BCA positions and SCP were significantly greater than those in the 110 and 100° BCA positions. Additionally, the AP in the 120° BCA position was significantly less than that of the 130° BCA position, but not the 140° BCA position and SCP. The FI values showed a small amount of decline as the BCA was reduced. However, only the FI in the 100° BCA position was significantly less than the 130 and 140° BCA positions and the SCP. The PP and AP produced in the ORP were greater than those in the SCP, but only the AP was significantly different between the two positions.

Statistical results were similar for both the corrected and standard power calculation methods. The only difference was in the FI results, where the 100° BCA position was also significantly less than the 110° BCA position using the standard method.

Similar to the controlled kinematic parameters, there were no significant differences in the kinetic data between the control and familiar groups. However, the AP of the control group was consistently less than that produced in the familiar group. This occurred for both the recumbent positions as well as the SCP.

2.4.3 Lower-Extremity Kinematics: Changes in power output with BCA were accompanied by changes in lower extremity kinematics (Table 2.4). The 10° increases in

BCA produced roughly 10° increases in hip angles (Figure 2.3). All recumbent hip angles were significantly different from each other, except for the maximum hip angles in the 120 and 110° BCA positions. The hip angles in the SCP were significantly greater than all the recumbent position hip angles, except for the 140° BCA position. The hip angles of the control group were generally greater, but only the minimum hip angle in the 130° BCA was significantly different, from those of the familiar group.

Changes in BCA did not solicit any consistent changes in knee angle. None of the knee angles in the recumbent positions were significantly different from each other. However, the knee angles in the SCP were significantly lower than the knee angles of all recumbent positions. The knee angles of the control group were generally greater, but only the minimum knee angle in the 120° BCA was significantly different from those of the familiar group.

Ankle angles exhibited a general increase of about 10° total as the BCA increased across the studied range. Ankle angles in the 130 and 140° BCA positions were significantly greater than those of the 100 and 110° BCA positions. Average and minimum ankle angles in the 120° BCA position were also significantly greater than those in the 100° BCA position. Ankle angles in the SCP were significantly greater than all those in the recumbent positions except for the 130 and 140° BCA positions. There were no generalizable differences between the ankle angles of the control and familiar groups.

There were no significant differences in the pedal angles of the recumbent positions. However, pedal angles in the recumbent positions were significantly greater than those in the SCP, as expected by the great difference in HOA between the recumbent and SCP.

Even though the BCA of the ORP was only 1° more than that of the SCP, six out of nine of the lower-extremity joint-angle values were significantly different (Table 2.4). The hip and ankle angles were lower in the ORP compared to the SCP, with the max hip angle and the average and minimum ankle angles significantly lower. All knee angles were significantly greater in the ORP compared to the SCP.

2.5 Discussion

2.5.1 Effect of Altering Body Configuration Angle (BCA): Changing the BCA through backrest angle while maintaining a constant HOA had similar effects on both the power output and kinematics for the familiar and control group cyclists. This similarity supports the combining of the data into one group. A small range was evident around the 130 to 140° BCA (ORP = 135° BCA) where PP may be maintained, but noticeable losses occur with BCA changes as small as 10° from this zone. The small zone of stable power output followed by a significant (11%) decrease in peak-power output with reduced BCA found in this study, is consistent with the findings by Yoshihuku and Herzog (1996). Yoshihuku and Herzog (1996) found PP output to be stable near the optimal hip angle with power dropping from 10 to 17% (depending on definition of muscle model) as the pelvis was rotated forward up to 30° from the optimal position. It is expected that the 40° change in BCA in this study was due to both changes in pelvic tilt and, to a small degree, spinal flexion. However, pelvic tilt could not be measured due to obstruction of view by the hip belt.

The optimal zone around the 130 to 140° BCA is consistent with the majority of the work where the effects of BCA on cycling performance were examined (Heil *et al.*, 1995;

Umberger *et al.*, 1998; Welbergen and Clijsen, 1990). However, several studies were not necessarily supportive of these findings. From the measurements taken by Price and Donne (1997) the BCA could not be determined, and Heil *et al.* (1997) found no consistent trends except that subjects were most efficient in BCA positions that matched their road bicycles.

Too (1991) reported an optimal BCA near 115°, outside the optimal zone found in this study. Other factors such as altering HOA, limited number of positions tested, and subject population may have contributed to the different results between this study and Too (1991). Too (1991) altered both BCA and HOA, while HOA was not altered here. Too (1994) found that HOA did effect power output when BCA was maintained. While the effect of HOA on power output was not the direct goal of this study, two distinct HOA were used between the recumbent positions and the SCP. The ORP, with BCA similar to the SCP but with different HOA, did not produce reduced power as would be suggested by Too (1994). However, Too (1994) utilized toe clips as the foot-to-pedal interface rather than clipless pedals. While toe clips help secure the foot to the pedals, they do not provide the security that the newer clipless pedals provide (Broker and Gregor, 1996). This may cause reduced power output, especially in the recumbent cycling positions with negative HOA, where the foot is not supported above the pedals by gravity.

Since all but one of the positions tested by Too (1991) incorporated a positive HOA, the foot-to-pedal interface probably would not account for the large difference in optimal BCA. An increased number of positions tested might have reduced the discrepancy as well, but the 140° BCA tested here is very similar to a position tested by Too (1991).

Too (1991) found this position to be slightly less powerful than the most powerful 115° BCA position. The most likely reason for the difference in optimal BCA is a small contribution from the above factors, coupled with the subject populations tested. Both studies used subjects classified as 'recreational' cyclists. However, the subjects here were recreational off-road cyclists while the subjects in Too (1991) were recreational road cyclists. The two types of cycling require slightly different BCA. The ORP BCA found here matched the preferred BCA of the subjects in the SCP. Too (1991) did not test the subjects in the SCP, but the BCA which was found to be optimal is very similar to that which has been measured on track cyclists (Cavanagh and Sanderson, 1986). The track cycling BCA is expected to be very similar to the crouched road cycling BCA utilized when sprinting. Given adequate training, the muscles acting at the hip may be able to alter their force-length properties enough to change the joint angles where peak power is achieved (Herzog *et al.*, 1991).

BCA alterations caused the greatest changes in hip angle with smaller changes in ankle angle and virtually no changes in knee angle. These findings are consistent with those of others (Heil *et al.*, 1995; Heil *et al.*, 1997; Price and Donne, 1997; Too, 1991; Umberger *et al.*, 1998). However, this is the first study to find significant differences in ankle angle with changes in HOA. This is most likely due to the relatively large number of subjects studied here, as well as the relatively large changes in HOA compared to the previous studies. Similar ankle angle trends have been noticed by others (Heil *et al.*, 1995; Heil *et al.*, 1997; Price and Donne, 1997).

It appears that the body attempts to maintain the knee motion at the expense of hip and ankle motion. While it would be impossible for the hip motion not to be altered and

a person still be able to cycle, there could be a more even distribution of change across the hip, knee, and ankle. This suggests that the uniarticular quadriceps muscle or short head of the biceps femoris acting across the knee joint may be the most critical muscles for power production in cycling, in terms of operating length and joint moments. The bi-articular muscles acting across the knee (rectus femoris, long head of biceps femoris and other hamstring muscles, and gastrocnemius) may be compensated by alterations of motion at the hip and ankle. This is plausible given that the knee joint muscle power is greater than that of both the hip and ankle, and that the knee joint muscle power is substantial in both extension and flexion (Broker and Gregor, 1996). Additionally, the ankle joint is more of a transfer joint than one for generating power, making the ankle angle less critical than the knee angle (Yoshihuku and Herzog, 1996).

Alternatively, changing the reaction forces and skeletal loading of the knee may affect power output. However, without more in depth analysis of the musculoskeletal biomechanics, including kinetics, little can be concluded regarding how the muscles are affected by the altered BCA, especially since pelvic rotation and familiarity may also play a role.

It also appears that there is a preferred pedal orientation for force application while cycling, which is maintained at the expense of the hip and ankle motion. Changing the pedal orientation may reduce the effective forces on the pedal, or cause detrimental joint reaction forces.

2.5.2 Recumbent Familiarity: Familiarity with recumbent cycling may have produced some noticeable, but not significantly different, changes in both power output and cycling kinematics. However, the degree to which the differences between groups

may be attributed to the recumbent familiarity is limited. Participants were not pre-tested eight weeks prior to being post tested, so general fitness level and cycling kinematics prior to any recumbent training could not be compared. Additionally, the control group was not required to add any further SCP cycling training to their regimen to account for the additional cycling of the familiar group. The additional cycling by the familiar group could account for the slightly increased AP compared to the control group, since AP was elevated even in the SCP. The lack of consistent differences in PP output between the groups is plausible given the similar BCA of the recumbent trainers and the limited amount of intense recumbent training by the familiar group. Even though the familiar group was aware that they would be tested with a sprint type test at the end of eight weeks of training, the majority of training was of relatively low intensity and could not be expected to improve PP dramatically.

While the differences in power output between the two groups could be explained by the additional cycling and possible group differences prior to participation, regardless of position, it is highly unlikely that the differences in kinematics could come solely from group differences prior to participation. Both groups had similar cycling histories, suggesting that fitness levels and cycling techniques should have been similar. Subjects of both groups were set-up at the beginning of each test session with a HPD of 105% of their standing greater trochanter to floor length. However, the control group was consistently below this at the midpoint of the Wingate test for all the recumbent positions, while the familiar group maintained the set HPD. The reduced HPD was most likely caused by posterior rotation of the pelvis as evidenced by the accompanied reduced TA and extended BCA of the control group relative to the familiar group in all positions. The

extended BCA was even evident in the SCP, showing that the familiar group probably had become accustomed to cycling with the slightly reduced BCA of the recumbent trainer.

Additionally, the reduced HPD produced slightly greater hip, knee, and pedal angles in virtually all positions in the control group relative to the familiar group. The slight reduction in HPD by the control group was not enough to expect significant changes in power output (Too, 1993). However, it might allow the hip musculature to operate effectively at a slightly reduced length, by increasing hip angle, which the control group may have been more accustomed to using in the SCP.

2.5.3 Recumbent Cycling Versus the Standard Cycling Position (SCP): As long as the BCA that is preferred by the subject in the SCP is maintained in the recumbent position, PP and AP are not reduced by cycling recumbently. However, this may not be the case in more extreme recumbent HOAs. In fact, PP and AP may increase slightly as shown in the ORP compared to the SCP. This slight improvement may be due to having a firm seat and backrest to push against while cycling recumbently.

The kinematics produced in the ORP were the most similar of the recumbent positions compared to the SCP. However, the differences were generally large enough to be significant. These differences may be a result of comparing the best of the 10°-incremented recumbent positions with that of the subject-selected SCP. There may also be some changes induced in the kinematics from the altered HOA, and an altered pull from gravity on the segments of the lower extremity. The altered pull on the segments may produce slightly different moments and reaction forces at the joints resulting in different preferred joint angles.

Additionally, the forces on the pedals may be altered, causing slightly different cycling kinematics. In the SCP the gravitational force is acting positively for cycling during the propulsive phase of the pedal cycle. However, while in the recumbent positions, with the hips behind the bottom bracket, gravity is acting positively after the propulsive phase is considered over. There is also an inertial contribution to the pedal force which may be altered by the different segment orientations. However, these gravitational and inertial effects do not seem to alter the BCA that was found to be optimal, or the ability to produce power in the positions tested. This is consistent with the findings in a steady-state, low-power output study by Brown *et al.* (1996) who found that lower extremity kinematics were altered by changes in HOA. However, it was suggested that these changes were not large enough to produce significant changes in muscle lengths and, therefore, power output.

2.6 Conclusions

From this investigation five main conclusions may be drawn. 1) Small changes on the order of 10° from the optimal BCA 'zone' may not reduce peak-power output significantly, but may reduce power output sufficiently to influence the top-speed while sprint cycling in a less than optimal BCA. 2) If large training effects occur when recumbent cycling compared to standard cycling, a longer time period, increased intensity, vastly different BCA, or a combination of these variables is needed to elicit these changes. 3) The optimal recumbent cycling BCA is most similar to the BCA chosen by the rider when tested in the SCP. The power output in the optimal recumbent cycling BCA is not reduced relative to the SCP, and may actually be enhanced by having

a firm seat to push against. 4) Power output and kinematics are altered similarly by altering the BCA through changes in TA while maintaining the same HOA, or changes in HOA while maintaining the same TA. Manipulating HOA will induce small changes in the lower-extremity kinematics. However, these effects on power output are insignificant. 5) While this research adds to our knowledge of recumbent cycling, more investigation is needed into the areas related to the influences of training on BCA and power output. An increased understanding of why one position may be optimal relative to another and how the rider attempts to compensate when placed in a less than optimal position for producing power would also be of great benefit.

2.7 Acknowledgments

Special thanks to Randy Wilber, Ph.D. of the USOC's Sport Science & Technology Division for his assistance with the experimental design as well as use of selected pieces of equipment. Also, thanks to all participants, without whom this project would not have been possible. This project was sponsored in part by the U.S. Department of Education Graduate Assistance in the Areas of National Need program (award #P200A70433).

2.8 References

Bar-Or, O. (1987). The Wingate anaerobic test: an update on methodology, reliability and validity. *Sports Medicine*, **4**, 381-394.

Broker, J.P. and Gregor, R.J. (1996). Cycling biomechanics. In *High-Tech Cycling* (Edited by Burke, E.R.). Human Kinetics Publishers: Champaign, pp. 145-166.

Brown, D.A., Kautz, S.A., and Dairaghi, C.A. (1996). Muscle activity patterns altered during pedaling at different body orientations. *J. Biomechanics*, **29**(10), 1349-1356.

Browning, R.C., Gregor, R.J., and Broker, J.P. (1992). Lower extremity kinetics in elite athletes in aerodynamic cycling positions. *Medicine & Science in Sports and Exercise*, **24**(5S), s186.

Cavanagh, P.R. and Sanderson, D.J. (1986). The biomechanics of cycling: studies of the pedaling mechanics of elite pursuit riders. In *Science of Cycling* (Edited by Burke, E.R.). Human Kinetics Publishers: Champaign, pp. 91-122.

Hagberg, J. and McCole, S. (1996). Energy expenditure during cycling. In *High-Tech Cycling* (Edited by Burke, E.R.). Human Kinetics Publishers: Champaign, pp. 167-184.

Herzog, W., Guimaraes, A.C., Anton, M.G., and Carter-Erdman, K.A. (1991). Moment-length relations of rectus femoris muscles of speed skaters/cyclists and runners. *Medicine & Science in Sports and Exercise*, **23**(11), 1289-1296.

Gross, A.C., Kyle, C.R., and Malewicki, D.J. (1983). The aerodynamics of human-powered land vehicles. *Scientific American*, **249**(6), 142-152.

Heil, D.P., Derrick, T.R., and Whittlesey, S. (1997). The relationship between preferred and optimal positioning during cycle ergometry. *Eur. J. Appl. Physiol.*, **75**, 160-165.

Heil, D.P., Wilcox, A.R., and Quinn, C.M. (1995). Cardiorespiratory responses to seat-tube angle variation during steady-state cycling. *Medicine & Science in Sports and Exercise*, **27**(5), 730-735.

Price, D. and Donne, B. (1997). Effect of variation in seat tube angle at different seat heights on submaximal cycling performance in man. *J. Sports Sciences*, **15**, 395-402.

Sports Medicine (1998). OptoSensor 2000™ User's Manual. Sports Medicine Industries, Inc. St. Cloud, Minnesota.

Too, D. (1994). The effect of trunk angle on power production in cycling. *Research Quarterly for Exercise and Sport*, **65**(4), 308-315.

Too, D. (1993). The effect of seat-to-pedal distance on anaerobic power and capacity in recumbent cycling. *Medicine & Science in Sports and Exercise*, **25**(5S), s68.

Too, D. (1991). The effect of hip position/configuration on anaerobic power and capacity in cycling. *Int. J. of Sport Biomechanics*, **7**, 359-370.

Umberger, B.R., Scheuchenzuber, H.J., and Manos, T.M. (1998). Differences in power output during cycling at different seat tube angles. *J. Human Movement Studies*, **35**, 21-36.

Welbergen, E. and Clijsen, L.P.V.M. (1990). The influence of body position on maximal performance in cycling. *Eur. J. Appl. Physiol.*, **61**, 138-142.

Yoshihuku, Y. and Herzog, W. (1996). Maximal muscle power output in cycling: a modelling approach. *J. Sports Sciences*, **14**, 139-157.

2.9 Appendix: Nomenclature

Ankle Angle (AA) – Included angle between knee joint, ankle joint, and toe markers*

Average Power (AP) – Average-power output during entire 30-second Wingate test

Backrest Angle (BA) – Angle of seat backrest relative to horizontal*

Body Configuration Angle (BCA) – Included angle between torso, hip, and bottom bracket* (unless specified as included angle between backrest and seat-tube angle)

Fatigue Index (FI) – Percentile difference between peak and minimum power divided by peak power

Hip Angle (HA) – Included angle between mid-torso, hip joint, and knee joint markers*

Hip Orientation Angle (HOA) – Angle produced by line connecting hip joint with center of bottom bracket relative to horizontal*

Hip-to-Pedal Distance (HPD) – linear distance between hip joint marker and center of pedal spindle at maximum separation of these two points during pedaling

Knee Angle (KA) – Angle between hip joint, knee joint, and ankle joint markers with zero referenced at full extension and angle increasing with knee flexion*

Optimal Recumbent Position (ORP) - Recumbent cycling position that produced greatest peak power for each subject

Pedal Angle (PA) – Angle produced by line connecting toe marker with center of pedal spindle relative to vertical*

Peak Power (PP) – Highest mean power in five consecutive seconds during Wingate test

Standard Cycling Position (SCP) - 75° hip orientation angle with forward lean of torso

Torso Angle (TA) – Angle produced by mid-torso, hip joint marker, and horizontal*

* Displayed graphically in Figure 2.1

2.10 Tables

Table 2.1: Anthropometrics

Group		Age (yrs)	BM (kg)	Height	Thigh	Shank	Foot	HPD
Familiar		26.5	73.6	176	41	44	15	97
	N=8	*(4.7)*	*(13.8)*	*(10)*	*(3)*	*(4)*	*(1)*	*(7)*
Control		27.1	77.9	179	44	46	17	102
	N=10	*(3.9)*	*(6.5)*	*(11)*	*(3)*	*(2)*	*(1)*	*(5)*
Whole		26.8	76.0	178	42	45	16	99
	N=18	*(4.2)*	*(10.3)*	*(10)*	*(3)*	*(3)*	*(1)*	*(6)*

Height, Thigh, Shank, Foot length, and HPD (max hip-to-pedal distance) in cm
() indicate standard deviation

Table 2.2: Controlled Kinematics

BCA	100	110	120	130	140	ORP	SCP
HOA	-15	-15	-15	-15	-15	-15*	75
	(1)	*(2)*	*(1)*	*(2)*	*(2)*	*(2)*	*(2)*
Torso Angle	63*	53*	45*	33*	25*	30*	120
	(9)	*(6)*	*(8)*	*(5)*	*(7)*	*(8)*	*(10)*
Backrest Angle	70	60	50	40	30	—	—
	—	—	—	—	—	—	—
BCA (measured)	102*	111*	119*	131*	140*	135	134
	(9)	*(7)*	*(8)*	*(6)*	*(8)*	*(9)*	*(11)*
HPD	104	103‡	104	104	105	105	105
	(3)	*(3)*	*(3)*	*(3)*	*(2)*	*(3)*	*(3)*

HPD reported as percent standing floor to greater trochanter length, angles reported in degrees
() indicate standard deviation
Note: Not all statistically different parameters marked in table, see text for complete description
*($p<0.05$) between ORP and SCP ‡ ($p<0.05$) with 105 HPD
*($p<0.05$) with all recumbent positions

Table 2.3A: Corrected Relative Power Output (W/kg BM)

BCA	100	110	120	130	140	ORP	SCP
Peak	11.3	11.8	12.4	12.7^{+}	12.7^{+}	12.9	12.8
	(0.9)	*(0.8)*	*(0.9)*	*(0.7)*	*(0.8)*	*(0.8)*	*(0.7)*
Average	9.0	9.2	9.5	9.7^{+}	9.6^{+}	9.8*	9.6
	(0.6)	*(0.6)*	*(0.6)*	*(0.5)*	*(0.6)*	*(0.5)*	*(0.6)*
Fatigue Index [%]	41‡	44	44	45	45	45	45
	(8)	*(7)*	*(6)*	*(6)*	*(7)*	*(6)*	*(6)*

Table 2.3B: Standard Relative Power Output (W/kg BM)

BCA	100	110	120	130	140	ORP	SCP
Peak	11.0	11.5	11.9	12.2^{+}	12.2^{+}	12.3	12.2
	(0.8)	*(0.7)*	*(0.7)*	*(0.6)*	*(0.7)*	*(0.6)*	*(0.7)*
Average	8.9	9.1	9.4	9.6^{+}	9.5^{+}	9.7*	9.5
	(0.6)	*(0.6)*	*(0.6)*	*(0.5)*	*(0.6)*	*(0.5)*	*(0.6)*
Fatigue Index [%]	38‡	41	40	41	41	41	41
	(8)	*(7)*	*(6)*	*(6)*	*(7)*	*(6)*	*(6)*

Note: Not all statistically different parameters marked in table, see text for complete description
() indicates standard deviation
*($p<0.05$) between ORP and SCP
$^{+}$($p<0.05$) with 100 and 110° BCA
‡ ($p<0.05$) with 45% FI in (A) and 41% FI in (B)

Table 2.4: Lower-Extremity Kinematics

BCA	100	110	120	130	140	ORP	SCP
Hip Angle							
Maximum	87+	94	99	110+	118+	113*	122
	(7)	*(7)*	*(7)*	*(4)*	*(8)*	*(9)*	*(9)*
Average	64+	72+	79+	91+	100+	95	100
	(7)	*(8)*	*(8)*	*(5)*	*(9)*	*(10)*	*(11)*
Minimum	41+	49+	58+	72+	81+	76+	80
	(8)	*(9)*	*(9)*	*(6)*	*(11)*	*(13)*	*(14)*
Knee Angle							
Maximum	114	116	117	115	114	114*	108
	(4)	*(5)*	*(5)*	*(4)*	*(6)*	*(6)*	*(4)*
Average	83	86	86	84	83	83*	74
	(4)	*(5)*	*(5)*	*(4)*	*(6)*	*(5)*	*(5)*
Minimum	48	50	51	48	48	47*	38
	(8)	*(8)*	*(8)*	*(7)*	*(7)*	*(7)*	*(8)*
Ankle Angle							
Maximum	124	123	127	130‡	132‡	132	135
	(9)	*(9)*	*(9)*	*(11)*	*(11)*	*(10)*	*(10)*
Average	107	109	112	116‡	117‡	117*	121
	(8)	*(6)*	*(7)*	*(9)*	*(7)*	*(8)*	*(7)*
Minimum	93	95	99	103‡	102‡	103*	107
	(7)	*(6)*	*(7)*	*(9)*	*(7)*	*(8)*	*(6)*
Pedal Angle							
Maximum	316	314	316	312	319	315*	64
	(22)	*(18)*	*(18)*	*(16)*	*(16)*	*(15)*	*(22)*
Average	281	281	287	283	289	284*	26
	(19)	*(18)*	*(13)*	*(13)*	*(14)*	*(12)*	*(18)*
Minimum	256	257	261	258	261	257*	-12
	(19)	*(17)*	*(16)*	*(14)*	*(16)*	*(12)*	*(19)*

Angles reported in degrees

() indicate standard deviation

Note: Not all statistically different parameters marked in table, see text for complete description

*($p<0.05$) between ORP and SCP ‡ ($p<0.05$) with 100 and 110° BCA

*($p<0.05$) with all recumbent positions

2.11 Figures

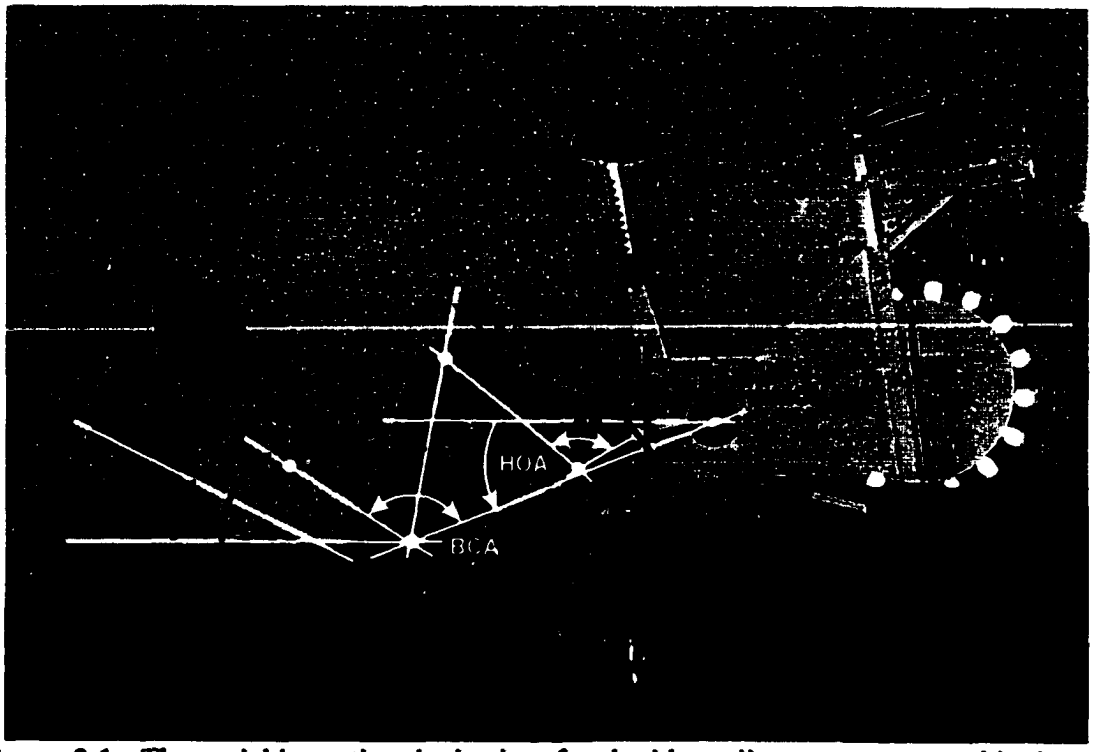

Figure 2.1: The variable seating device interfaced with cycling ergometer used in data collection with overlay of defined terms: ankle angle (AA), backrest angle (BA), body configuration angle (BCA), hip angle (HA), hip orientation angle (HOA), knee angle (KA), pedal angle (PA), and torso angle (TA).

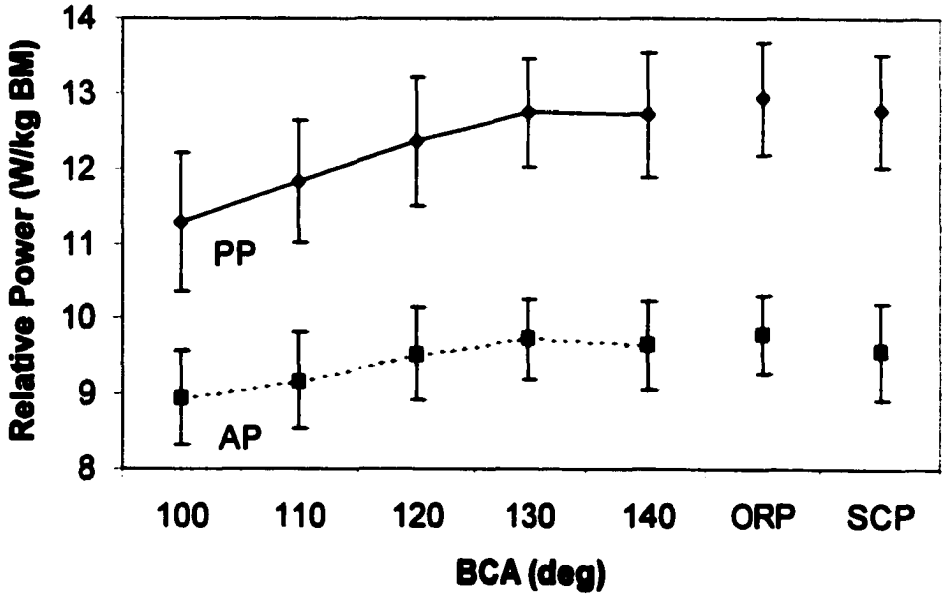

Figure 2.2: Whole group peak-power (PP) and average-power (AP) output relative to subject body mass.

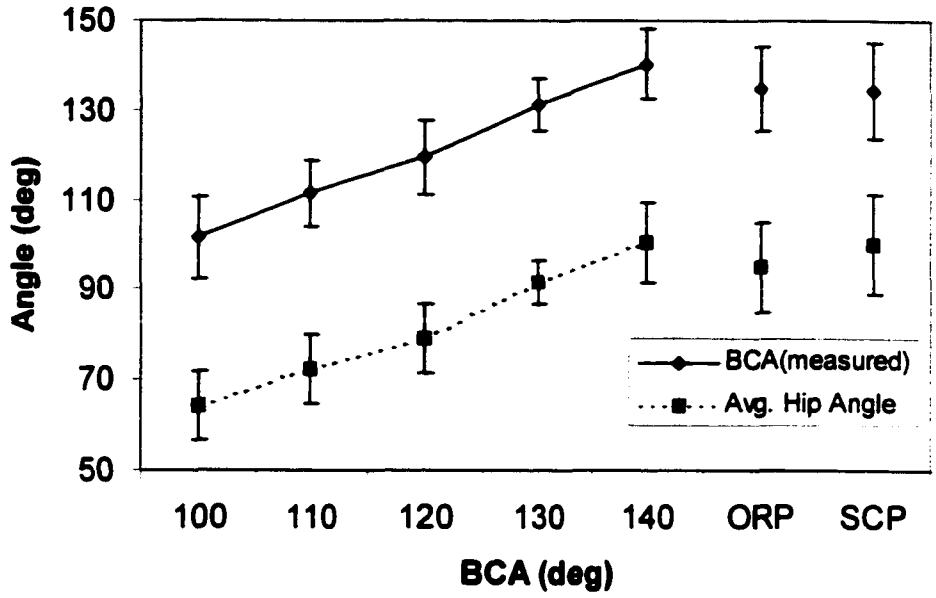

Figure 2.3: Average measured whole group body configuration angles (BCA) and hip angles.

Chapter 3

Anaerobic Cycling Power Output with Variations in Hip Orientation

3.1 Abstract

While the recumbent cycling position has become increasingly popular for both high-performance human-powered vehicles and sport/comfort cycles, questions still remain regarding the optimal riding position for maximal power output. The effect on anaerobic power output of altering the hip orientation angle (HOA, angle of hip joint to bottom bracket relative to horizontal) while maintaining a constant body configuration angle (BCA, included angle between torso, hip, and bottom bracket) was examined. In this way, changes in power output and cycling kinematics could be attributable to the altered pull of gravity on the segments of the lower extremity. Nineteen male recreational cyclists with no recent recumbent cycling experience completed 30-second Wingate tests in three recumbent positions (HOA of -20, -10, and 0°) and the standard cycling position, all with a 130° BCA. Peak power (12.8, 12.9, 12.8, and 13.0 W/kg body mass, respectively) and average power (9.9 W/kg body mass in all positions) were not significantly different across all positions ($p \leq 0.01$). Hip angles increased slightly, knee angles decreased slightly, and ankle angles did not change as HOA increased (hip angle referenced to decrease with flexion, knee angle to increase with flexion, and ankle angle to increase with plantar flexion). No differences were found in the lower-extremity

kinematics of the three recumbent cycling positions. However, significant differences did exist in the hip and knee angles between the recumbent and standard cycling positions. These findings suggest that while HOA does have a small effect on cycling kinematics, these effects are not large enough to alter short-term power output. Additionally, when BCA is matched, anaerobic power output while recumbent cycling is similar to that of the standard cycling position.

3.2 Introduction

The recumbent cycling position has become increasingly popular for both high-performance human-powered vehicles and sport/comfort cycles. Popularity for high-performance vehicles is mainly due to a recumbent's reduced aerodynamic drag compared to a fully-crouched, standard racing position (Gross *et al.* 1983). The reduced aerodynamic drag of a recumbent is also beneficial for sport/comfort riding since it reduces muscular fatigue by allowing a person to pedal with less effort over the same distance compared to the standard cycling position (SCP). Additionally, less fatigue is incurred in the neck, wrists, back, and crotch while riding recumbently compared to the SCP (Martin, 1984; Wilson *et al.*, 1984; Kita, 1997; Ice and Waite, In Preparation). Recumbents may also be safer than the SCP, since a lower center of mass creates a more stable vehicle, the head naturally faces forward keeping the oncoming road in the field of view, and in a crash situation the head is protected by not leading the body when thrown over the handlebars as in the SCP.

While a recumbent position may have many advantages compared to the standard position, questions still remain about power output in the recumbent position. Presently,

it is unclear what the optimal position of the hip joint relative to the crank, termed hip orientation angle (HOA), is for peak anaerobic power output (see Appendix and Figure 3.1 for more detailed definition of terms). Additionally, it is unclear how the recumbent positions compare to the SCP, in terms of both power output and cycling kinematics.

3.2.1 Review of Literature: Previously, Reiser *et al.* (Accepted – Dissertation Chapter 2) investigated the effects on anaerobic cycling power output of altering the body configuration angle (BCA) through changes in backrest angle (BA) while maintaining a constant HOA (-15°). In this way, power output variations were attributable to changes in the lower-extremity joint ranges of motion, primarily at the hip. BA was varied from 30 to 70° in 10° intervals, and the 30 and 40° BA positions proved to be most powerful, with power dropping off as the BA was elevated further. The BCA of these two low-angled backrest cycling positions was similar to the BCA selected by the subjects in the SCP (130°). Additionally, power output in these two recumbent positions was similar to the power output produced in the SCP.

While Reiser *et al.* (Accepted – Dissertation Chapter 2) demonstrated that BCA is a major determinant of power output and that the optimal recumbent BCA is similar to that in the SCP, their protocol did not examine the effects of altered HOA on power output beyond the single recumbent HOA and the standard cycling position HOA. It is believed that altering the HOA changes the relative phasing of propulsive leg extension relative to gravity pulling the leg down on the pedal. For example, in the SCP, leg extension occurs in phase with gravity acting on the leg segments to produce propulsive forces at the same time (Kautz and Hull, 1993). In contrast, a recumbent cycling position with a HOA near 0° would have leg extension approximately 90° out of phase with the propulsive forces

from gravity. The net propulsive effect from the gravitational forces on the cycling task will be zero, regardless of the HOA, due to the conservative nature of the system during a complete pedal cycle. However, the pull of gravity on the limbs in different orientations about the bottom bracket may cause the segmental angles of the lower extremity joints to vary. Alone, or in combination, the altered phasing of propulsive power components and lower extremity kinematics may cause changes in power output.

Brown *et al.* (1996) examined similar BCA with different HOA while subjects cycled steady-state at relatively low levels of power output (80 W while pedaling at 60 rpm). This work found that the altered phasing of gravity produced changes in muscle activation dynamics, joint moments, as well as lower-extremity kinematics. However, since the subjects cycled at low levels of power output, it could not be determined if these kinematic and kinetic changes were enough to produce significant differences in peak-power output. The two different HOA with similar BCA examined by Reiser *et al.* (Accepted – Dissertation Chapter 2) confirmed the slight changes of lower extremity kinematics, but found no significant changes in peak-power output between the two positions. However, with only two different HOA examined, no definite conclusions regarding the effects of altered HOA on power output could be made from the protocol.

In a separate investigation, Too (1994) isolated the effects on power output of gravity changes on the legs by altering HOA while cycling. The 105° BCA (defined as the angle between backrest and seat-tube angle), which was determined to be the most powerful in a previous study [where both BCA and HOA were manipulated simultaneously (Too, 1991)], was maintained while altering the HOA in 30° increments from -15 to 45°. Power output in the -15° HOA was found to be significantly less than the power output in

the 15 and 45° HOA positions. The power outputs in the 15 and 45° HOA positions, however, were not significantly different. This finding suggested that HOA may have an influence on the power output produced while cycling.

The conflicting results between Reiser *et al.* (Accepted – Dissertation Chapter 2) and Too (1994) suggest that further investigation is needed relating to the effects of different HOA on anaerobic-power output. Without additional knowledge of the effects of gravity, the optimal recumbent cycling position can not be determined.

3.2.2 Purpose: The objective of this investigation is to extend the literature in the area of anaerobic-power output while recumbent cycling by determining the effects on power output and cycling kinematics of altering the HOA while keeping the BCA constant. In this way, alterations in HOA will be the main effect in any power output differences. The sensitivity of the body to small changes in HOA (10° increments) will be determined with practical HOA for a streamlined aerodynamic vehicle. Additionally, in order to understand the differences between recumbent cycling and the SCP more clearly, a comparison to the standard cycling position will also be made.

3.3 Methods

3.3.1 Subjects: Nineteen male recreational cyclists participated in this study [age = 26.8 ± 4.6 yrs, (AVG ± STD) body mass = 75.7 ± 8.8 kg, height = 180 ± 8 cm, thigh = 43 ± 4 cm, shank = 45 ± 3 cm, foot = 17 ± 1 cm, and maximum hip-to-pedal distance (HPD) = 99 ± 6 cm]. All leg lengths were measured on the right side. The thigh length was measured from the greater trochanter to the knee center of rotation, the shank length from the knee center of rotation to the lateral malleolus, and the foot length from the lateral

malleolus to the head of the 5th metatarsal. The HPD while cycling was set at the beginning of each cycling session at 105% of the standing leg length from greater trochanter to the floor. Subjects had performed no significant recumbent cycling training within the three-month period prior to testing.

3.3.2 Equipment: To accommodate the changes in BA and HOA required of this study and maintain consistent HPD for different sized individuals, a four-degrees-of-freedom, variable-seating device was interfaced with a Monark 824E bicycle ergometer (Monark Exercise AB, Varberg, Sweden) (Figure 3.1). The ergometer was equipped with 175 mm crank arms and Shimano SPD® compatible clipless pedals. Constant foot position on the pedals was achieved by requiring the subjects to maintain the same cleat positioning on their shoes during the testing period.

3.3.3 Experimental Protocol: Five test sessions were required of each subject. The first session was used to obtain university-approved informed consent along with information on cycling experience and health status. Additionally, anthropometric measurements were made and a test administered in a random position to familiarize subjects with the apparatus and procedures (Wingate pilot testing showed a one-test learning curve with no further improvements after the second test). Each of the remaining four sessions tested a different cycling position. Three of the cycling positions tested were recumbent with -20, -10, and 0° HOA coupled with BA of 30, 40, and 50°, respectively, in order to maintain a 130° BCA. The fourth position was a SCP with 75° HOA and no backrest so that the subject could choose their own angle of torso lean (each subject was also allowed to adjust handlebar height and rotation).

The 130° BCA was chosen because it was found to be optimal in a similar set of subjects (Reiser *et al.*, Accepted – Dissertation Chapter 2). The -20 to 0° HOA combined with the 30 to 50° BA, respectively, was selected for its practicality in a streamlined recumbent vehicle. Rotating the rider HOA below -20°, while maintaining the 130° BCA, interfered with forward vision as well as dropped the heart level below the working musculature. Rotating the rider HOA above 0° produced a larger frontal area for the vehicle which would result in an increase in aerodynamic drag.

All subjects were tested in each cycling position with the testing sequence randomly determined. However, the position tested in the familiarization session was repeated in the fifth session. There was a minimum of 24 hours between test sessions with each subject testing at the same time of each day with a minimum of exercise during the hours of that day prior to testing. Once testing commenced, all sessions were completed within a 14 day period. Subjects were weighed prior to every session in order to ensure consistent body mass (BM). For each recumbent position, the subject was strapped to the seating device with both a hip and mid-torso belt. No belts were worn during the SCP testing. However, the subjects were required to remain seated during the entire SCP test.

To acquire lower-extremity kinematics while cycling, reflective markers were placed on each subject's right mid-torso (mid-rib cage, in line with hip/shoulder axis), hip (approximating the greater trochanter), knee (lateral femoral epicondyle), ankle (lateral malleolus), and toe (head of 5^{th} metatarsal). Markers were also placed on the ergometer at the crank- and pedal-spindle centers (Figure 3.1).

The 30-second Wingate test was chosen as the measure of maximal anaerobic power output with the administered test protocol similar to that utilized by the Sport Science &

Technology Division of the United States Olympic Committee (R.L. Wilber, personal communication, March 1998). The test protocol consisted of a five minute warm-up with self-selected cadence and resistive load of 2.0% BM in the test position of that session. During the warm-up period two short sprints of five second duration with a load of 4.1% BM were administered at the three and four minute marks. A three minute recovery period followed the warm-up prior to the initiation of the test. The recovery period allowed the subject to continue cycling with zero load or to stop and stretch. To begin the test, each subject cycled at 60 rpm against zero load until, after a five second countdown, the resistance was increased to 8.5% BM. Simultaneous with the increase in resistance, the subject began pedaling as hard and fast as possible, and continued for the next 30 seconds. After completion of the test, the subject was allowed to continue cycling against a light load for recovery.

Power output during the test was measured with the OptoSensor 2000™ (Sports Medicine Industries, Inc., St. Cloud, Minnesota). This system used an optical sensor to measure rotation of the ergometer flywheel. Power was then calculated at one second intervals throughout the test based on flywheel properties, flywheel kinematics, and the applied load to the flywheel. Also during the test, subjects were videotaped by a camera positioned orthogonally to the plane of motion at a distance of approximately 3 m and operating at 30 Hz with a shutter speed of 0.001 second.

3.3.4 Data Analysis: From each test, the five second intervals with the highest and lowest average power output were selected for the peak- (PP) and minimum-power outputs, respectively. The PP and minimum power were then used to calculate the fatigue index (FI). The 30-second average power (AP) over the entire test was also

calculated. Power output results were computed by the OptoSensor 2000™ software for both a standard method as well as a corrected method. Standard power-output (P_S) results were computed using the velocity of the flywheel and the braking resistance:

$$P_S = T_{BF} \cdot \omega_F \qquad [3.1]$$

where T_{BF} is the belt friction torque and ω_F is the angular velocity of the flywheel. A corrected-power (P_C) calculation used the velocity of the flywheel and braking resistance and the inertial contribution of both the flywheel and crank:

$$P_C = P_S + I_F \cdot \alpha_F \cdot \omega_F + I_C \cdot \alpha_C \cdot \omega_C \qquad [3.2]$$

where I is the moment of inertia of the flywheel (F) and crank (C), α is the angular acceleration of the flywheel (F) and crank (C), and ω_C is the angular velocity of the crank. I_F and I_C are constants equal to 0.396 kgm^2 and 0.08 kgm^2, respectively (Sports Medicine 1998). Flywheel moments of inertia on Monark ergometers have been measured as high as 0.8 kgm^2 (G. Street, personal communication, December 1999). However, since independent verification of flywheel inertial properties was impractical, the conservative estimate of flywheel inertia was utilized. By choosing the conservative value for the flywheel inertia, power output values might be slightly underestimated, however, trends between positions would not be compromised. All power calculations were normalized by dividing by the subject's BM to report relative power outputs (W/kg BM).

The reflective markers were automatically digitized (Peak Motus System, Peak Performance Technologies, Inc., Englewood, Colorado) at 30 Hz for three successive pedal revolutions beginning at top-dead center (right crank arm pointing vertically

upward). The three pedal revolutions that were digitized were those that crossed the 15 second point into the test. Two-dimensional coordinate data were then smoothed at 5 Hz using a recursive, low-pass Butterworth filter. Crank-arm length, HPD, HOA, torso angle (TA), BCA, maximum, average, and minimum hip (HA), knee (KA), ankle (AA), and pedal angles (PA) were all calculated from the coordinate data. Maximum and minimum value kinematic parameters are an average of the three maxima or minima from the digitized pedal cycles, while the remaining kinematic parameters are an average over the entire three pedal cycles. Crank-arm length was computed to verify digitizing accuracy, and BCA, HPD, HOA, and TA were computed to verify the experimental set-up.

The power output and kinematic data were tabulated for the three different recumbent positions (HOA from -20 through 0°) and the SCP. Average and standard deviations were calculated for each cycling position. The three recumbent positions and SCP were compared using repeated measures ANOVA with post-hoc analysis using Tukey's HSD (due to the extreme differences in TA and PA between the recumbent positions and the SCP, the SCP was held out of the statistical procedures for these two parameters). All significance was evaluated at the $p \leq 0.01$ level.

3.4 Results

3.4.1 Controlled Parameters: Average crank-arm length across all positions for each group was 175 ± 0 mm (Table 3.1). The HPD (percent of the subject's standing leg length) was constant across all positions with an average of 105 ± 0%. BCA was maintained by the simultaneous changes in HOA and BA within 3° of the experimentally

designed 130° for all positions, including SCP. None of the BCA were significantly different from each other.

3.4.2 Power Output: Requiring the subjects to begin the Wingate test pedaling at 60 rpm produced large flywheel accelerations during the first ten seconds with peak cadences recorded above 150 rpm. These large flywheel accelerations made it necessary to use the power output values corrected for inertial effects, rather than the standard calculations, for accurate assessment of power production (Table 3.2A). However, since the majority of the Wingate results reported in the literature use the standard method, these are also presented (Table 3.2B). PP outputs were approximately 5% higher when using the corrected method compared to the standard method. Similarly, the AP outputs were approximately 1% greater, and FI's approximately 10% greater compared to the standard method of power calculation. PP, AP, and FI did not vary significantly across the four positions.

3.4.3 Lower-Extremity Kinematics: The maximum, average, and minimum hip angles (HA) exhibited a slight increase as HOA increased from -20 through 0° with the HA in the SCP slightly greater than all the recumbent positions (Table 3.3). A slight inflection in the HA at the -10° HOA position was noticeable, consistent with the BCA. None of the recumbent HA were significantly different. However, the SCP HA were generally significantly different (six out of nine comparisons) from the recumbent positions. (All kinematic and kinetic parameters significantly different are noted in Table 3.3.)

The maximum, average, and minimum knee angles (KA) did not change significantly across the recumbent positions, but did tend to decrease slightly (increasing extension) as

the HOA increased (Table 3.3). The KA of the SCP was consistently less than those of the recumbent positions, and they were generally significantly different (five out of nine comparisons).

The maximum, average, and minimum ankle angles (AA) exhibited no consistent changes across both the recumbent and SCP (Table 3.3). A slight inflection in the AA of the -10° HOA position is noticeable in line with the BCA and HA. However, no statistical significance was found among any of the AA.

The maximum, average, and minimum pedal angles (PA) changed in accordance with the HOA (Table 3.3). Each PA was significantly different from the others.

3.5 Discussion

3.5.1 Effect of Altering Hip Orientation Angle (HOA): Small increases in HA accompanied by small decreases in KA were evident as HOA increased. These changes are consistent with the findings of Brown *et al.* (1996) and Reiser *et al.* (Accepted – Dissertation Chapter 2). Brown *et al.* (1996) and Reiser *et al.* (Accepted – Dissertation Chapter 2) also noticed changes in AA with HOA, while no differences in AA were found here. Since changes in AA with HOA were found to be small, and sometimes not consistent, in previous studies, it is possible that the small variations in AA from the slightly varying BCA could have masked the effects of HOA on AA. Too (1994) reported no changes in lower-extremity kinematics as the HOA was altered. However, Too (1994) made all kinematic measurements statically, which could account for the discrepancies when compared to dynamically measured kinematics.

A small inflection of the HA and AA is noticeable in the -10° HOA position. This inflection coincides with a similar inflection in the BCA data. Changes in the HA and AA in coordination with the BCA, with no apparent change in the KA, are consistent with the previous findings of Reiser *et al.* (Accepted – Dissertation Chapter 2). Reiser *et al.* (Accepted – Dissertation Chapter 2) found that changes in BCA elicit consistent changes in HA and AA, but not KA. The small variation in BCA found here is not expected to result in any significant changes in a person's power output. Reiser *et al.* (Accepted – Dissertation Chapter 2) found that changes of BCA on the order of 10° from optimal were needed to elicit changes in power output.

While lower-extremity kinematics were altered slightly by changes in HOA, these changes did not effect power output. This is consistent with the previous findings by Reiser *et al.* (Accepted – Dissertation Chapter 2) who found no difference between similar BCA of a -15° HOA recumbent position and a 75° HOA SCP. Additionally, Brown *et al.* (1996) concluded that kinematic variations from altered HOA were not large enough to significantly alter muscle force production. Too (1994), in contrast, found significant differences between similar BCA positions with positive and negative HOA. However, Too (1994) incorporated toe-clips, rather than clipless pedals, into the experimental design. Toe-clips do not provide the secure interface provided by clipless pedals (Broker and Gregor, 1996). The less-secure interface may be why power output in the low hip orientation position was less than that of the two other positions. With the foot effectively underneath the pedal in the -15° HOA, gravity tends to separate the foot from the pedal, and thus may cause reduced power output while cycling with toe-clips.

When the foot is above the pedals, as in the 15 and 45° HOA positions, gravity is always acting to keep the foot in contact with the pedal.

3.5.2 Recumbent Cycling Versus the Standard Cycling Position (SCP): Cycling in the recumbent position does not seem to reduce, or improve, anaerobic power output compared to the SCP. While Reiser *et al.* (Accepted – Dissertation Chapter 2) found that an 'optimal' recumbent position may be slightly (but not significantly) more powerful than the SCP, it was not verified here. The 'optimal' recumbent position was selected from the most powerful recumbent position of each subject. Their protocol found that two, possibly three, BCA positions tested had similar power output. Daily variations in power output could account for one position being slightly greater than another. Selecting this 'optimal' and comparing it against a position that was tested just once, like the SCP, could account for a slight increase in power output in the recumbent position compared to the SCP, when, in fact, having a backrest to push against may have no influence on power output.

3.6 Conclusions

HOA does have a small effect on lower-extremity kinematics when cycling with maximal effort. However, these effects are not large enough to produce significant changes in power output, at least in the practical range of positions tested for a streamlined human-powered vehicle. These results support previous findings that the recumbent cycling position is as effective for producing high levels of power output as the SCP. These results also indicate that proper selection of BCA is more important for power output than HOA. Additionally, more investigation is still needed concerning the

musculoskeletal kinematics and kinetics in order to understand why power output is or is not altered under these and previously examined experimental conditions. Furthermore, investigation is still needed into the effects of foot-to-pedal interface when the foot is effectively underneath the pedal while cycling.

3.7 Acknowledgments

Special thanks to the Shimano American Corp. (Irvine, California) for their support of this project and R. L. Wilber, Ph.D. of the U.S. Olympic Committee's Sport Science & Technology Division for assistance with developing the testing protocol. Also, thanks to all participants, without whom this project would not have been possible. Support for the first author was provided by the Graduate Assistance in Areas of National Need program in The U.S. Department of Education (award #P200A70433).

3.8 References

Broker, J.P. and Gregor, R.J. (1996). Cycling biomechanics. In *High-Tech Cycling* (Edited by Burke, E.R.). Human Kinetics: Champaign, pp. 145-166.

Brown, D.A., Kautz, S.A., and Dairaghi, C.A. (1996). Muscle activity patterns altered during pedaling at different body orientations. *J. Biomechanics*, **29**(10), 1349-1356.

Gross, A.C., Kyle, C.R., and Malewicki, D.J. (1983). The aerodynamics of human-powered land vehicles. *Scientific American*, **249**(6), 142-152.

Ice, R. and Waite, J. (In Preparation). Overuse injuries in cycling. To be submitted to: *Int. J. Sports Medicine.*

Kautz, S.A. and Hull, M.L. (1993). A theoretical basis for interpreting the force applied to the pedal in cycling. *J. Biomechanics*, **26**(2), 155-165.

Kita, J. (1997). The unseen danger (Special report: impotency and cycling), *Bicycling Magazine*, August, pp. 68-73.

Martin, G. (1984). Notes on human powered practicality. *Proceedings of the Second International Human Powered Vehicle Scientific Symposium.* Long Beach, CA: IHPVA, Box 2068, Seal Beach, CA, pp. 115-117.

Reiser, R.F., Peterson, M.L., and Broker, J.P. (Accepted – Dissertation Chapter 2). Anaerobic cycling power output with variations in recumbent body configuration. *J. Applied Biomechanics.*

Sports Medicine (1998). OptoSensor 2000™ User's Manual. Sports Medicine Industries, Inc.: St. Cloud, Minnesota.

Too, D. (1994). The effect of trunk angle on power production in cycling. *Research Quarterly for Exercise and Sport,* **65**(4), 308-315.

Too, D. (1991). The effect of hip position/configuration on anaerobic power and capacity in cycling. *Int. J. Sport Biomechanics,* **7**, 359-370.

Wilson, D.G., Forestall, R., and Hendon, D. (1984). Evolution of recumbent bicycles and the design of the Avatar Bluebell. *Proceedings of the Second International Human Powered Vehicle Scientific Symposium.* Long Beach, CA: IHPVA, Box 2068, Seal Beach, CA, pp. 92-103.

3.9 Appendix: Nomenclature

Ankle Angle (AA) – Included angle between knee joint, ankle joint, and toe markers*

Average Power (AP) – Average-power output during entire 30-second Wingate test

Backrest Angle (BA) – Angle of seat backrest relative to horizontal*

Body Configuration Angle (BCA) – Included angle between torso, hip, and bottom bracket* (unless specified as included angle between backrest and seat-tube angle)

Fatigue Index (FI) – Percentile difference of Wingate peak power minus minimum power divided by peak power

Hip Angle (HA) – Included angle between mid-torso, hip joint, and knee joint markers*

Hip Orientation Angle (HOA) – Angle produce by line connecting hip joint with center of bottom bracket relative to horizontal*

Hip-to-Pedal Distance (HPD) – linear distance between hip joint marker and center of pedal spindle at maximum separation of these two points during pedaling

Knee Angle (KA) – Angle between hip joint, knee joint, and ankle joint markers with zero referenced at full extension and angle increasing with knee flexion*

Pedal Angle (PA) – Angle produced by line connecting toe marker with center of pedal spindle relative to vertical*

Peak Power (PP) – Highest average power output during five consecutive seconds during a 30-second Wingate test

Standard Cycling Position (SCP) - 75° HOA with rider selected forward lean of torso

Torso Angle (TA) – Angle produced by line connecting mid-torso marker with hip joint marker relative to horizontal*

* Displayed graphically in Figure 3.1

3.10 Tables

Table 3.1: Controlled Parameters

HOA	-20	-10	0	SCP
Hip-to-Pedal [%]	105	105	105	105
	(2)	*(2)*	*(1)*	*(2)*
Torso Angle	30**	39**	47**	124
	(7)	*(5)*	*(5)*	*(9)*
HOA(measured)	-21**	-13**	0**	77
	(2)	*(1)*	*(1)*	*(2)*
BCA	129	128	133	133
	(7)	*(6)*	*(6)*	*(9)*

Angles reported in degrees

() indicate standard deviation

**($p<0.01$) with SCP and all other recumbent positions

Table 3.2A: Corrected Relative Power Output (W/kg BM)

HOA	-20	-10	0	SCP
Peak	12.8	12.9	12.8	13.0
	(0.9)	*(1.0)*	*(0.9)*	*(0.8)*
Average	9.9	9.9	9.9	9.9
	(0.8)	*(0.8)*	*(1.0)*	*(0.9)*
Fatigue Index	45	46	46	46
[%]	*(5)*	*(7)*	*(6)*	*(6)*

Table 3.2B: Standard Relative Power Output (W/kg BM)

HOA	-20	-10	0	SCP
Peak	12.3	12.3	12.3	12.4
	(0.8)	(0.8)	(0.8)	(0.7)
Average	9.7	9.8	9.7	9.8
	(0.7)	*(0.8)*	*(0.9)*	*(0.8)*
Fatigue Index	41	42	42	42
[%]	*(5)*	*(7)*	*(6)*	*(6)*

() indicate standard deviation

No values statistically different at $p<0.01$

Table 3.3: Lower-Extremity Kinematics

HOA	-20	-10	0	SCP
Hip Angle				
Maximum	108*	107*	112*	119
	(6)	*(5)*	*(6)*	*(8)*
Average	90*	89*	93	97
	(6)	*(5)*	*(6)*	*(9)*
Minimum	70	69*	73	76
	(8)	*(6)*	*(7)*	*(12)*
Knee Angle				
Maximum	112	112	111	108
	(4)	*(5)*	*(3)*	*(7)*
Average	82*	82*	81*	76
	(3)	*(4)*	*(4)*	*(7)*
Minimum	46*	47*	46*	41
	(5)	*(5)*	*(5)*	*(9)*
Ankle Angle				
Maximum	137	135	138	137
	(10)	*(11)*	*(11)*	*(10)*
Average	123	121	122	122
	(9)	*(8)*	*(8)*	*(7)*
Minimum	109	107	107	107
	(9)	*(10)*	*(7)*	*(6)*
Pedal Angle				
Maximum	314**	323**	339**	67
	(13)	*(12)*	*(10)*	*(12)*
Average	282**	292**	306**	34
	(14)	*(11)*	*(11)*	*(15)*
Minimum	255**	266**	279**	-6
	(18)	*(12)*	*(12)*	*(18)*

Angles reported in degrees
() indicate standard deviation
***(p<0.01) with SCP only**
****(p<0.01) with SCP and all other recumbent positions**

3.11 Figures

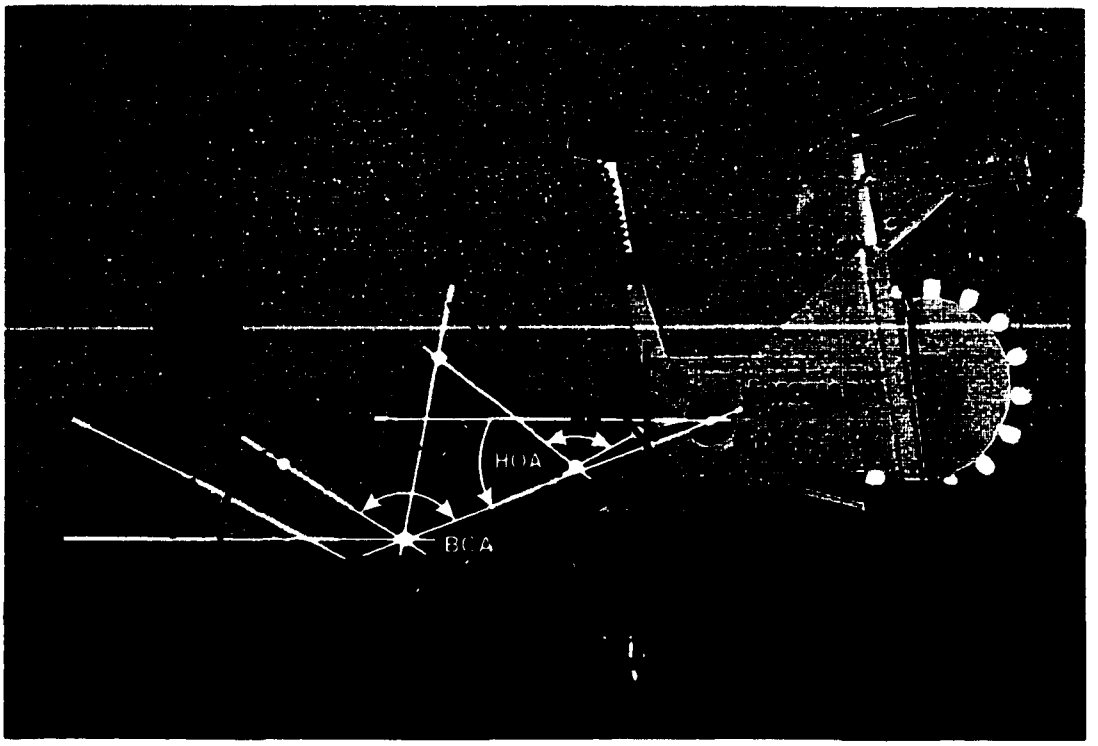

Figure 3.1: The variable seating device interfaced with cycling ergometer used in data collection with overlay of defined terms: ankle angle (AA), backrest angle (BA), body configuration angle (BCA), hip angle (HA), hip orientation angle (HOA), knee angle (KA), and pedal angle (PA).

Chapter 4

Instrumented Bicycle Pedals for Dynamic Measurement of Propulsive Cycling Loads

4.1 Abstract

A system was developed for measuring and analyzing the forces placed on a bicycle pedal during cycling operation of a stationary ergometer in a laboratory setting. The pedals measure forces in the plane parallel to the ergometer, independent of the lateral location of the applied force, in the directions normal and tangential to the surface of the pedals. These forces are not the only loads placed on the pedals. However, they are of greatest interest because they encompass the only plane where propulsive forces are generated. The instrumented pedals are designed to be structurally and functionally equivalent to a standard clipless pedal used in road or off-road bicycling. In order to instrument the pedal, the pedal spindle and bearing assembly of the original pedal was replaced. A new spindle was machined out of stainless steel and instrumented with eight foil strain gages, arranged into two complete Wheatstone bridges. The bearings were relocated from inside the pedal body to the crank-arm/pedal-spindle interface. This was necessary to keep the wires of the strain gages from wrapping up as the cyclist pedals. The original pedal body was then pinned to the newly machined spindle. In addition to sensing forces, the pedals were instrumented with optical encoders to measure the angle

of the pedal relative to the crank arm. An optical encoder was also mounted near the crank-arm spindle to measure crank-arm angle; allowing the pedal angle relative to the crank arm to be converted to a pedal angle relative to ground. Signals were transmitted from the pedals to an instrumented chassis via a cable tethered to the cyclist's leg and away from the ergometer. Inside the instrumented chassis, strain gage signals were conditioned and the digital optical encoder signals converted to analog signals. From the instrumented chassis the signals were routed to a laptop computer equipped with an analog-to-digital board and data analysis software. Data collected from this new system has proven to be both comparable to previously published literature and highly accurate when compared to expected power output values.

4.2 Introduction

Knowledge of loads applied to the pedals is important for a number of applications in bicycle design and the biomechanics of cycling. Pedal loads are the primary force input into the bicycle (Bolourchi and Hull, 1985) and thus are the most significant factor in the design of bicycle frames and components. Pedal loads are only one factor, since a number of other factors also impact the design of bicycle components and the frame. However, since the legs generate the propulsive force for a bicycle, any optimization of the bicycle for a particular rider is almost completely dependent on an accurate measurement of the forces and resulting power output from the rider.

4.2.1 Pedal Loads: Forces and moments on the pedals are best described in a right-hand reference system fixed to the center of the pedal spindle (Figure 4.1). Components of force may be directed tangential to the surface of the pedal (F_T), normal to surface of

the pedal (F_N), or along the long axis of the pedal spindle, laterally (F_L). Each of these axes may also have an associated moment (M_T, M_N, and M_L). The moment about the long axis of the pedal spindle (M_L) is generally assumed to be negligible, since pedals are designed to rotate freely about this axis. The only opposition to rotation about the long axis of the pedal is produced by bearing friction.

While all of these forces and moments are present to varying degrees, only the forces normal and tangential to the body of the pedal may provide propulsive energy (assuming the moment about the long axis of the pedal spindle is zero). The force component in the F_T - F_N plane directed normal to the long axis of the crank arm provides propulsive energy while the force component directed tangential to the long axis of the crank arm provides no propulsive energy (Figure 4.1). For these reasons, the normal component to the crank arm can be referred to as the effective force (F_E) while the tangential component is referred to as the ineffective force (F_I).

4.2.2 Cycling Analysis: In any analysis of rider efficiency, both the ineffective and effective forces play a role. One of the key tools for the optimization of a bicycle configuration is use of energy minimization techniques that can be applied to an inverse-dynamics model of the rider. Knowing the position versus time of all the links that make up the rider-bicycle system as well as the loads applied to the pedals, makes it possible to perform a minimization on the forces and moments which are applied to the system. Minimization requires that both the effective and ineffective forces be known prior to performing the analysis (Kautz and Hull, 1996). The inverse-dynamics model then can lead to an understanding of the effects of rider positioning and cadence on power output, fatigue, and injury (Broker and Gregor, 1996).

For example, in the case of knee loading, the effect of float of clipless pedals (rotation about the F_N axis) on the load on the knee joint has been debated. Through the use of an inverse-dynamics model, it is possible to determine the F_N axis moment on the knee of a cyclist both with and without pedal float (Wheeler *et al.*, 1995). Similar studies have been performed which considered the optimization of human movement through the use of inverse-dynamic models (Gregor *et al.*, 1991). As a result, obtaining the power output at the pedal, rather than any other location, is highly desirable, since it allows both effective and ineffective forces to be measured and supports biomechanical calculations.

However, further criteria limit the options available for obtaining data on the rider's power output and efficiency. In those cases where power output is of primary interest and no optimization will be performed using inverse dynamics, only the effective component of the output pedal force is required. Power output and aerobic efficiency of trained cyclists is highly dependent on maintaining a familiar position and feel for the rider on the bicycle (Heil *et al.*, 1997). This suggests that the optimization of position for elite riders should be performed on their own equipment, or nearly identical equipment; making several other options for obtaining this power output problematic. In this regard, for example, it is possible to fully instrument the frame of a bicycle to obtain information on symmetry and input power. However, this arrangement precludes the use of a rider using a familiar bicycle and requires that, at a minimum, multiple size frames be equipped with this capacity. The use of modified frames is advantageous because it eliminates the cabling problems that are present in force-pedal designs to get the signal from the rotating pedal spindle to the data acquisition system. However, the difficulties associated with constructing models based on frame loads have limited this approach.

Another alternative is to only measure the forces in the crank arms of the bicycle. The measurement of crank bending forces limits the measurements to the effective forces, and does not simplify the cabling to the pedals. This problem has been solved in one commercial power measurement system that uses instrumented crank arms (Schroberer Rad MeBtechnik, Weldorf, Germany). This approach is effective as a training tool, but is not suitable for the optimization calculations associated with the inverse-dynamics modeling. In addition, it is necessary to provide crank arms which are of the same length as those used in training. While it is less difficult to provide the acquired range of crank-arm lengths, than bicycle frames, this decreases measurement flexibility. Thus, the best approach to obtaining the information required for the optimization of the rider mechanics is construction of instrumented pedals which measure the applied forces to pedals in all axes.

4.2.3 Literature Review: In fact, instrumented pedals date back to the late 1800's (Sharp, 1993). These first pedals incorporated springs mounted to measure the force component orthogonal to the pedal surface, similar to a bathroom scale. More recently, Hoes *et al.* (1968) measured the loads orthogonal to the surface of the pedal with foil strain gages. Dal Monte *et al.* (1973) then added the tangential component of force to the measurement of reaction forces on the pedal. Hull and Davis (1981) were the first to design a set of pedals that measured all three forces and moments. This design was very bulky and complex, requiring 32 strain gages and extensive calibration equipment and procedures. Several iterations of this design were made (Newmiller *et al.* 1988; Wootten and Hull, 1992; Boyd *et al.*, 1996) as were different designs that incorporated

piezoelectric transducers (Ericson *et al.*, 1984; Broker and Gregor, 1990; Wheeler *et al.*, 1992).

One key design challenge for these pedals was to maintain the correct distance between the pedal spindle and platform. Additional height in this area can require significant fit adjustment on the bicycle to maintain proper body positioning.

4.2.4 Purpose: While all of these designs have provided useful information related to the loading of the bicycle pedal, they have all been limited to measurements inside a laboratory. Recently, however, a simplified design has been developed to measure the forces normal and tangential to the surface of the pedal when cycling outside the laboratory (Alvarez and Vinyolas, 1996; Rowe *et al.*, 1998). The design incorporates 8 strain gages mounted on the shaft of the pedal and two angular position sensors to measure pedal angle relative to the crank arm and crank-arm angle relative to ground. The acquired data are then stored on board for later analysis or telemetered to a nearby data acquisition system. This basic design has been incorporated into a new pedal-force measuring system for laboratory use which may be converted to an on-road measurement system in the future. The goal of this study is to present the new system and compare the results and performance with other recent designs.

4.3 Methods

The complete system consists of two modified clipless pedals and slightly modified crank arms, an optical encoder mounted near the crank arm spindle (bottom bracket) for measuring the angle of the crank arms relative to ground, an instrumentation chassis, and a laptop computer containing the analog-to-digital data acquisition and analysis hardware

and software (Figure 4.2). The modified clipless pedals and crank arms measure the forces normal and tangential to the surface of the pedal along with the angle of the pedal relative to the crank arm. The instrumentation chassis houses the power supply, strain gage signal-conditioning modules, and optical encoder signal conversion circuit boards. With knowledge of pedal angle relative to the crank arm and crank-arm angle relative to ground, the angular position of the pedal relative to ground may be determined.

4.3.1 Pedal Design: The pedals consist of a commonly used Shimano PD-6500 clipless pedal body (Shimano American Corporation, Irvine, California) that has the original bearing and spindle assembly removed. Clipless pedals have become popular in recent years for both road and off-road cyclists. Clipless pedals require the use of a cleat that is attached to the bottom of the cyclist's shoe. This cleat snaps into a spring loaded mechanism, securing the foot to the pedal. The cyclist is able to detach the cleat from the pedal by rotating the heel in or out (depending on the pedal design). This pedal design produces a lighter and more secure foot-to-pedal attachment than the previously preferred toe clips and cleats. The secure attachment of the clipless pedal design also allows the cyclist to produce propulsive forces on the pedal throughout the pedal stroke, which was difficult with the toe-clip design.

A new bearing and spindle design was required for the instrumentation. In order to minimize the bulk of the pedals and retain functional equivalence to the commercially available pedals, the pedal spindle was instrumented with strain gages rather than instrumenting a specially designed platform between the foot and pedal spindle. However, traditional pedal design has the pedal spindle screw into the crank arm. The bearing assembly is then located between the spindle and pedal body to allow for free

rotation of the pedal body about the F_L axis. Screwing the pedal spindle into the crank arm would cause the wires coming off of the instrumented spindle to wrap up as the crank arms rotated. To alleviate this problem, the bearing assembly was moved to the pedal spindle-crank arm interface (Figure 4.3). The pedal body is then fixed directly to the spindle.

To accommodate the new bearing design, the threaded hole for the traditional pedal spindle of an after-market alloy crank was enlarged. A needle bearing was then pressed into the enlarged hole (B-69, The Torrington Co., Torrington, Connecticut). Each side of the crank was faced off perpendicular to the axis of the through hole for seating of thrust bearings on each side of the crank arm (NTA-613, The Torrington Co., Torrington, Connecticut). Each thrust bearing was accompanied by two finely ground thrust washers on each side. The thrust washers on the crank arm side were slightly thinner than the washers on the outside of each thrust bearing (0.79 mm compared to 1.56 mm). A thicker outside washer was chosen since the complete face of the outside washer was not entirely covered by the fixing lock nut on the inside of the crank arm or the spindle flange on the outside of the crank arm.

This bearing assembly design isolates the needle bearings from the thrust forces and some of the bending moments produced by the offset pedal forces. This was required due to the size limitations placed on the needle bearing by the thickness and width of the crank arm. To minimize the amount of material removed from the crank arm, a needle bearing with outside diameter of 14.29 mm and width of 14.27 mm was selected. The diameter of the pedal spindle shaft through this bearing was 9.52 mm. This needle bearing has an ISO 281 basic dynamic load rating of 9,000 N, just over the maximum

expected load of 8,000 N when a 90 kg person stands with all their weight on one pedal (Rowe *et al.*, 1998). The large flange on the pedal spindle is expected to reduce the moment transferred to the needle bearings, increasing the factor of safety slightly. The thrust bearings have the same inner diameter as the needle bearing and outside diameter of 20.62 mm and thickness of 1.98 mm. This bearing has a basic dynamic load rating of 4,800 N, which is well above the maximal thrust forces expected by the sum of the laterally placed loads (approximately 100 N (Hull and Davis, 1981)) and transferred force from the moment by the flange. The thrust and axial load bearings are readily available and easily replaced if loads prove to be higher, wearing the bearings at a faster than anticipated rate.

The strain gage configuration requires a relatively long spindle section with the same cross-section. The diameter of the cross-section was restricted by the internal diameter of the pedal body and the space requirements of the strain gages and wiring. A practical diameter for this section was 9.52 mm, the same as the diameter of the section passing through the crank arm. With a maximum force applied near the outer edge of the pedal, approximately 60 mm from the outside of the flange, where the smallest factor of safety occurs, a stress of nearly 700 MPa could be expected on the surface of the shaft. This stress level exceeds the yield strength of untreated Cromoly (Sy = 550 MPa) which is traditionally used for pedal spindles. Normal pedal spindles are stepped down in diameter, being thickest near the crank arm and thinnest at the outermost end which could not be accommodated with the modified design. The pedal spindle was instead made from 17-4 PH stainless steel due to its higher yield strength (Sy = 1175 MPa) and high machinability. With this diameter and material properties, a maximum strain of

approximately 3,500 microstrain would be expected, well within the strain gage measurement accuracy while remaining below the maximum of 50,000 microstrain.

The pedal spindle shaft was then enlarged at the outermost edge to fit snuggly into the pedal body where the original bearing assembly was housed. A small hole was then drilled through the pedal body and spindle to attach the two together with a roll pin.

The strain gage configuration consists of eight miniature foil gages per pedal. The gages are laid out with four placed in 90° intervals around the shaft at the base of the flange near the crank arm and four placed similarly at the lateral edge of the spindle section just prior to the expanded section that inserts into the pedal body (Figure 4.3). The two gages in one row, 180° from each other, are wired with the two gages aligned similarly in the second row; making two complete Wheatstone bridges (Figure 4.4). Each bridge measures either the applied force component normal or tangential to the surface of the pedal.

4.3.2 Pedal Forces from Strain Gages: This strain gage configuration was chosen because the measured force in each bridge is decoupled from the orthogonal force component. The other forces and moments are also decoupled because the applied force measured is independent of the location of the force. Decoupling the normal force components reduces error and improves their ease of use. Measuring the force independent of its location is necessary since the point of force application varies from cyclist to cyclist as well as throughout the pedal revolution (Broker and Gregor, 1990).

The premise behind each bridge configuration being able to measure the force independent of the location lies in the fact that the applied force is proportional to the difference in the strains at each row of gages. To illustrate, the moment at the lateral row

of bridges (M_L) due to an applied force (F) which is a distance (x) away at the pedal-cleat location (Figure 4.3) is:

$$M_l = F \cdot x \qquad [4.1]$$

While the moment at the medial row of bridges (M_M) due to the same applied force (F) a slightly further distance (x plus L, where L is the distance between the two rows of gages) away is:

$$M_M = F \cdot (x + L) \qquad [4.2]$$

Solving Equation 4.1 for x and placing it in Equation 4.2 while solving for F yields the dependence of the applied force only on the difference between the two moments and the fixed distance between the two rows of gages:

$$F = \frac{M_M - M_L}{L} \qquad [4.3]$$

The moments at the medial and lateral gage locations are directly related to the surface strains (M_M and M_L, respectively) measured by the gages:

$$M_M = \frac{\varepsilon_M \cdot I \cdot E}{c} \qquad [4.4]$$

$$M_L = \frac{\varepsilon_L \cdot I \cdot E}{c} \qquad [4.5]$$

I, E, and c are the moment of inertia, Young's Modulus, and maximum distance from the neutral surface, respectively. I and c will remain the same at both rows of gages as long as the cross-section of the shaft is identical. Substituting Equation 4.4 and Equation 4.5 into Equation 4.3 provides the required applied force relation based on strain while independent of the location of the applied force:

$$F = \frac{I \cdot E}{c} \cdot \frac{\varepsilon_M - \varepsilon_L}{L} \qquad [4.6]$$

If each Wheatstone bridge is wired appropriately (Figure 4.4), the force measurement independent of its location is maintained. In the illustrated configuration, the excitation output voltage (e_N) for the normal force entering the strain gage conditioning module is:

$$e_N = \frac{K \cdot V}{4} \cdot (\varepsilon_1 - \varepsilon_2 - \varepsilon_3 + \varepsilon_4) \qquad [4.7]$$

where K, V, and M_i are the gage factor, bridge excitation voltage, and the unitary excitation strain from gages 1 through 4, where:

$$\varepsilon_1 = -\varepsilon_3 = F \cdot \frac{(x+L) \cdot c}{I \cdot E} \qquad [4.8]$$

$$\varepsilon_2 = -\varepsilon_4 = F \cdot \frac{x \cdot c}{I \cdot E} \qquad [4.9]$$

Substituting Equation 4.8 and Equation 4.9 into Equation 4.7 and solving for F finds the applied force directly proportional to the excitation output voltage from the bridge:

$$F_N = e_N \cdot \frac{2 \cdot I \cdot E}{K \cdot V \cdot c \cdot L} \qquad [4.10]$$

The applied force in the tangential direction (F_T) may be found similarly using gages 5 through 8:

$$F_T = e_T \cdot \frac{2 \cdot I \cdot E}{K \cdot V \cdot c \cdot L} \qquad [4.11]$$

The excitation output from each bridge is wired to a sensor module (160MK, CALEX Manufacturing Corporation, Inc., Concord, California) which allows for manual setting of gain, offset, and filtering. The gain was set to provide a 5 V (maximum allowable input voltage of analog-to-digital data acquisition board) output at maximum load. The offset was set to zero, and the filter set to its lowest cutoff frequency, 10 kHz.

4.3.3 Pedal Calibration: While the force measurements from each bridge are theoretically decoupled from each other as well as from the lateral force and all moments, slight misalignments during gage application may introduce possible cross-sensitivities to the other loads (Alvarez and Vinyolas, 1996; Rowe *et al.*, 1998). The cross-sensitivity of the normal force circuit to a tangentially applied load and the tangential force circuit to a normally applied load may be measured and accounted for in a simple calibration procedure.

To measure the sensitivity of the normal force circuit to a tangentially applied load, the pedal was progressively loaded and unloaded with a tangentially applied load while both the normal and tangential output voltages were measured. To accomplish this without introducing any additional forces or moments on the pedal, a special calibration cage was constructed (Figure 4.5). The calibration cage clipped into the pedal with the standard cleat so that the loading would be in a manner identical to that produced by a cyclist. Weights could then be incrementally added and subtracted to the cage for calibration. Both the cleated block and weight hanger of the calibration cage could be adjusted to balance the cage and keep the load on the pedal in the desired direction. The cleated block could be rotated 90° so that the calibration procedure could be repeated to measure the sensitivity of the tangential force circuit to normally applied loads.

The loading and unloading response of both circuits was highly linear with the response of the loaded circuit a magnitude of 10 times greater than the unloaded circuit (Figure 4.6). For the calibration procedure, the slope of the least squares linear regression line through zero was needed for both channels in each loading condition: the slope of the normal force channel output with a tangentially applied load (S_{NT}) and with a

normally applied load (S_{NN}), and the slope of the tangential force channel with a tangentially applied load (S_{TT}) and with a normally applied load (S_{TN}). These values are the coefficients for the sensitivity matrix in the calibration system of equations:

$$\begin{bmatrix} V_T \\ V_N \end{bmatrix} = \begin{bmatrix} S_{NT} & S_{NN} \\ S_{TT} & S_{TN} \end{bmatrix} \cdot \begin{bmatrix} F_T \\ F_N \end{bmatrix} \qquad [4.12]$$

V_T and V_N are the tangential and normal output voltages, respectively, and F_T and F_N are the tangential and normal applied forces, respectively. This system of equations was then solved for the applied forces, given the measured bridge output voltages and sensitivity coefficients:

$$\begin{bmatrix} F_T \\ F_N \end{bmatrix} = \begin{bmatrix} S_{NT} & S_{NN} \\ S_{TT} & S_{TN} \end{bmatrix}^{-1} \cdot \begin{bmatrix} V_T \\ V_N \end{bmatrix} \qquad [4.13]$$

Additionally, the slight misalignments of the gages make the bridges sensitive to laterally directed loads, moments about each axis, and the location of the load. However, Rowe *et al.* (1998) found that the sensitivities of the circuits to these loads introduced an error of less than 2% at full scale and Alvarez and Vinyolas (1996) found that the location of the load (within the surface of the pedal) introduced a similar error of less than 2% at full scale.

The natural frequency of the pedal could also introduce error if similar to that of a person using the pedal. Rowe *et al.* (1998) and Alvarez and Vinyolas (1996) measured their similarly designed pedals to have natural frequencies of approximately 200 Hz, while the natural frequency of the system with a 75 kg person clipped into the pedals and standing with half of their weight supported was 137 Hz (Rowe *et al.*, 1998). While the non-calibratable cross-sensitivities and the natural frequency of the present instrumented pedal were not directly measured, they were not expected to vary significantly from those

previously measured on similarly designed pedals. Additionally, if the non-calibratable cross-sensitivities and natural frequency of the present instrumented pedal were significantly different from the previous designs, they would have been noticeable in the data.

4.3.4 Pedal Angle Measurements: The excitation voltage and ground supplied to each bridge on the pedal spindle is also used to power the optical encoder measuring the angle between the pedal body and crank arm (Figure 4.4). The optical encoder is housed in an aluminum box located between the pedal body and crank arm (Figure 4.7). The aluminum box also serves to gather and protect the wires from the strain gages as well as hold the nine pin D-sub connector that plugs into the cable leading to the instrumentation chassis.

The shaft of the optical encoder is offset from the pedal spindle. Angle measurements are made through a 1:1 ratio gear system with one gear on the encoder and one attached to the outside of the crank arm, centered about the pedal spindle around the lateral thrust bearing assembly (Figure 4.7). In this configuration, one full turn of the pedal relative to the crank arm generates one complete revolution of the optical encoder. The optical encoder produces 512 pulses per revolution in two channels (A and B), so that direction of pedal turn may be measured (S1 Series Encoder, US Digital Corporation, Vancouver, Washington). Additionally, the optical encoder produces a fixed location zero pulse (Z) once every revolution. This pulse easily resets the count to zero in the same location each revolution; maintaining pedal calibration from one pedal usage to the next.

All nine pins of the D-sub connector on the pedal are necessary: one each for the supply voltage and ground, two each for each of the Wheatstone bridge excitation voltage outputs, and three for the optical encoder outputs. As discussed previously, the Wheatstone bridge outputs are wired directly to bridge sensors. The three optical encoder outputs are wired directly to custom circuit boards that convert the digital pulses to a single analog output that varies from 0 V at the Z pulse to 2.1 V just prior to resetting with a new Z pulse at the completion of one revolution (Figure 4.8). With the digital to analog conversion, the encoders mimic linear, continuous–turn potentiometers. However, optical encoders are advantageous to potentiometers because they do not have a 'dead' spot at the turnover point. The 'dead' spot of a potentiometer may be as little as 5°. However, the angle measure must be interpolated during this spot, introducing error to the system. Optical encoders do not have a 'dead' spot and, therefore, require no interpolation of position at any point during the rotation of the pedal.

A single analog channel is also preferable to three digital channels for several reasons. By converting to an analog signal, all channels could be easily measured by a single analog-to-digital board in the laptop computer. The analog output has also proven to be easier to trouble shoot because of the reduction in the number of wires which must be monitored to ensure that the system is functional during testing of subjects.

The aluminum box containing the optical encoder is cantilevered off the inside of the pedal body. The encoder box is held securely to the pedal body with three allen-head set screws that are recessed into the body. The box is machined so that there is some slight adjustability in the location of the optical encoder inside the box as well as in the location of the box on the pedal body. This allows for the appropriate mesh between the two

gears measuring the angle between the pedal and crank arm. The top of the box is below the level of the cleat on the cyclist's shoe so that there are no interference problems between the foot and pedal during cycling.

4.3.5 Complete Pedal and Crank-Arm Assembly: This design produces a pedal that is structurally and functionally equivalent to an uninstrumented clipless pedal. The instrumented pedal and modified crank arm are only 0.134 kg (21%) heavier than the same unmodified pedal and crank arm assembly. The pedal is also only 0.35 cm (7%) wider, from crank arm to cleat location, than the original pedal. The shaft was made slightly wider than the original shaft in order to keep the optical encoder close to the pedal spindle. This was necessary to keep the mass of the aluminum box down as well as the gear sizes. Additionally, minimizing the profile of the aluminum box is necessary to protect it in case of bicycle fall over in the event of a crash when the pedal system is installed on a bicycle rather than the present stationary bicycle ergometer.

4.3.6 Crank-Arm Angle Measurement: To measure crank-arm angle relative to ground, an identical optical encoder was mounted near the crank-arm spindle (Figure 4.9). A two-gear system with 1:1 ratio was utilized similar to that on the pedal. However, since the encoder shaft and crank-arm spindle separation was greater than that between the encoder shaft and pedal spindle, larger gears were necessary. The encoder was mounted on a piece of right-angle aluminum which was bolted to the frame of the ergometer. Adjustability was built into the mount so that appropriate gear mesh could be achieved. Similar to the pedal encoders, the three digital outputs were converted to a single analog channel in the instrumentation chassis.

4.3.7: Instrumentation Chassis: In addition to the strain-gage bridge conditioning modules and the digital-to-analog converter boards for the optical encoders, the instrumentation chassis houses the power supply for the entire system. Power is required for the strain gages, optical encoders, bridge conditioning modules, digital-to-analog converter boards, and two small fans mounted inside the chassis to prevent heat build-up. The four analog force channels and three angle channels are also bundled for output to the data acquisition system.

4.3.8 Data Acquisition System: The data acquisition system is set up in two stages. The first stage collects the seven channels of raw time series data and the second stage processes individual pedal revolutions extracted from the raw data. Raw data are collected through a PCMCIA analog-to-digital card (PCM-DAS08, ComputerBoards, Inc., Middleboro, Massachusetts) at 450 Hz with Labview® (National Instruments Corp., Austin, Texas). Prior to the collection of dynamic pedal data, zero offsets for each channel may be collected, manually input, or accepted from previous values. These offset values are then subtracted from the data prior to any processing of the data.

Continuous force-channel data are filtered with a fourth-order recursive, low-pass Butterworth filter at 12 Hz and then converted to forces with the calibration coefficients previously determined. Angular-channel data are similarly filtered after the raw saw-tooth waveforms that vary from 0 to 360° are cropped to a single revolution, otherwise, filtering the discontinuous angle signals would corrupt the data. The processed force channel data and raw angle channel data are then stored in a file for later processing of individual pedal revolutions.

4.3.9 Data Processing: To analyze an individual pedal revolution in stage two, the user selects the start and endpoint of the desired pedal revolution by viewing the graphically displayed crank-arm angle data. The data segment of each channel is then cropped out with the angle channels padded at each end with continuous data, and filtered. The pedal-angle data are then converted from the crank-arm reference system to a ground-based system with use of the crank-arm angle data.

Using the angular data and forces normal and perpendicular to the surface of the pedal, several additional computations are performed. The magnitude of force, direction of force, force components in a ground based reference frame with axes horizontal and vertical, effective and ineffective forces, and crank-arm angular velocity are all calculated. The crank-arm angular velocity is used in conjunction with the effective force and crank-arm length to calculate instantaneous power output. The Labview® program displays all these data sets graphically as well as several simple computations, including total average power output, and the percent of total power from the left and right pedal. For ease of analysis, data are displayed relative to crank-arm angle rather than time. The data sets are interpolated so that one data point exists for every degree of pedal revolution. The data are also stored in a file for further analysis if desired.

4.4 Results

4.4.1 Verifying Accuracy: The accuracy of the measured data was confirmed in two ways. First, cyclic trends and magnitudes of each parameter were compared against previous pedal data under similar conditions (Broker, 1991: See Dissertation Chapter 5 for comparable data in standard cycling position). Second, average power output from

both pedals and cadence was compared against the power output level and cadence set on the stationary ergometer. In one measurement, 19 subjects cycled with the ergometer set for a power output of 250 W (125 W expected per pedal). The average right pedal power measured across all subjects was 125 ± 14 W. Both methods showed the data from the pedals to be highly accurate.

4.4.2 Exemplar Data: The pedal angle varies roughly through a 50° sinusoid while cycling (Figure 4.10A). The pedal angle is calculated relative to ground with 0° when the surface of the pedal faces forward with the nose down. The angle increases as the nose elevates with 90° when the surface of the pedal is horizontal. Cycling data are most easily interpreted when they are presented relative to crank-arm angle which is defined as 0° when the right crank arm is pointing vertically up. The crank-arm angle increases through 359°, before resetting to 0° at the completion of a revolution. Rather than presenting forces relative to the surface of the pedal which are hard to comprehend and analyze, the pedal forces are displayed relative to a ground based reference frame (Figure 4.10B). When cycling recumbently the forces in the horizontal direction (Fx, positive force pushing the pedal forward) far exceed those in the vertical direction (Fy, positive force pulling the pedal up). Another valuable display of the forces is presentation in terms of the force normal to the crank arm, or effective force (F_E), and the force tangential to the crank arm, or ineffective force (F_I) (Figure 4.10C). Generally, the magnitude of F_E is slightly greater than F_I. However this subject cycled with a technique that produced effective and ineffective forces with equal magnitude. The effective force is combined with the crank arm angular velocity and length to calculate instantaneous

power output (Figure 4.10D). Since angular velocity does not vary greatly during the pedal cycle, the power output trend mimics that of the effective force.

4.5 Discussion

This new instrumented pedal system meets the previously discussed design criterion. The measurements are highly accurate. The design provides structural and functional equivalence to an uninstrumented bicycle and pedal. The system may be installed on a variety of bicycles with very little modification. The system is simple to use, and produces data in a form that is convenient for analysis.

4.5.1 Comparison with Uninstrumented Pedal: The only differences between the instrumented pedal system and an unmodified system is the slight increase in mass, slight increase in pedal width, and a cable coming off of the pedal that must be tethered to the leg and then back to the instrumentation chassis. The slight increase in mass was unavoidable due to the sensors. However, this extra mass is minimal. The slight increase in width of the pedal was also unavoidable and was not commented on by any of the cyclists who were tested using the system. The slight increase in stance width required by the cyclist from the new pedals produces an increase in the hip abduction angle of less than 1°, and the influence on other joints of the lower extremity are even less. The cable tethered to the leg also has no influence on pedal dynamics. The cable is tethered loosely so that movement is not restricted and blood flow not compromised.

4.5.2 Possible Additional Modifications: In order to install the pedal-force measuring system on another stationary bicycle only the mounting bracket for the optical encoder measuring crank-arm angle needs to be modified. This is a relatively minor

modification that could include strapping the bracket to the frame rather than bolting. The crank arms and pedals may be moved from one bicycle to another with no modification.

Presently only one set of crank arms have been machined to accommodate the instrumented pedals. However, the modifications to the crank arms are minor and easily reproduced, if a longer or shorter crank-arm length were needed. All components may be moved from one crank-arm assembly to the next, except for the pressed in radial needle bearing, which must be purchased at very little additional expense.

In order to convert the system from stationary laboratory use to in-the-field use, a new instrumentation chassis with on board data collection and storage or telemetry would be necessary. These types of systems have been previously developed by others (Alvarez and Vinyolas, 1996; Rowe *et al.*, 1998). However, to simplify the data collection these previous systems used potentiometers rather than optical encoders for measuring angular positions. A slightly different on-board device would be needed to accommodate the analog and digital channels of the present design.

4.5.3 Comparison with other Instrumented Pedals: Besides the different type of sensor used for angular measurement, the new pedal design has several other differences to both the designs by Rowe *et al.* (1998) and Alvarez and Vinyolas (1996). The new design is based on a single-sided Shimano clipless road pedal with the aluminum box housing the encoder cantilevered off the pedal body while Rowe *et al.* (1998) based their design around a double-sided Shimano 737 clipless off-road pedal with the aluminum box attached directly to the pedal shaft. Rowe *et al.* (1998) also threaded the end of the spindle to secure the pedal body, rather than pinning the two together. Additionally,

Rowe *et al.* (1998) used a single combination bearing, rather than three independent bearings. The combination bearing contained a radial needle bearing assembly and single row of ball bearings in one housing. This bearing combination is adequate for the radial loads, however, it is limited in its ability to react to thrust loads in both medial and lateral directions.

The differences between the new pedal design and that by Alvarez and Vinyolas (1996) are more pronounced. Their pedal design is based on a Time clipless road pedal (Time Sport USA, Hayward, California) which utilizes a slightly different cleat configuration from the Shimano pedals. Their design does not incorporate an aluminum box between the pedal body and crank arm. Instead, the potentiometer is located on the lateral edge of the pedal body with a shaft running down the center of the pedal spindle that attaches to a plate on the inside of the crank arm. The internal plate also prevents medial movement of the pedal spindle. A single press-fit (double row) ball bearing is located at the crank-arm/pedal-spindle interface. As with the Rowe *et al.* (1998) design, thrust forces are not taken up well by this bearing assembly. The strain gage and potentiometer measurements are taken off of the pedal at the lateral edge of the pedal with the cable directed outward. This potentiometer and cable location makes them highly susceptible to damage in the event of a bicycle fall-over or crash. The crank-arm angle measurement assembly is also slightly different, using two identical diameter pulleys and a timing belt rather than directly meshed gears to rotate the potentiometer with crank-arm rotation.

4.6 Conclusions

A successful pedal-force measurement system for laboratory use was developed. This system measures the forces normal and tangential to the surface of a commonly used clipless pedal. The modifications to the original pedal design necessitated to measure both force and angular position resulted in no structural or functional differences compared to the original pedal. The instrumented pedal measures the normal and tangential forces with high accuracy and very little cross-sensitivity to out of plane forces and moments. The cross-sensitivity of the normal force measurement to a tangentially applied load and vice versa are accountable and factored out. The newly developed pedal design is similar in many respects to previously presented instrumented pedals. However, this new design improves on the angular measurement capabilities and bearing designs of these previous systems. The pedals were designed with field applications in mind. A minor modification to the crank-arm angle sensor bracket and new on-board data collection or telemetry system is necessary for field use.

4.7 Acknowledgements

Special thanks to the Shimano American Corporation for providing the PD-6500 pedals used in this project and The U.S. Department of Education's Graduate Assistance in Areas of National Need program (award #P200A70433) for their partial sponsorship of the project.

4.8 References

Alvarez, G. and Vinyolas, J. (1996). A new bicycle pedal design for on-road measurements of cycling forces. *J. Applied Biomechanics*, **12**, 130-142.

Boyd, T., Hull, M.L., and Wootten, D. (1996). An improved accuracy six-load component pedal dynamometer for cycling. *J. Biomechanics*, **29**(8), 1105-1110.

Broker, J.P. (1991). Mechanical energy management during constrained human movement. *Unpublished Doctoral Dissertation.* University of California, Los Angeles.

Broker, J.P. and Gregor, R.J. (1990). A dual piezoelectric element force pedal for kinetic analysis of cycling. *Int. J. Sport Biomechanics*, **6**, 394-403.

Broker, J.P. and Gregor, R.J. (1996). Cycling biomechanics. In *High-Tech Cycling* (Edited by Burke, E.R.). Human Kinetics: Champaign, pp. 145-165.

Bolourchi, F. and Hull, M.L. (1985). Measurement of rider-induced loads during simulated bicycling. *Int. J. Sport Biomechanics*, **1**, 308-329.

Dal Monte, A., Manoni, A., and Fucci, S. (1973). Biomechanical study of competitive cycling. In *Biomechanics III* (Edited by Cerquiglini, S., Venerando, A., and Wartenweiler, J.). Karger: Basel, pp. 434-439.

Ericson, M.O., Nisell, R., and Ekholm, J. (1984). Varus and valgus loads on the knee joint during ergometer cycling. *Scand. J. Sports Sci.*, **6**, 39-45.

Gregor, R.J., Broker, J.P., and Ryan, M.M. (1991). The biomechanics of cycling. In *Exercise and Sport Sciences Reviews* (Edited by Holloszy, J.O.). Williams & Wilkens: Baltimore, Vol. 19, pp. 127-169.

Heil, D.P., Derrick, T.R., and Whittlesey, S. (1997). The relationship between preferred and optimal positioning during submaximal cycle ergometry. *Eur. J. Appl. Physiol.*, **75**, 160-165.

Hoes, J.J., Binkhorst, R.A., Smeekes-Kuyl, A.E., and Vissers, A.C. (1968). Measurement of forces exerted on pedal and crank during work on a bicycle ergometer at different loads. *Int. Zeitschrift fur Ang. Physiol.*, **26**, 33-42.

Hull, M.L. and Davis, R.R. (1981). Measurement of pedal loading in bicycling: I. Instrumentation. *J. Biomechanics*, **14**(12), 843-856.

Kautz, S.A. and Hull, M.L. (1996). Cycling biomechanics. In *High-Tech Cycling* (Edited by Burke, E.R.). Human Kinetics: Champaign, pp. 117-143.

Newmiller, J., Hull, M.L., and Zajac, F.E. (1988). A mechanically decoupled two force component bicycle pedal dynamometer. *J. Biomechanics*, **21**(5), 375-386.

Rowe, T., Hull, M.L., and Wang, E.L. (1998). A pedal dynamometer for off-road bicycling. *J. Biomechanical Engineering*, **120**, 160-164.

Sharp, A. (1993). *Bicycles and Tricycles*. Longmans Green and Co.: London, 1896. Fifth reprinting, M.I.T. Press: Cambridge, pp. 268-270.

Wheeler, J.B., Gregor, R.J., and Broker, J.P. (1992). A dual piezoelectric bicycle pedal with multiple shoe/pedal interface compatibility. *Int. J. Sport Biomechanics*, **8**, 251-258.

Wheeler, J.B., Gregor, R.J., and Broker, J.P. (1995). The effect of clipless float design on shoe/pedal interface kinetics and overuse injuries during cycling. *J. Applied Biomechanics*, **11**, 119-141.

Wootten, D. and Hull, M.L. (1992). Design and evaluation of a multi-degree-of-freedom foot/pedal interface for cycling. *Int. J. Sport Biomechanics*, **8**, 152-164.

4.9 Figures

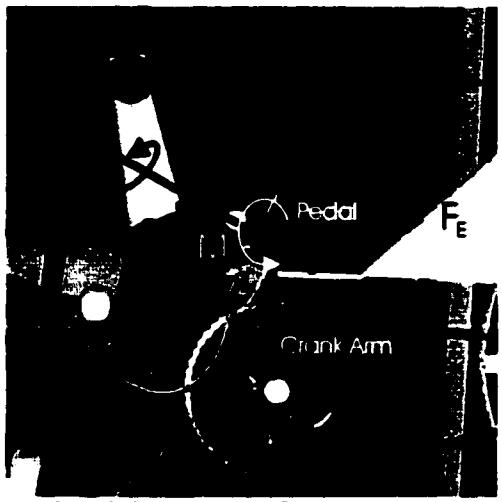

Figure 4.1: The instrumented pedals measure forces on the pedal spindle directed normal (F_N) and tangential (F_T) to the surface of the pedal. In addition to these two loads, forces may also exist on the pedal in the lateral direction (F_L, positive out of page), and moments may exist about each axes (M_T, M_N, and M_L). However, the only propulsive loads exist in the $F_T - F_N$ plane, with M_L assumed to be zero. In this plane, the force component directed normal to the crank arm may be effective in producing propulsion (F_E) while the force component directed tangential to the long axis of the crank arm is ineffective in producing propulsion (F_I). Note: subject is cycling in a recumbent position.

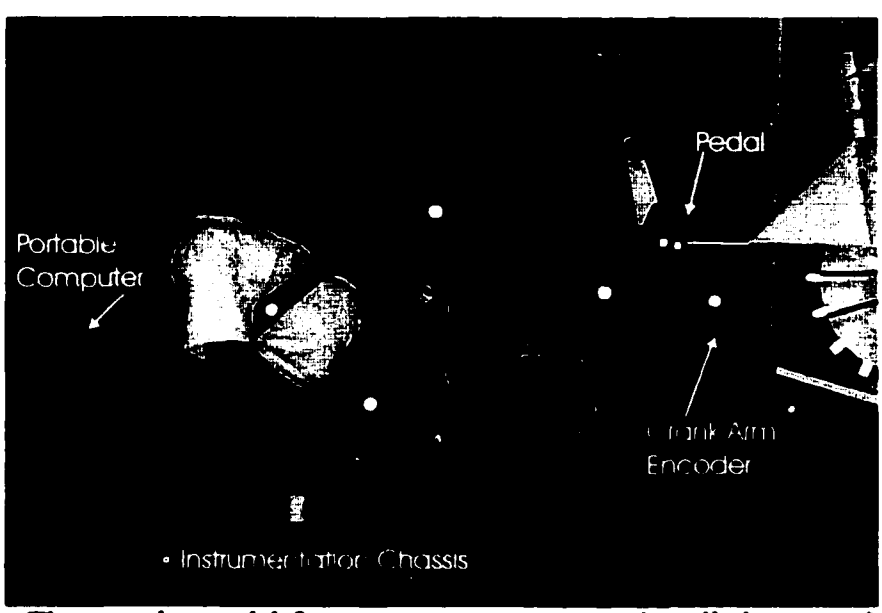

Figure 4.2: The complete pedal-force measurement system installed on a stationary ergometer that may be used to collect cycling data in a recumbent or standard cycling position: pedals, crank-arm angle encoder, instrumentation chassis, and data acquisition computer. Note: subject is outfitted with reflective markers and all other reflective items, including the pedals, have been masked with black tape to collect easily digitizible sagittal-plane videography to accompany the force pedal measurements.

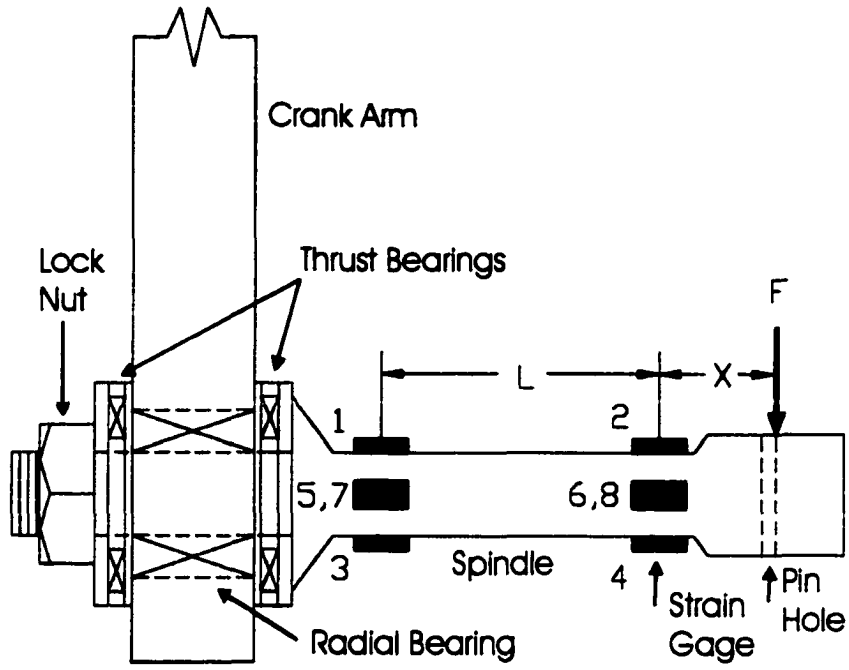

Figure 4.3: Pedal spindle and lower portion of crank arm with other components removed. A new bearing assembly was incorporated that includes two flat thrust bearings on each side of the crank arm and one radial bearing pressed into the crank arm, indicated by regions with an 'X' through them. Strain gages were placed (with measurement grids in line with the long axis of the spindle) in two rows separated by the distance, L, on a section with similar cross-section. The gages in each row were 90° apart. Forces (F) are placed on the pedal body located a short distance (X) lateral to the second row of strain gages.

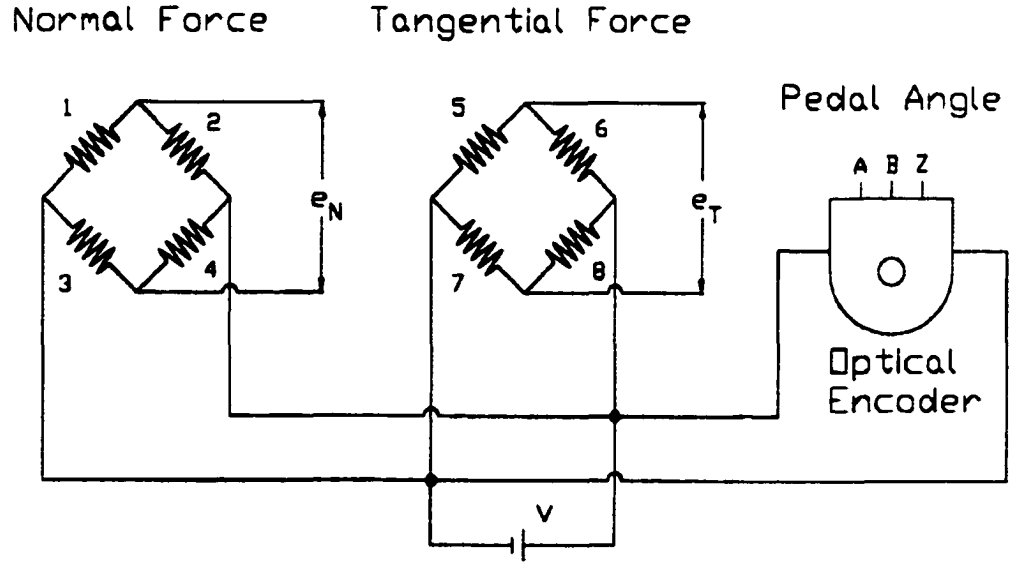

Figure 4.4: Each pedal is wired similarly with a common 5 V excitation (V). The strain gages, which are labeled to correspond with their location in Figure 4.3, are configured into two complete Wheatstone bridges to measure the normal (e_N) and tangential (e_T) forces. In addition to the forces, pedal angle relative to the crank arm is measured with an optical encoder which has three digital outputs (A, B, and Z).

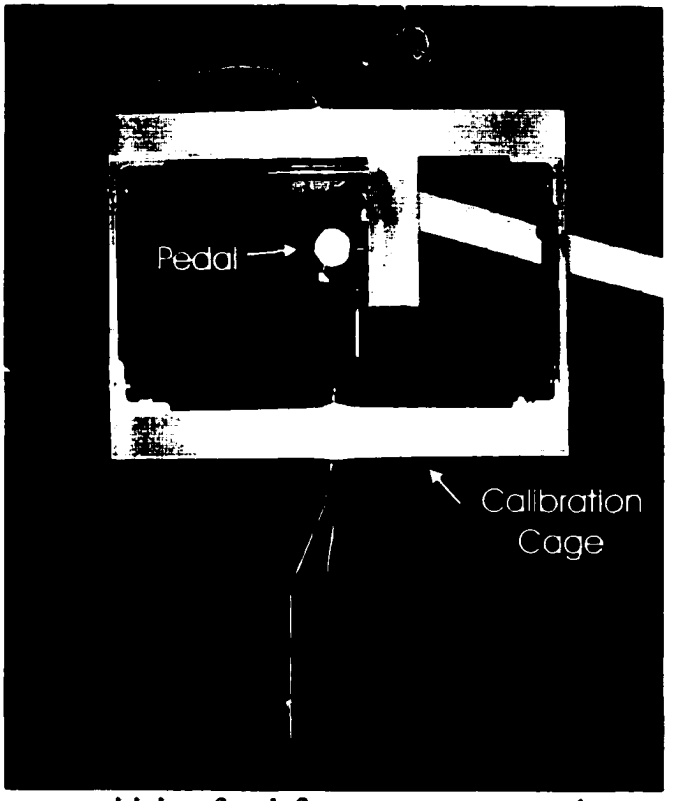

Figure 4.5: The cross-sensitivity of each force component may be accounted for by calibrating the pedals. Pedals are calibrated by loading and unloading the pedal purely in the tangential direction (pictured) and in the normal direction while both force channel output voltages are measured. Note: as in the previous views, the pedal is blackened and the pedal spindle location marked with reflective tape, ready for simultaneous videography.

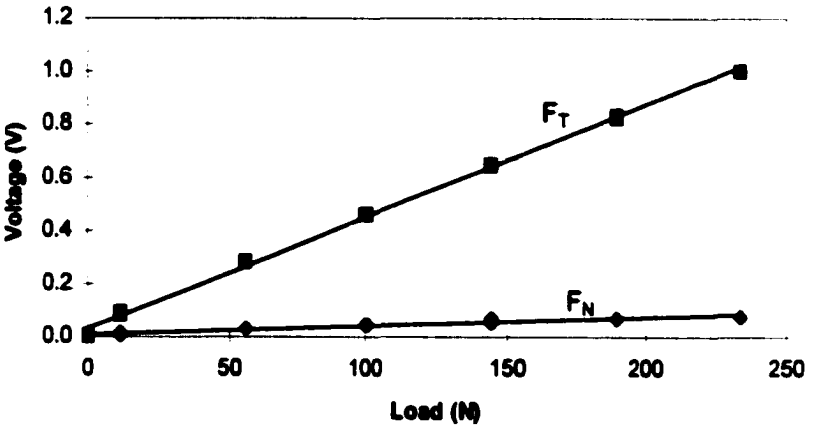

Figure 4.6: Similar for both calibration loading conditions, the loaded channel (F_T in this case) responds with approximately 10 times the output of the unloaded channel (F_N).

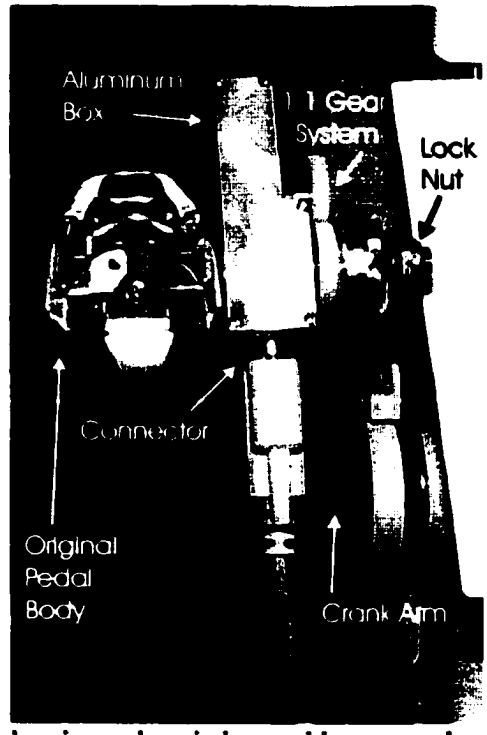

Figure 4.7: A machined aluminum box is located between the pedal body and crank arm (left pedal viewed from above and slightly behind). The aluminum box contains the optical encoder in the forward narrow section while the posterior portion allows for shaft pass-through, strain gage wiring, and cable connection.

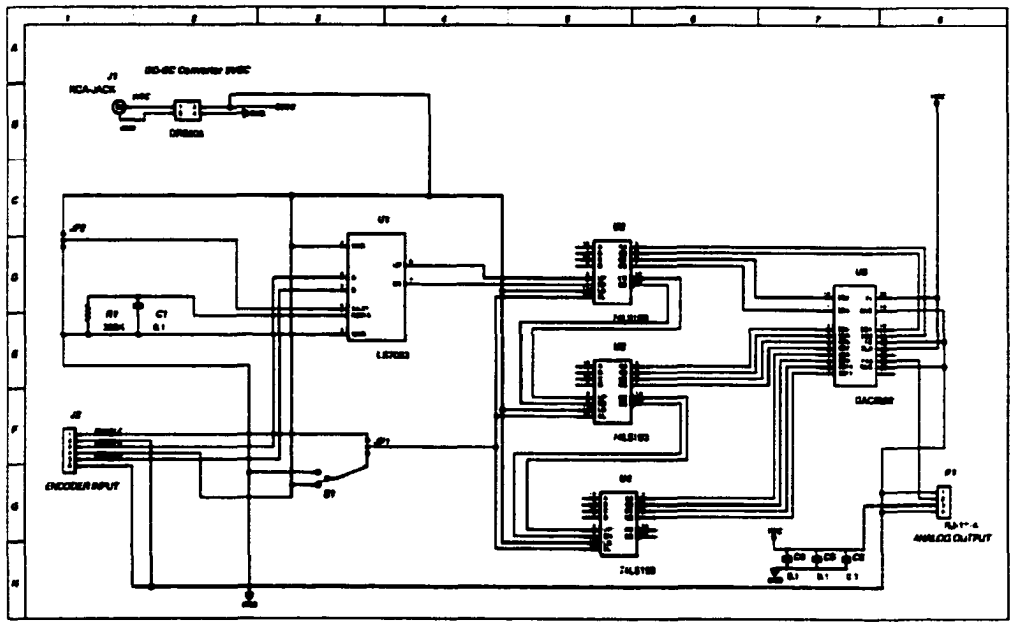

Figure 4.8: Digital to analog conversion circuit utilized with optical encoders. The heart of the circuit is a 12 bit cascading counter (three 74LS193 chips) that supplies the digital to analog converter (DAC8562). From the DAC852 a single analog output, linear to the angular position of the optical encoder, is sent to a terminal connector.

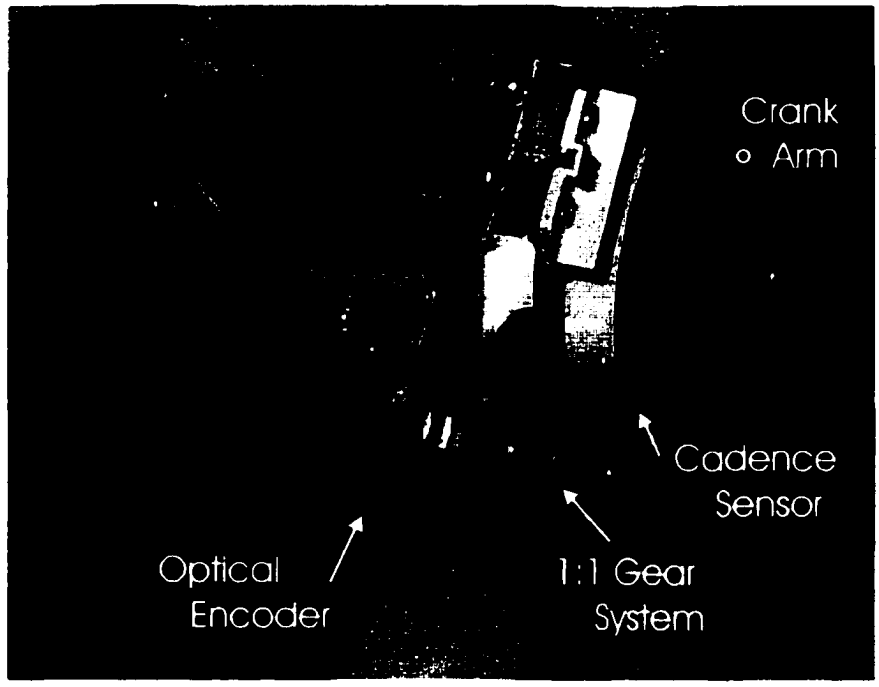

Figure 4.9: A third optical encoder is used to measure the crank-arm angle relative to ground. This is accomplished with a 1:1 ratio gear assembly with the gear offset from the crank-arm spindle on the encoder. The encoder is mounted securely to the frame of the ergometer. Note: also visible is the cadence sensor of the ergometer, located just lateral to the gear mounted on the crank-arm spindle.

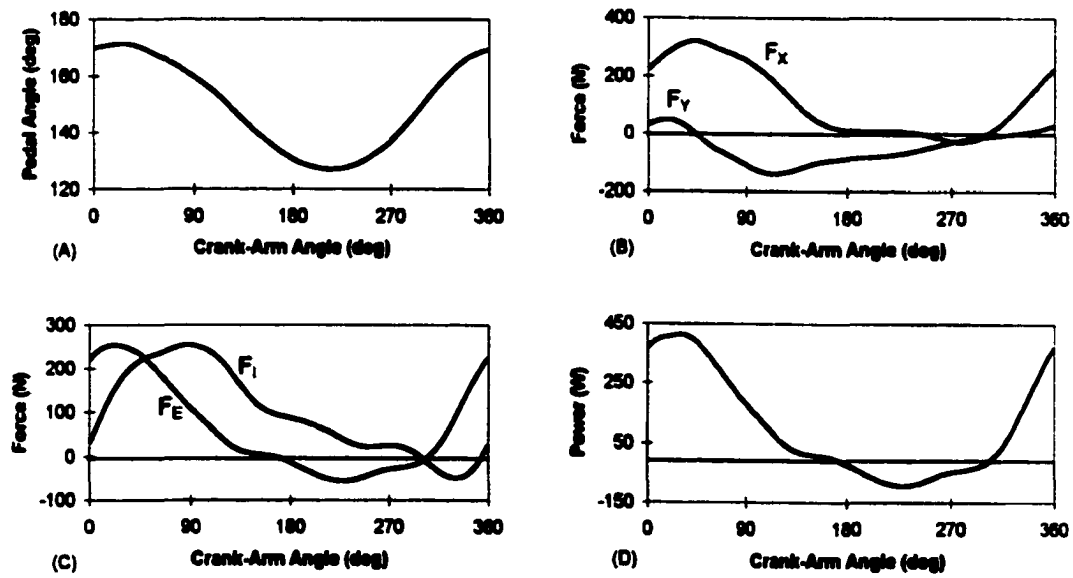

Figure 4.10: Exemplar system data collected on a cyclist riding recumbently with a cadence of 90 rpm and total power output of 250 W: pedal angle (A), horizontal (Fx) and vertical (Fy) pedal reaction forces (B), effective (F_E) and ineffective (F_I) pedal reaction forces (C), and pedal power output (D).

Chapter 5

Biomechanical Analysis of Recumbent Cycling with Comparison to the Standard, Upright Cycling Position

5.1 Abstract

The recumbent cycling position (RCP) has become increasingly popular in recent years as a mode of cycling in both stationary and moving conditions. However, very little is known about the recumbent position, especially related to how it compares biomechanically to the standard, upright cycling position (SCP). It is expected that subtle, but important, differences exist between the two positions mainly due to the altered phasing of the effective contribution of gravity to the pedal forces with respect to the propulsive muscular forces in the RCP compared to the SCP. To investigate these differences, 19 recreational cyclists (12 males and 7 females, mean age 24.6 ± 4.2 years of age) with no prior recumbent cycling experience were acclimated to recumbent cycling over a two-week period prior to measuring pedal reaction forces and lower-extremity kinematics in both a recumbent and SCP (cadence = 90 rpm; power output = 250 W). The included angle between the crank-spindle center, hip joint center, and mid-torso were matched between the two cycling positions so that only the effects of altered hip orientation were investigated. In the RCP the hip joint was level with the crank spindle, and in the SCP a 75° seat-tube angle was employed. Pedal force and lower-extremity

measurements were combined and an inverse-dynamics analysis performed with significant differences evaluated at $p \leq 0.01$. As a result of the altered phasing of effective gravitational and propulsive muscular forces in the RCP, pedal force magnitudes were found to be significantly reduced with the positive effective forces encompassing a significantly increased percentage of the pedal cycle compared to the SCP. Lower-extremity kinematics were not different between the two positions. However, a slight redistribution of energy from the sources did occur. The work performed at the hip joint from the reaction forces was significantly reduced and the amount of work performed by knee flexion significantly increased in the RCP relative to the SCP. Total work at the knee was not different between the two positions. The added demands of the knee flexors in the RCP are most likely trainable, so that performance between positions would not be affected by this. However, since less propulsive energy is transferred from the upper body to the pedals in the RCP, the demands of the lower-extremity muscles are increased in the RCP, possibly reducing the overall performance of the cyclist in the RCP relative to the SCP.

5.2 Introduction

In recent years, recumbent cycling has become increasingly popular. Stationary recumbent ergometers are now widely available in health clubs, gymnasiums, and medical clinics as well as being available for purchase and use in the home. Recumbent bicycles are also increasing in numbers. While bicycles configured for riding in the standard, upright cycling position still far outnumber recumbent bicycles, the recumbent bicycle is no longer the oddity it once was. Recumbent bicycles have proven themselves

to be successful for a wide variety of applications, including touring, sprinting, and leisurely riding.

The increased popularity of the recumbent cycling position (RCP) may be attributed to two main factors: comfort and aerodynamics. In the RCP, low-back and neck stress is greatly reduced compared to the standard cycling position (SCP) (Ice and Waite, In Preparation; Wilson *et al.*, 1984). Additionally, since the upper body is not leaning forward over the hands in the RCP, less stress is placed on the shoulders, elbows, and wrists compared to the SCP (Ice and Waite, In Preparation; Wilson *et al.*, 1984). Also, the saddle is generally larger on a recumbent bicycle, spreading out the seat load over a greater area compared to the standard cycling saddle (Kita, 1997; Wilson *et al.*, 1984). These factors all increase cycling comfort compared to the SCP.

The aerodynamics of the RCP are often improved compared to the SCP by reducing the effective frontal area (Gross *et al.*, 1983). This is accomplished in two ways: 1) the hips are placed almost directly behind the crank, horizontally, and 2) the torso is raised only slightly so that the rider may see forward (Figure 5.1). The location of the hip joint relative to the crank is best described by the angle these two points make with the horizontal, termed the hip orientation angle (HOA) (Figure 5.1, nomenclature also included in Appendix). The HOA is similar to the seat-tube angle often used to describe the hip position of the SCP. However, because the line of the seat tube does not pass through the hip joint in the recumbent position, as it generally does in the SCP, the seat-tube angle does not describe the hip position accurately in the RCP. The torso position is best described by an angle made between the mid-rib cage, the hip, and the horizontal, termed the torso angle (Figure 5.1). In the recumbent position the torso angle is similar

to the backrest angle. However, the backrest angle does not take into account any slight curvature of the back that may exist, nor is it applicable to both the recumbent and SCP. The HOA and torso angle may be manipulated independently to modify the aerodynamics of the vehicle. However, together they define the overall configuration of the rider. The included angle formed by the HOA and torso angle is termed the body configuration angle (BCA).

While the RCP is increasing in popularity, very little is known about this position, especially in comparison to the SCP that it is replacing. Recumbent position cycling is expected to be slightly different from standard position cycling due to the influence of the altered orientation of the cyclist compared to the direction of gravity. Gravity is believed to affect the control of limb movement as a result of both changes in sensory input (Young, 1984) and task mechanics (Davis and Cavanagh 1993; McMahon, 1984). The sensory input of relevance to cycling includes items such as foot pressure and vestibular orientation. The task mechanics of cycling encompasses the projection of limb segment centers of mass in the gravitational plane.

Understanding how gravity alters the lower-extremity kinematics and kinetics of cycling is necessary. With the increased number of recumbent ergometers and bicycles, people now have choices regarding the mode of cycling they wish to pursue. Without an understanding of the similarities and differences between the two modes, uninformed choices will be made which may not be appropriate for the rider. For example, cycling has often been used in rehabilitation settings when patients are not yet ready for the loading demands of walking and running. However, if the lower-extremity joint ranges

of motion or muscular contributions are different between the recumbent and SCP, one cycling position may be advantageous to another, depending on the desired effect.

In another example, the RCP has become extremely popular for high-performance human-powered vehicle competitions. However, elite riders are often recruited for these competitions that have very little recumbent cycling experience. Therefore, they have very little time to train and adapt to any differences that may exist between the two cycling positions. Knowing the specific demands of each cycling position will help riders train appropriately and become ready for recumbent cycling events with minimal preparation.

5.2.1 Review of Literature: Recently, Brown *et al.* (1996) investigated the effects of gravity on cycling by testing 11 healthy subjects in nine different HOA, ranging from 0 to 80° in 10° increments. BCA was kept constant at 180° by rotating the backrest in conjunction with HOA. Subjects cycled steady state in each position at 60 rpm and 80 W. A surface EMG and inverse-dynamics analyses were performed in order to assess changes in muscle activation dynamics and muscle group energy contributions. HOA was found to systematically alter net joint moments: mean hip moments showed increased flexor values, knee moments showed increased extensor values, and ankle moments showed increased dorsiflexor values as HOA increased towards vertical. These changes were supported by the EMG. Additionally, lower-extremity joint angles were found to vary slightly with altered HOA.

While these results suggest that significant differences may exist in the kinetics between recumbent cycling with a HOA near 0° and SCP with a HOA near 75°, the experimental protocol did not directly compare the two. The BCA tested was

approximately 45° greater than that normally chosen by cyclists in the SCP (Reiser *et al.*, Accepted – Dissertation Chapter 2; Reiser *et al.*, In Review-a – Dissertation Chapter 3). This extended BCA would reduce the lengths of the hip extensor muscles and increase the lengths of the hip flexor muscles, affecting their abilities to contribute to the cycling task in a preferred manner (Yoshihuku and Herzog, 1996). The contribution of each muscle group may then be altered, affecting the dynamics of the entire cycling task. Therefore, little, if any, information gained from Brown *et al.* (1996) is directly applicable for understanding the differences between the recumbent and SCP.

Additionally, the hip joint was modeled by Brown *et al.* (1996) in the inverse dynamics as a stationary point. While this approximation may be justified in their experimental design, where the hips were securely strapped to a back board, generally the hips are free to rotate back and forth in the SCP. Energy is transferred across the hip joint by means of this linear motion (Broker, 1991). Allowing the hips to move freely is necessary for an accurate comparison of the two types of cycling, since linear hip motion is expected to be reduced in the RCP compared to the SCP.

Another confounding factor to the application of Brown *et al.*'s (1996) results was the level of effort examined. Brown *et al.* (1996) studied a power output level of only 80 W at a cadence of 60 rpm. Most cyclists generally cycle at cadences near 100 rpm with sustained levels of effort around 250 W (Broker, 1991; Coast, 1996). It is possible that an increased level of effort could alter relative muscle group contributions (Broker, 1991) as well as increase the magnitude of the kinematic and kinetic differences noted by Brown *et al.* (1996).

Others have also examined the effects of lower-body orientation relative to gravity on recumbent cycling performance by altering HOA, backrest angle, or both while measuring aerobic (Too, 1988), anaerobic (Kyle and Caiozzo, 1986; Too, 1991b; Too, 1994), or muscle activation parameters (Too, 1991a). However, no one has compared recumbent performance in a BCA similar to that in the SCP with actual performance in the SCP. If the BCA is not matched, other variables, rather than just the effects of gravity, may be involved; making the results difficult to analyze and interpret. Only Reiser *et al.* (Accepted – Dissertation Chapter 2) and Reiser *et al.* (In Review-a – Dissertation Chapter 3) matched the BCA utilized in the RCP with that selected by subjects in the SCP. In both investigations, anaerobic performance was examined with the 30-second Wingate test. Results indicated that anaerobic performance is not altered, regardless of the HOA, as long as BCA is maintained between the recumbent and SCP. However, altering the orientation of gravity relative to the lower extremity does alter joint angular kinematics. Since lower-extremity kinematics are altered by gravity, it is possible that muscle group contributions are also altered, with total power output remaining unchanged. Unfortunately, the limited data collected could not assess this issue.

5.2.2 Purpose: The goal of this experimental investigation is to determine how lower-extremity cycling kinematics and kinetics are altered between the recumbent and SCP. In order to isolate the gravitational effects on the movements, identical BCA will be utilized in both positions. Additionally, in order to produce results which are applicable to a large number of situations, the BCA will be identical to that self-selected

by cyclists in the SCP with cadence and power output set to a challenging, yet realistic, level.

5.3 Methods

5.3.1 Subjects: Nineteen recreational cyclists participated in this study [12 male, 7 female, age = 24.6 ± 4.2 years (AVG ± STD), body mass = 73.0 ± 10.3 kg, height = 178 ± 9 cm, thigh = 45 ± 2 cm, shank = 45 ± 4 cm, and foot = 14 ± 1 cm]. All leg lengths were measured on the right side. The thigh length was measured from the greater trochanter to the knee center of rotation, the shank length from the knee center of rotation to the lateral malleolus, and the foot length from the lateral malleolus to the head of the 5th metatarsal. Subjects had performed no significant recumbent cycling training within the three-month period prior to testing. Prior to participation, university-approved informed consent was obtained from all subjects.

5.3.2 Experimental Protocol: To minimize the effects of testing subjects unfamiliar with recumbent cycling, a two-week acclamation period was required of each participant. During this period, subjects cycled a stationary recumbent ergometer (205P, Schwinn Cycling & Fitness, Boulder, Colorado) on six different occasions for 30 minutes a session. Subjects were allowed to vary the flywheel resistance and pedaling cadence as they desired. The Schwinn 205P ergometer was chosen due to its similar BCA to that utilized in the SCP and HOA near 0°; producing the recumbent cycling position which was to be tested and compared to the SCP.

Within three days of completing the acclamation period, data were collected from each subject while cycling in both the RCP (HOA = 0°; backrest angle = 50° from

horizontal) and the SCP (HOA = 75°; self-selected forward torso lean). Both positions had the subjects pedaling the same Monark 824E bicycle ergometer (Monark Exercise AB, Varberg, Sweden). For the SCP, the ergometer was placed on the floor while for the RCP the ergometer was mounted on a platform attached to a custom-built recumbent-seating device (Figure 5.1). The ergometer was loaded so that a 250W power output was maintained when cycling steady state at 90 rpm. Cadence was monitored with the ergometer's digital display.

The order of testing positions was randomly determined with both data collections occurring in the same session. Prior to each data collection, subjects warmed up in the test position for a minimum of five minutes. The maximum hip-to-pedal distance while cycling was controlled in each position; set to 105% of the subject's standing hip-to-floor length. For the RCP, the subject was strapped to the seating device with both a hip and mid-torso belt. No belts were worn during the SCP testing. However, the subjects were required to remain seated during the SCP test.

To acquire lower-extremity joint kinematics while cycling, reflective markers were placed on each subject's right mid-torso (mid-rib cage, in line with hip/shoulder axis), hip (approximating the greater trochanter), knee (lateral femoral epicondyle), ankle (lateral malleolus), and toe (head of 5^{th} metatarsal). Markers were also placed on the ergometer at the crank- and pedal-spindle centers (Figure 5.1). Subjects were required to wear dark cycling shorts, a dark shirt, and dark socks in addition to stiff-soled cycling shoes.

The ergometer was equipped with 175 mm crank arms and modified PD-6500 clipless pedals (Shimano American Corp., Irvine, California). The pedals were modified with strain gages and optical encoders to measure normal and tangential components of the

applied load and the angle of the pedal with respect to the crank arm (Reiser *et al.*, In Review-b – Dissertation Chapter 4). Additionally, an optical encoder was used to measure the angle of the crank arm with respect to the ergometer frame.

Three seconds of force and position output data from the force-pedal system were collected at 450 Hz once steady-state cycling was achieved and maintained at 90 rpm. Joint marker displacements were recorded at 30 Hz (shutter speed = 1/250 second) with a camera positioned orthogonal to the plane of motion at a distance of approximately 3 m. Pedal-system data were synchronized with the joint-marker displacements using a light emitting diode (LED) placed in the camera field of view. The LED was illuminated by the pedal system just prior to data collection. Both right and left pedal data were recorded to ensure total output was as expected and that all subjects cycled symmetrically (no subject pedaled with more than an 55:45% power output differential between their two limbs).

5.3.3 Data Analysis: Kinematic and kinetic data describing three pedal revolutions beginning and ending with the right crank arm at top-dead center (pointing vertically upward) were isolated for analysis. Each revolution was analyzed individually with ten additional samples before and after the start and end of each revolution. The data were padded to facilitate smoothing of the endpoint effects. Pedal-system data (normal and tangential forces, pedal angle, and crank-arm angle) were smoothed at 12 Hz using a 4^{th} order, recursive, low-pass Butterworth filter. The normal and tangential pedal loads were resolved into horizontal (FP_X) and vertical (FP_Y) components of the ground based coordinate frame as well as the effective and ineffective force components. The effective pedal force (FP_E) is directed normal and the ineffective pedal force (FP_I) directed

tangential to the long axis of the crank arm. Instantaneous pedal power output (P_{PED}) was then calculated by multiplying the effective pedal force by the crank-arm length (L_{CA}) and crank-arm angular velocity (C_{CA}):

$$P_{PED} = FP_E \cdot L_{CA} \cdot \omega_{CA} \qquad [5.1]$$

Mean pedal power was then determined by averaging P_{PED} over the complete revolution and work determined by integrating P_{PED} with respect to time over the complete revolution (W_{PED}). Cadence was determined using the total time to complete the pedal revolution.

Coordinate data describing torso, hip, knee, ankle, toe, pedal-spindle center, and crank-spindle center motion were obtained by automatically digitizing the video images (Peak Motus System, Peak Performance Technologies, Inc., Englewood, Colorado). Coordinate data were smoothed at 5 Hz using the same Butterworth filter and then converted to 180 Hz using a spline interpolation. From the 180 Hz data, segment inclination angles were computed. Linear and angular velocities and accelerations were then computed using finite difference techniques.

5.3.4 Inverse Dynamics: In order to synchronize the pedal system data with the coordinate data, all parameters were converted to crank-arm angle based data sets rather than time series data sets. One data point for every degree of crank-arm angle was calculated for each parameter using a spline interpolation.

Anthropometric data (segment mass, center of mass location, and moment of inertia) were obtained from the regression equations developed by Dempster (1955). The mass of the foot segment was increased to account for the mass of the shoe and the rotational inertia of the pedal added to the foot segment using the parallel axis theorem. Since the

foot was locked to the pedal, the pedal's rotational inertia is transferred to the foot (Broker, 1991). However, since the pedal loading is measured between the foot and pedal, the mass of the pedal is not added to that of the foot segment. Additionally, since the pedal is assumed to rotate freely, the moment about the long axis of the pedal spindle was assumed to be negligible.

The lower extremity was modeled as a planar, three-segment, rigid-body system with external reaction forces (FP_X and FP_Y) located at the distal end of the foot segment (Figure 5.2). Axes of rotation were considered to be fixed at the joint centers, internal joint friction was assumed negligible, and any redistribution of segment masses due to muscular contraction was ignored. Equations of motion for the planar model were formulated using conventional Newtonian mechanics:

Foot Segment:

$$I_f \cdot \ddot{\Theta}_f = M_A + FP_x \cdot d_f \cdot \sin\Theta_f - FP_y \cdot d_f \cdot \cos\Theta_f - FA_x \cdot r_f \cdot \sin\Theta_f + FA_y \cdot r_f \cdot \cos\Theta_f \quad [5.2]$$

$$m_f \cdot a_{fx} = FA_x + FP_x \quad [5.3]$$

$$m_f \cdot a_{fy} = FA_y + FP_y - m_f \cdot g \quad [5.4]$$

Shank Segment:

$$I_s \cdot \ddot{\Theta}_s = M_K + M_A - FA_x \cdot d_s \cdot \sin\Theta_s + FA_y \cdot d_s \cdot \cos\Theta_s - FK_x \cdot r_s \cdot \sin\Theta_s + FK_y \cdot r_s \cdot \cos\Theta_s \quad [5.5]$$

$$m_s \cdot a_{sx} = FK_x - FA_x \quad [5.6]$$

$$m_s \cdot a_{sy} = FK_y - FA_y - m_s \cdot g \quad [5.7]$$

Thigh Segment:

$$I_t \cdot \ddot{\Theta}_t = M_H - M_K - FK_x \cdot d_t \cdot \sin\Theta_t + FK_y \cdot d_t \cdot \cos\Theta_t - FH_x \cdot r_t \cdot \sin\Theta_t + FH_y \cdot r_t \cdot \cos\Theta_t \quad [5.8]$$

$$m_t \cdot a_{tx} = FH_x - FK_x \quad [5.9]$$

$$m_t \cdot a_{ty} = FH_y - FK_y - m_t \cdot g \quad [5.10]$$

Generalized muscle moments at the hip (M_H), knee (M_K), and ankle (M_A) represent the net effect of all muscles and periarticular structures acting across each joint. I_i, m_i, d_i, and r_i represent the segment moment of inertia, mass, distance from distal end of segment to the center of mass, and distance from the proximal end of segment to the center of mass, respectively, for the foot (f), shank (s), and thigh (t). I_i represents segmental angular position with one superior dot indicating velocity and two indicating acceleration while a_{ix} and a_{iy} represent segment center of mass linear accelerations. FA_x and FA_y, FK_x and FK_y, and FH_x and FH_y represent the components of joint reaction forces for the ankle, knee, and hip, respectively, and g represents the acceleration due to gravity.

5.3.5 Energy Analysis: In the planar model, there are five locations where mechanical energy may enter or exit the system (Figure 5.3). Energy may enter or exit the system through joint angular motion accompanied by a generalized muscular moment, or through the hip joint and foot/pedal interface when linear motion is accompanied by a reaction force. Energy transfers may also occur within the system, at the knee and ankle joints, when linear joint motion is accompanied by a joint reaction force.

The instantaneous power (P_{Mj}) associated with the energy generation (or absorption) at each joint due to a muscular moment may be calculated by multiplying the muscular moment (M_j) by the joint angular velocity ($\dot{\Theta}_j$):

$$P_{Mj} = M_j \cdot \dot{\Theta}_j \quad [5.11]$$

where j represents the hip, knee, or ankle joint. For computation of the hip muscular power only the motion of the thigh segment was included in the calculation of the hip angular velocity. The torso motion was not included in the hip angular velocity because motion of the torso marker was not necessarily reflective of pelvic rotation. Pelvic rotation is the desired motion to include with thigh segment rotation for accurate calculation of hip angular velocity.

The instantaneous power (P_{Fj}) associated with the energy generation, absorption, or transfer across a joint due to a reaction force was calculated by adding the contributions from the horizontal and vertical joint reaction forces (FJ_X and FJ_Y):

$$P_{Fj} = FJ_x \cdot v_{jx} + FJ_y \cdot v_{jy} \qquad [5.12]$$

where j and J represent the joint and v_{jx} and v_{jy} represent the linear joint velocities.

The instantaneous powers, P_{Mj} and P_{Fj}, were then integrated with respect to time over the complete pedal cycle to compute net, positive, and negative work done by each of the four sources (W_{MJ} and W_{FJ}). The sum of the work done by all sources is equal to the sum of the work done on the pedal plus any change in potential and kinetic energy of the segments from the beginning to the end of the pedal revolution (dEsys):

$$W_{MH} + W_{MK} + W_{MA} + W_{FH} = W_{PED} + dEsys \qquad [5.13]$$

Since subjects were cycling at steady state, dEsys is expected to be zero. However, to ensure that there was no net acceleration or deceleration of the cyclists between positions, the overall mean crank-arm velocity at the beginning of the pedal revolution was compared against the mean crank-arm velocity at the end of the pedal revolution.

5.3.6 Statistical Analysis: For each subject and position, the three pedal revolutions were averaged to create one representative pedal revolution. The mean power output for

each representative pedal revolution of the two cycling positions were compared to ensure that variation in mean power output within each subject was not more than 5 W. For seven of the 19 subjects, mean power output differences in the representative pedal revolutions were greater than 5 W. However, by selecting just one pedal revolution from each position for these seven subjects, rather than averaging three revolutions, variation was kept within the 5 W limit. Prior to selecting just one revolution from the three, parameters were visually analyzed to ensure that the one revolution was representative of the three.

Means ± one standard deviation were computed for all continuous variables for each cycling position. These variables included pedal kinematic and kinetic data (pedal angles and reaction forces), joint kinematics (ankle, knee, and hip angles), joint kinetics (ankle, knee, and hip generalized muscle moments), and energy transfer data (ankle, knee, and hip muscle powers and force powers, and pedal power). Additionally, from each subject the maximum, average, and minimum value for each parameter was extracted and compared across positions with Student's t-test with repeated measures. In instances where parameters had both local and global maxima, both were analyzed. Likewise, average cadence, maximum hip-to-pedal distance, torso angle, HOA, and BCA were analyzed. Since work values mimicked average power values, no statistical procedures were run independently on work parameters. All statistical significance was evaluated at the $p \leq 0.01$ level.

5.4 Results

5.4.1 Controlled Parameters: Cycling cadence, mean power output, maximum hip-to-pedal distance, torso angle, HOA, and BCA were well controlled between cycling positions in the experiment (Table 5.1). Mean cadence was within one rpm and mean power output was identical between the two cycling positions. Maximum hip-to-pedal distances differed by only 1 cm, which was not statistically significant. Additionally, HOA and torso angles were within two degrees of their prescribed values, producing BCAs between the SCP and RCP which were within two degrees of each other and were not statistically significant.

5.4.2 Pedal Forces: The effective and ineffective pedal forces were very similar between the two positions (Figure 5.4). However, events were shifted in the pedal cycle by the 76° difference in HOA between the two cycling positions. When taking this phase shift into account, effective pedal forces in both positions were near zero at the beginning of the pedal cycle (top-dead center), increased to a maximum near 90° and decreased back to zero just after 180°. Effective pedal forces then dropped below zero for the remainder of the pedal cycle before returning to zero at the end of the cycle (top-dead center). Peak effective forces were significantly higher in the SCP (302 ± 44 versus 260 ± 43 N) while the effective forces were positive for a significantly greater portion of the pedal cycle in the RCP (66 versus 60%). A positive effective force adds energy to the cycling task while a negative effective force takes energy from the system.

Ineffective forces maintained trends similar to the effective forces, except they were shifted in the pedal cycle by approximately 60° (Figure 5.4). The magnitudes of the ineffective forces were less than those of the effective forces, with the peak ineffective

forces in the SCP significantly greater than those of the RCP (280 ± 54 versus 236 ± 45 N). Additionally, the ineffective forces produced in the RCP were positive for a significantly greater duration of the pedal cycle compared to those in the SCP (80 versus 70%). A positive ineffective force is directed along the crank arm with a tendency to lengthen the arm while a negative force would attempt to shorten the arm.

5.4.3 Lower-Extremity Kinematics: Similar to the effective and ineffective pedal forces, trends in lower-extremity joint kinematics were similar between the two cycling positions when adjusted for the phase difference in the pedal cycle (Figure 5.5). Ankle angle, defined as the included angle between the foot and shank segments, decreased slightly during the first 90° of the pedal cycle before increasing during the second 90° and then slowly declining towards its original level at the end of the pedal cycle. Knee angles, defined by the shank and thigh segments to increase with flexion from 0° at full extension, were maximal at the beginning of the pedal cycle, decreased through the first half of the pedal cycle, and increased back to a maximum near the end of the pedal cycle. Hip angles, defined as the included angle between the thigh and torso segment, were mirror images of the knee angles.

The maximum, minimum, and average ankle, knee, and hip angle values between positions were not significantly different from each other (Table 5.2). The pedal angles, defined as the included angle between the surface of the pedal and vertical, were approximately 82° greater in the RCP compared to the SCP, 6° greater than the difference in HOA.

5.4.4 Muscular Moments: Similar to the pedal forces and lower-extremity kinematics, trends in lower-extremity joint muscular moments were similar between the

two cycling positions when adjusted for the phase difference in the pedal cycle (Figure 5.6). Ankle muscular moments started near zero at the beginning of the pedal cycle, decreased through 110°, and then increased back to zero at the end of the pedal cycle. A negative ankle moment is indicative of a net plantar-flexor torque. Knee muscular moments began positive and continued to increase through 90° before declining to a negative minimum near 180°. Knee moments then increased through the remainder of the pedal cycle. A positive knee moment is indicative of a net extensor torque while a negative knee moment is indicative of a net flexor torque.

Hip muscular moments began negative and stayed at their initial levels through 90° before dropping to a minimum near 135°. Hip moments then increased to a positive maximum near 270° before dropping back to their initial negative values at the end of the pedal cycle. A negative net hip moment is indicative of an extensor torque while a positive net hip moment is indicative of a flexor torque.

Even though muscular moment trends were similar between the two positions, several significant differences exist in the average and minimum values (Table 5.3). Maximum and minimum ankle muscular moments were similar between positions with the average ankle moment significantly greater (less negative) in the SCP. Maximum, average, and minimum knee muscular moments were greater in the SCP, however, only the average and minimum knee moments were significantly greater. The maximum, average, and minimum hip muscular moments were all very similar with none significantly different.

5.4.5 Muscular Powers: Since lower-extremity kinematics and generalized muscle moments were similar between the two positions, combining the joint kinematics with the joint muscular moments produced similar trends in joint muscular power, when adjusted

for the phase difference in the pedal cycle (Figure 5.7). Ankle muscular power begins the pedal cycle near zero and stays low until about 90°, where it rapidly increases to a peak near 125°. The ankle muscular power then drops back near zero at 180° and maintains virtually no power output through the remainder of the pedal revolution. Knee muscular power begins the pedal cycle slightly above zero, rapidly increases to a peak near 90°, then drops below zero near 110° before rebounding with a slightly reduced peak near 200°. After the second peak, the knee muscular power output drops just below zero late in the pedal cycle before coming back above zero at the end of the cycle. Hip muscular power begins the pedal cycle slightly below zero, increases to a positive peak near 135°, then drops below zero near 180° before rebounding to just above zero near 270°. After 270°, the hip muscular power drops below zero again until the end of the pedal cycle.

As with the muscular moments, there are some differences in the maximum, average, and minimum joint muscular power values, even though trends were similar between the two positions (Table 5.3). The maximum, average, and minimum muscular powers of the ankle, knee, and hip were all greater in the SCP, however, none of the values were found to be significantly greater. When the knee and hip muscular powers were broken down into their two distinct regions of positive power output, the peak of the second region of knee power output was significantly greater in the RCP compared to the SCP.

5.4.6 Force Powers: Joint force and pedal powers were similar between the two cycling positions when adjusted for the phase difference in the pedal cycles (Figure 5.8). Force powers begin the pedal cycle near 0 W, then rise to a peak near 90° before falling back to zero near 180°. Force powers are then generally negative in the second half of the pedal cycle before returning to zero at the end of the pedal cycle. However, the hip

force power does have positive peak values in both the power (crank-arm angle from 0 to 180°) and recovery phases (crank-arm angle from 180 to 360°). The knee force power has a slight rise in the recovery phase and peaks near zero. The ankle and pedal force powers do not rise and peak again in the recovery phase.

The ankle force power is offset from the pedal force power only by the contribution of the mass of the foot segment on the pedal, inertia of the foot, and the small amount of power generated by the ankle muscular moment. The knee force power is substantially reduced from the ankle force power mainly due to the contribution of the knee muscular moment on the ankle force power and, to some extent, the mass and inertia of the shank. The hip force power is substantially reduced from the knee force due to contributions at the knee from the hip muscular moment as well as mass and inertia of the thigh.

Pedal power represents the flow of energy between the foot and the pedal, ankle force power represents the flow of energy between the shank and the foot, knee force power represents the flow of energy between the thigh and the shank, and hip force power represents the flow of energy between the pelvis and the thigh. During the propulsive phase, energy flows from proximal to distal while during the recovery phase energy flows from distal to proximal. This reversal in the order of force powers in the recovery phase compared to the propulsive phase illustrates the change in direction in the flow of energy.

Since joint force powers reflect contributions from both joint muscular power and the gravitational contribution from the segment masses, differences exist in maximum, average, and minimum joint force power values even though the trends are similar between the two positions (Table 5.3). Maximum, average, and minimum ankle and knee joint force powers are greater in the SCP with the maximum and minimum values

significantly greater. At the hip, however, even though power values were extremely similar between the two positions, the average and minimum hip force power values were significantly greater in the SCP compared to the RCP. Additional analysis of the recovery phase peaks in knee and hip force powers found the recovery phase peak of the hip force power to be significantly greater in the SCP.

5.4.7 System Energy: By integrating the joint muscular and force powers with respect to time to calculate work and employing the system energy equation (Equation 5.13), relative task contributions may be analyzed (Table 5.4). The majority of the work in both cycling positions was produced by the knee musculature (approximately 55%), followed by the hip musculature (approximately 25%), then the ankle musculature (approximately 11%), and finally the hip reaction force (approximately 8%). There were slight differences between the two cycling positions, however, only the work done by the hip force power was significantly different. Increased motion at the hip joint in the SCP produced slightly more work compared to the hip joint in the RCP. Additionally, the hip force power produced positive work for a significantly greater portion of the pedal cycle in the SCP compared to the RCP (82 versus 62%). Analyzing the hip force power further, the total amount of work done in the power phase of the pedal cycle was not different between the two cycling positions even though this accounted for only 75% of the positive work in the SCP and 94% of the positive work in the RCP. The additional work done in the recovery phase of the pedal cycle in the SCP was significantly greater than that produced in the same phase of the RCP.

At the other three energy sources, there were virtually no changes in duration of the pedal cycles where positive or negative work was being performed. However, there was

a notable redistribution of work performed in the pedal cycle for the knee musculature. In the SCP, 67% of the positive work was done in the power phase of the pedal cycle and only 55% of the positive work during this same phase in the RCP. This redistribution of work generation was significant, even though total positive work from the knee musculature was not different, between the two positions.

Summing the work of each source produced significantly more work in the SCP compared to the RCP (Table 5.4). This was accompanied by a net 3.5°/second increase in mean crank-arm angular velocity in the SCP compared to the RCP. An increase in crank-arm angular velocity is indicative of an increase in system energy in the SCP resulting from the increased work done in the SCP energy sources, even though work on the pedals was not significantly different between the two positions. As also indicated in the effective pedal forces, positive work was done over a significantly greater portion of the pedal cycle in the RCP compared to the SCP (66% versus 60%).

5.5 Discussion

5.5.1 Pedal Data: Pedal force and pedal angle profiles measured in this investigation in the SCP agree favorably with previously published data (Broker, 1991; Broker and Gregor, 1996; Cavanagh and Sanderson, 1986; Gregor *et al.*, 1985; Kautz and Hull, 1993). Slight differences between this data and that reported by others can easily be attributed to differences in cycling ability between subject populations, cycling cadence, power output, and cycling set-up.

The redistribution of positive effective and ineffective pedal forces over a greater percentage of the pedal cycle with reduced magnitude in the RCP compared to the SCP

was expected from the altered HOA between the two positions. In the SCP, the positive effective force from gravity acting on the lower extremity occurs in phase with the propulsive extension of the limbs. However, in the RCP, the positive effective forces from gravity acting on the lower-extremity begin when the propulsive extension forces from the limbs are declining. This out-of-phase nature of the effective muscular and gravitational force contributions in the RCP increases the duration of the pedal cycle where effective forces are positive and reduces the overall magnitude of the effective forces compared to those in the SCP. Additionally, the ineffective forces are redistributed between the two cycling positions in the same manner due to the out of phase occurrence of propulsive and gravitational forces in the RCP compared to the SCP.

5.5.2 Lower-Extremity Kinematics: The slight, but not significant, increases in hip and ankle joint extension in the SCP relative to the RCP were accompanied by a slight decrease in knee extension and pedal angle in the SCP relative to the RCP. The slight changes in kinematics between the two positions were most likely due to the redistribution of loads on the limbs as a result of their altered orientation relative to gravity. No statistical differences in lower-extremity kinematics are consistent with results reported by others who examined lower-extremity kinematics at less than maximal effort (Too 1994; Brown *et al.*, 1996). Too (1994) measured joint angles statically in three different recumbent cycling positions with different HOA and similar BCA. Brown *et al.*, (1996) found no statistical differences in hip and knee angles measured dynamically in their previously described study. However, they did find a significant increase in ankle angles from the 0 to 80° HOA. This finding is interesting since they also found slight decreases in ankle angles in the 40° HOA compared to the 0° HOA.

Since they did not find consistent changes in ankle angles with changes in HOA their results are difficult to interpret and compare with those found here.

In studies where lower-extremity kinematics were measured dynamically while subjects produced maximal effort, the changes in joint angles are more pronounced between positions with different HOA (Reiser *et al.*, Accepted – Dissertation Chapter 2; Reiser *et al.*, In Review-a – Dissertation Chapter 3). Reiser *et al.* (Accepted – Dissertation Chapter 2) found that hip and ankle angles were significantly greater and knee angles reduced in the SCP compared to the RCP with matched BCA and -15° HOA. However, in the follow-up study, while hip and knee angles were significantly different as previously found, ankle angles were not different (Reiser *et al.*, In Review-a – Dissertation Chapter 3). The authors noted that the lack of differences in ankle angles in the follow-up study could have been caused by some other slight, but not significantly different variations in BCA. Regardless, it is plausible that lower-extremity kinematics could be different between sub-maximal and maximal effort cycling since level of effort redistributes muscular energy contributions (Broker, 1991).

5.5.3 Lower-Extremity Kinetics: Joint moment and power profiles measured in the SCP are similar to those reported by others (Broker, 1991; Broker and Gregor, 1996; Gregor *et al.*, 1985). Similarly, the trends in average ankle, knee, and hip moments are similar between the two HOA tested here and those found by Brown *et al.* (1996): ankle moments became more dorsi-flexor, knee moments became more extensor, and hip moments became more flexor in the SCP compared to the RCP.

At the ankle, the average ankle muscular moment is significantly increased in the SCP compared to the RCP. However, the difference is only 2 Nm between positions and

the maximum and minimum values are not altered. This significant difference in average ankle moments between the two positions does not transfer across to any differences in instantaneous power output or work done by the muscular moment.

The ankle muscular moments are plantar flexor throughout the pedal cycles of both positions, accompanied by only a small region of ankle motion in the second half of the propulsive phase. This situation produces a small region of positive work by the ankle musculature. Since there is little ankle motion throughout the rest of the pedal cycle, there is little energy generated or absorbed in the remainder of the pedal cycle. Plantar-flexor activity, however, is required to maintain ankle position and allow appropriate transfer of energy generated at the hip and knee to the pedal. It is this stabilizing requirement that most likely accounts for the increased average ankle muscle moment in the SCP compared to the RCP.

The average and minimum knee muscular moments are significantly greater in the SCP compared to the RCP, suggesting reduced flexor activity in the SCP. This is indeed the case. Knee muscular moments are extensor during the majority of the propulsive phase before switching to flexor for the recovery phase. During the majority of the extensor activity the knee is also extending, just as during the flexor activity the knee is flexing, allowing the knee musculature to have two distinct regions of positive work. The peak-power output in the region of knee flexor activity is significantly greater in the RCP compared to the SCP. The increased amount of knee flexor activity in the recovery phase of the pedal cycle in the RCP is accompanied by a slight reduction in knee extensor activity in the propulsive phase compared to the SCP. The resulting reduced work of the knee extensors in the propulsive phase of the pedal cycle is offset by the increased work

of the knee flexors in the recovery phase, yielding no total change in the work done by the knee musculature between the two cycling positions. Relying more on the knee flexors in the RCP compared to the SCP may cause performance differences, especially if adequate training is not given to the cyclist prior to cycling for extended periods of time in the RCP.

The difference in average hip moments, though less negative in the SCP, was not found to be statistically significant as it was by Brown *et al.* (1996). In fact, the maximum, average, and mean hip moment values differ by 2 Nm or less. These differences are not large enough to produce a significant increase in the instantaneous power output or work from the hip musculature between the two cycling positions. The net hip muscle moment is extensor throughout, except for a brief period near the end of the pedal cycle. This extensor moment produces positive work in the propulsive phase and absorbs energy in the recovery. However, the magnitude of the extensor moment in the recovery phase is very small and therefore very little energy is absorbed compared to that produced by the hip musculature.

5.5.4 Lower-Extremity Energetics: In the RCP, the hip is secured by the seat, backrest, and waist belt, reducing hip motion when compared to the SCP. As a result of this motion, the upper body and pelvis may transfer more energy to the lower extremity in the SCP through the hip-joint reaction forces. In fact, 2 J of additional energy were transferred to the pedals from the hip reaction force. While this source of power is the smallest contributor to the pedaling task, the difference between the two cycling positions was consistent enough to be significantly different in both the amount of work done and

the percent of total work done. It was the only energy source to be significantly different between positions in either of these parameters.

The difference between cycling positions in work done by the hip force power occurs during the recovery phase of the pedal cycle. The total amount of work done in the propulsive phase of both cycling positions is similar, however, the positive work done in the recovery phase in the SCP is much improved. Even though this is only a 2 J improvement, it is 2 J less required from the lower-extremity musculature. Over an extended period of time this could cause premature fatigue when cycling in the RCP compared to the SCP.

It is interesting to note that Reiser *et al.* (Accepted – Dissertation Chapter 2) and Reiser *et al.* (In Review-a – Dissertation Chapter 3) found no differences in peak or 30-second mean power output between the SCP and RCP, even though there seems to be a reduced capacity to transfer energy from the upper body to the lower body in the RCP. It is possible that since subjects did not have to concern themselves with bicycle stability, steering, and visibility in the peak-power tests and since the seating restraints allowed some motion, they were able to manipulate the upper body in a way to transfer the same amount of energy from the upper body to the lower body in both the RCP and SCP. However, upper-body motion will be minimized in the RCP when stability and control becomes an issue, producing a similar situation to that in the submaximal tests in this study. The resulting likelihood will be a greater energy demand placed on the musculature of the lower extremity in the RCP compared to the SCP.

The force powers at the knee and ankle, which are responsible for transferring energy through the joints, are significantly greater in the SCP in maximum and average values

compared to the RCP. An increase in the maximum force powers may be attributed in part to the increased magnitudes of the pedal forces due to the in phase nature of the propulsive gravitational forces and propulsive pedal forces in the SCP compared to the RCP. However, this does not account for the significant increase in the average power transferred across these two joints.

When summing the source contributions in each position it was found that the total work done in the SCP was significantly greater than that done in the RCP. This was supported by the net increase in crank-arm angular velocity in the SCP relative to the RCP. While the net power delivered to the pedals was not different between the two positions, the additional energy generated in the SCP went towards increasing the kinetic energies of the lower-extremity segments. This energy was also transferred between the segments through the joints, accounting for the significant increase in the average force powers of the knee and ankle joints and some of the increase in the maximum force powers.

While it is expected that the majority of the differences in total source contributions between the two cycling positions be from the relative change in crank-arm angular velocities and subsequent changes in kinetic energies of the lower-extremity segments during the pedal cycle, other confounding factors exist. Since crank-arm angular velocities increased in both cycling positions, the total source contributions in each position should exceed the total pedal contributions. However, this is only the case in the SCP. The total source contributions in the RCP fall slightly below those of the total pedal output. This discrepancy has been found by others using inverse-dynamics models to analyze lower-extremity function in cycling without resolution (Broker, 1991; Ericson

et al., 1986; Ingen Schenau *et al.*, 1990; Sirin *et al.*, 1989). All energy into and out of the system is assigned to an energy source or sink in this modeling process and, therefore, should add up to balance the energy equation (Equation 5.13) when changes in segmental energies are included. The only possible place where discrepancies could be introduced is in the finite difference process used to calculate velocities and accelerations from angular and linear position data. Joint angles and angular accelerations along with positions and linear accelerations are used when computing joint moments and reaction forces through the inverse-dynamics model. This process should account for all the energies of the system. However, to calculate the individual energies through instantaneous power values, angular and linear velocities are used which were not required in the inverse-dynamics model to compute the moments and reaction forces. Errors in the position, velocity, and acceleration data relative to each other introduced by the finite difference method could account for a discrepancy when adding up individually computed sources and comparing them to the measured pedal values. The validity of this possible source of error has not been investigated.

5.6 Conclusions

Subtle, but important, differences exist in the lower-extremity function between cycling in the SCP and RCP. The magnitudes of the effective and ineffective pedal forces are reduced in the RCP which in-turn should reduce the magnitudes of the reaction forces at the joints of the lower-extremity. Forces are reduced by introducing a phase shift in the propulsive and gravitational forces acting on the pedal. The redistribution of pedal forces is accompanied by virtually no change in the cycling kinematics at sub-

maximal levels of power output. Reduced force magnitudes with no changes in joint ranges of motion could make the RCP an ideal choice for rehabilitation purposes compared to the SCP. However, energy contributions from the different sources are also slightly altered which need to be taken into account. The demands of the lower-extremity musculature are increased in the RCP due to less transfer of energy across the hip from the pelvis and upper-body. Additionally, the RCP demands more effort from the knee flexor muscles compared to the SCP. While the knee flexor muscles are most likely trainable and, therefore, adaptable to the increased demands in the RCP, overall performance in the RCP may be reduced due to the reduced ability to transfer energy across the hip joint from the pelvis and upper-body. The reduced amount of energy transferred across the hip joint may not significantly reduce power output under maximal cycling conditions. However, longer-duration performance may be reduced in the RCP due to the increased demands of the lower-extremity musculature.

5.7 Acknowledgements

Special thanks to the Shimano American Corporation for providing the PD-6500 pedals which were modified by us to measure pedal forces and angles, The U.S. Department of Education's Graduate Assistance in Areas of National Need program (award #P200A70433) for their support of the first author, and the Department of Health and Exercise Science at Colorado State University for providing office and laboratory space for the successful completion of this project.

5.8 References

Broker, J.P. (1991). Mechanical energy management during constrained human movement. *Unpublished Doctoral Dissertation*. University of California, Los Angeles.

Broker, J.P. and Gregor, R.J. (1996). Cycling biomechanics. In *High-Tech Cycling* (Edited by Burke, E.R.). Human Kinetics: Champaign, pp. 145-166.

Brown, D.A., Kautz, S.A., and Dairaghi, C.A. (1996). Muscle activity patterns altered during pedaling at different body orientations. *J. Biomechanics*, **29**(10), 1349-1356.

Cavanagh, P.R. and Sanderson, D.J. (1986). The biomechanics of cycling: studies of the pedaling mechanics of elite pursuit riders. In *Science of Cycling* (Edited by Burke, E.R.). Human Kinetics: Champaign, pp. 91-122.

Coast, J.R. (1996). Optimal pedaling cadence. In *High-Tech Cycling* (Edited by Burke, E.R.). Human Kinetics: Champaign, pp. 101-116.

Davis, B.L. and Cavanagh, P.R. (1993). Simulating reduced gravity: a review of biomechanical issues pertaining to human locomotion. *Aviat. Space Environ. Med.*, **64**, 557-577.

Dempster, W.T. (1955). Space requirements of the seated operator: geometrical, kinematic, and mechanical aspects of the body with special reference to the limbs. *Wright Air Development Center Report Nos. 55-159*. Dayton, Ohio.

Ericson, M.O., Bratt, A., Nisell, R., Arborelius, U.P., and Ekholm, J. (1986). Power output and work in different muscle groups during ergometer cycling. *Eur. J. Applied Physiology*, **55**, 229-235.

Gregor, R.J., Cavanagh, P.R., and LaFortune, M. (1985). Knee flexor moments during propulsion in cycling – a creative solution to Lombard's Paradox. *J. Biomechanics*, **18**(5), 307-316.

Gross, A.C., Kyle, C.R., and Malewicki, D.J. (1983). The aerodynamics of human-powered land vehicles. *Scientific American*, **249**(6), 142-152.

Ice, R. and Waite, J. (In Preparation). Overuse injuries in cycling. *Int. J. Sports Medicine*.

Ingen Schenau, G.J. van, Woensel, W.W.L.M. van, Boots, P.J.M., Snackers, R.W., and de Groot, G. (1990). Determination and interpretation of mechanical power in human movement: application to ergometer cycling. *Eur. J. Applied Physiology*, **61**, 11-19.

Kautz, S.A. and Hull, M.L. (1993). A theoretical basis for interpreting the force applied to the pedal in cycling. *J. Biomechanics*, **26**(2), 155-165.

Kita, J. (1997). The unseen danger (Special report: impotency and cycling). *Bicycling Magazine*, August, pp. 68-73.

Kyle, C.R. and Caiozzo, V.J. (1986). Experiments in human ergometry as applied to the design of human powered vehicles. *Int. J. of Sport Biomechanics*, **2**, 6-19.

McMahon, T.A. (1984). Mechanics of locomotion. In *Muscles, Reflexes, and Locomotion.* Princeton University Press: Princeton, pp. 189-233.

Reiser, R.F., Peterson, M.L., and Broker, J.P. (Accepted – Dissertation Chapter 2). Anaerobic cycling power output with variations in recumbent body configuration. J. Applied Biomechanics.

Reiser, R.F. Peterson, M.L., and Broker, J.P. (In Review-a – Dissertation Chapter 3). Anaerobic cycling power output with variations in hip orientation. *Ergonomics.*

Reiser, R.F. Peterson, M.L., and Broker, J.P. (In Review-b – Dissertation Chapter 4). Instrumented Bicycle Pedals for Dynamic Measurement of Propulsive Cycling Loads. *IEEE/ASME Transactions on Mechatronics.*

Sirin, A.V., Wells, R.P., and Patla, A.E. (1989). Bilateral power analysis of ergometer cycling. *Proceedings of the 13th Annual Meeting, American Society of Biomechanics.* University of Vermont Conferences: Burlington, Vermont, pp. 731.

Too, D. (1994). The effect of trunk angle on power production in cycling. *Research Quarterly for Exercise and Sport*, **65**(4), 308-315.

Too, D. (1991a). The effect of body orientation on EMG patterns in cycling. *Biomechanics in Sports IX* (Edited by Taut, C.L, Patterson, P.E., and York, S.L.). Iowa State University Press: Ames, Iowa, pp. 109-115.

Too, D. (1991b). The effect of hip position/configuration on anaerobic power and capacity in cycling. *Int. J. of Sport Biomechanics*, **7**, 359-370.

Too, D. (1988). The effect of body position, configuration, and orientation on cycling performance. *Unpublished Doctoral Dissertation*, University of Illinois at Urbana-Champaign.

Welbergen, E. and Clijsen, L.P.V.M. (1990). The influence of body position on maximal performance in cycling. *Eur. J. Appl. Physiol.*, **61**, 138-142.

Wilson, D.G., Forrestall, R., and Hendon, D. (1984). Evolution of recumbent bicycles and the design of the Avatar Bluebell. In *Proceedings of the Second International Human Powered Vehicle Scientific Symposium.* Long Beach, CA: IHPVA, Box 2068, Seal Beach, CA, , pp. 92-103.

Yoshihuku, Y. and Herzog, W. (1996). Maximal muscle power output in cycling: a modelling approach. *J. Sports Sciences*, **14**, 139-157.

Young, L.R. (1984). Perception of the body in space: Mechanisms. *Handbook of Physiology – The Nervous System*, Vol. 3 (Edited by Smith, I.). Academic Press: New York, pp. 1023-1066.

5.9 Appendix: Nomenclature

Ankle Angle (AA) – Included angle between knee joint, ankle joint, and toe markers*

Backrest Angle (BA) – Angle of seat backrest relative to horizontal*

Body Configuration Angle (BCA) – Included angle between torso, hip, and bottom bracket*

Hip Angle (HA) – Included angle between mid-torso, hip joint, and knee joint markers*

Hip Orientation Angle (HOA) – Angle produced by line connecting hip joint with center of bottom bracket relative to horizontal*

Hip-to-Pedal Distance (HPD) – linear distance between hip joint marker and center of pedal spindle at maximum separation of these two points during pedaling

Knee Angle (KA) – Angle between hip joint, knee joint, and ankle joint markers with zero referenced at full extension and angle increasing with knee flexion*

Pedal Angle (PA) – Angle produced by the surface of the pedal relative to vertical*

Recumbent Cycling Position (RCP) - 0° hip orientation angle with 50° torso angle

Standard Cycling Position (SCP) - 75° hip orientation angle with forward lean of torso

Torso Angle (TA) – Angle produced by line connecting mid-torso marker with hip joint marker relative to horizontal*

* Displayed graphically in Figure 1

5.10 Tables

Table 5.1: Controlled Parameters

Position	SCP	RCP
Cadence (rpm)	93.8	93.0
	(3.3)	*(2.7)*
Mean Power (W)	125	125
	(14)	*(14)*
Max Hip-to-Pedal (cm)	100	101
	(5)	*(6)*
Torso Angle (degrees)	125*	51
	(6)	*(6)*
HOA (degrees)	74*	-2
	(1)	*(1)*
BCA (degrees)	129	127
	(7)	*(6)*

() indicate standard deviation.

*($p<0.01$) between SCP and RCP

Table 5.2: Lower-Extremity Kinematics

Position	SCP	RCP
Ankle Angle		
Maximum	128	125
	(5)	*(6)*
Average	116	115
	(5)	*(4)*
Minimum	106	105
	(7)	*(5)*
Knee Angle		
Maximum	111	110
	(5)	*(4)*
Average	81	79
	(5)	*(4)*
Minimum	44	43
	(7)	*(6)*
Hip Angle		
Maximum	116	113
	(7)	*(7)*
Average	93	92
	(7)	*(7)*
Minimum	72	69
	(7)	*(8)*
Pedal Angle		
Maximum	92*	172
	(8)	*(6)*
Average	67*	149
	(5)	*(6)*
Minimum	41*	124
	(6)	*(7)*

Angles reported in degrees
() indicate standard deviation.
*($p<0.01$) between SCP and RCP

Table 5.3: Lower-Extremity Kinetics

	Muscular Moment (Nm)		Muscular Power (W)		Force Power (W)	
Position	**SCP**	**RCP**	**SCP**	**RCP**	**SCP**	**RCP**
Ankle						
Maximum	0	0	102	92	553*	447
	(3)	*(3)*	*(36)*	*(27)*	*(103)*	*(88)*
Average	-15*	-17	14	12	117*	99
	(4)	*(4)*	*(7)*	*(6)*	*(16)*	*(14)*
Minimum	-39	-38	-18	-21	-79	-95
	(7)	*(7)*	*(7)*	*(13)*	*(34)*	*(51)*
Knee						
Maximum	43	35	230	218	359*	304
	(17)	*(15)*	*(85)*	*(52)*	*(85)*	*(66)*
Average	4*	0	70	69	77*	62
	(8)	*(7)*	*(21)*	*(16)*	*(13)*	*(12)*
Minimum	-26*	-35	-47	-62	-55	-67
	(8)	*(11)*	*(39)*	*(31)*	*(23)*	*(29)*
Hip						
Maximum	8	7	166	156	45	47
	(10)	*(9)*	*(66)*	*(45)*	*(19)*	*(14)*
Average	-22	-24	35	30	11*	8
	(8)	*(6)*	*(18)*	*(16)*	*(5)*	*(2)*
Minimum	-54	-55	-42	-59	-6*	-12
	(16)	*(10)*	*(18)*	*(32)*	*(5)*	*(4)*

() indicate standard deviation.

*($p<0.01$) between RCP and SCP

Note: Knee and hip muscular and force powers exhibited two maxima. The second, smaller maxima of the knee muscular power and hip force power were significantly different.

Table 5.4: Source Contributions to System Energy

	SCP			RCP		
Source	**Work (J)**	**(% Total)**	**(% Cycle)**	**Work (J)**	**(% Total)**	**(% Cycle)**
Ankle Muscular						
Net	9.0	(10.7)		8.1	(10.5)	
Positive	10.6		(33.3)	9.9		(33.3)
Negative	1.6		(66.7)	1.8		(66.7)
Knee Muscular						
Net	45.1	(53.8)		44.3	(57.5)	
Positive	46.6		(82.2)	47.3		(78.9)
Negative	1.5		(17.8)	3.0		(21.1)
Hip Muscular						
Net	22.6	(26.9)		19.5	(25.3)	
Positive	26.4		(62.8)	25.3		(61.4)
Negative	3.8		(37.2)	5.8		(38.6)
Hip Force						
Net	7.2*	(8.6*)		5.2	(6.7)	
Positive	7.6		(81.9)	6.3		(61.9)
Negative	0.4		(18.1)	1.1		(38.1)
Total Source Contributions						
Net	83.9*	(100)		77.1	(100)	
Positive	91.2		(86.4)	88.8		(83.3)
Negative	7.3		(13.6)	11.7		(16.7)
Total Pedal Contributions						
Net	79.8			80.2		
Positive	90.8		(59.7)	88.5		(66.4)
Negative	11.0		(40.3)	8.3		(35.6)
dEsys (deg./sec)	+8.0			+4.5		

*($p<0.01$) between RCP and SCP

5.11 Figures

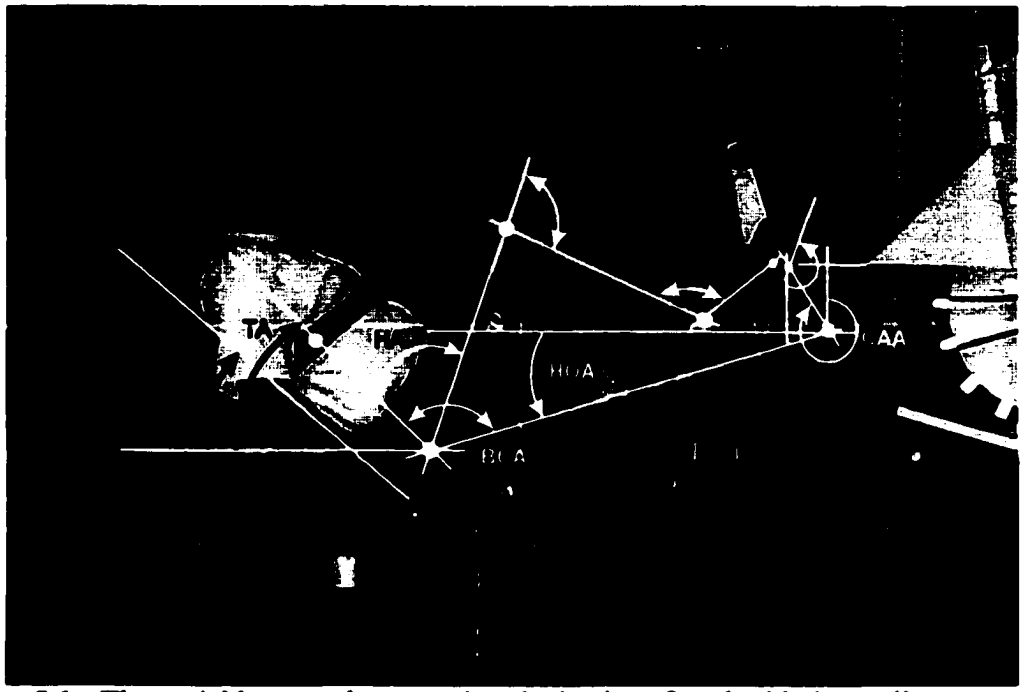

Figure 5.1: The variable recumbent-seating device interfaced with the cycling ergometer used in the collection of data with overlay of defined terms: ankle angle (AA), backrest angle (BA), body configuration angle (BCA), crank-arm angle (CAA), hip angle (HA), hip orientation angle (HOA), knee angle (KA), pedal angle (PA), and torso angle (TA).

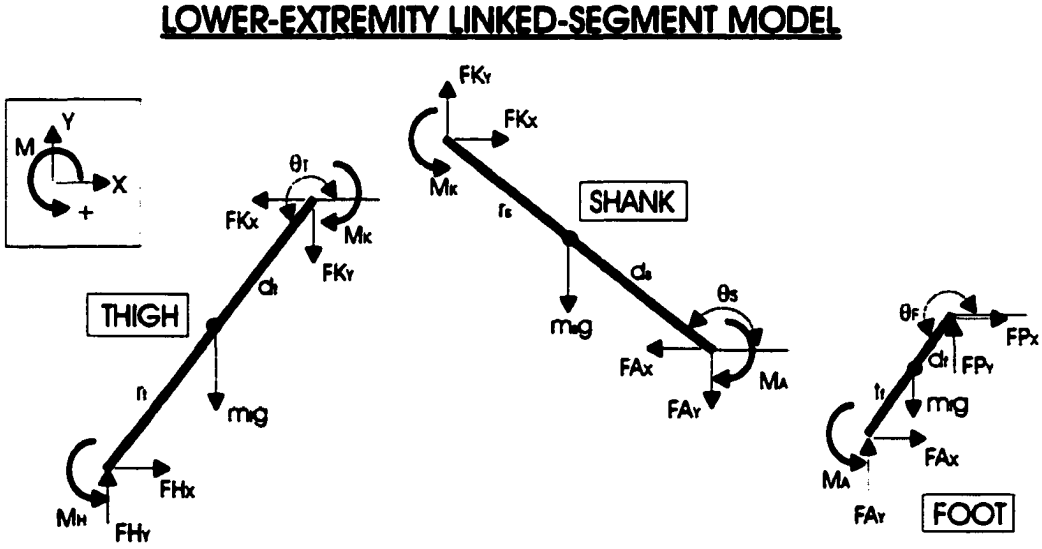

Figure 5.2: Linked-segment model of the lower extremity utilized to analyze kinetic features of cycling. External reaction forces at the pedal and lower-extremity kinematics are the inputs and joint reaction forces and moments the outputs to the model.

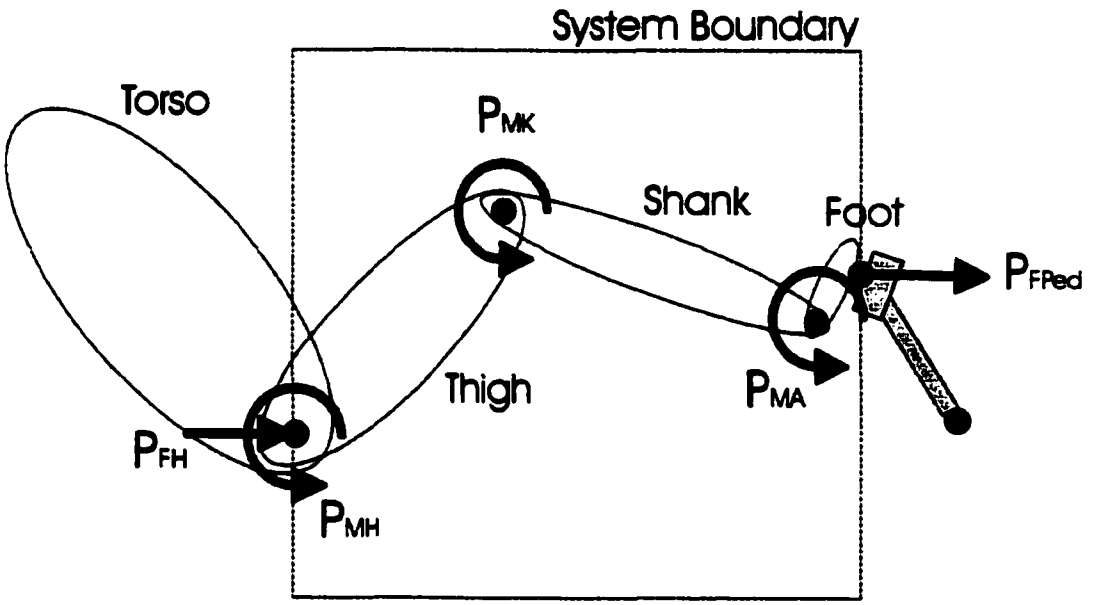

Figure 5.3: Control system describing the energy sources and sink of the lower-extremity during cycling. Energy sources include the three joint muscular powers and the hip joint force power. The pedal is the only energy sink. However, energy may also be absorbed by the energy sources, but the net contribution of each source is positive.

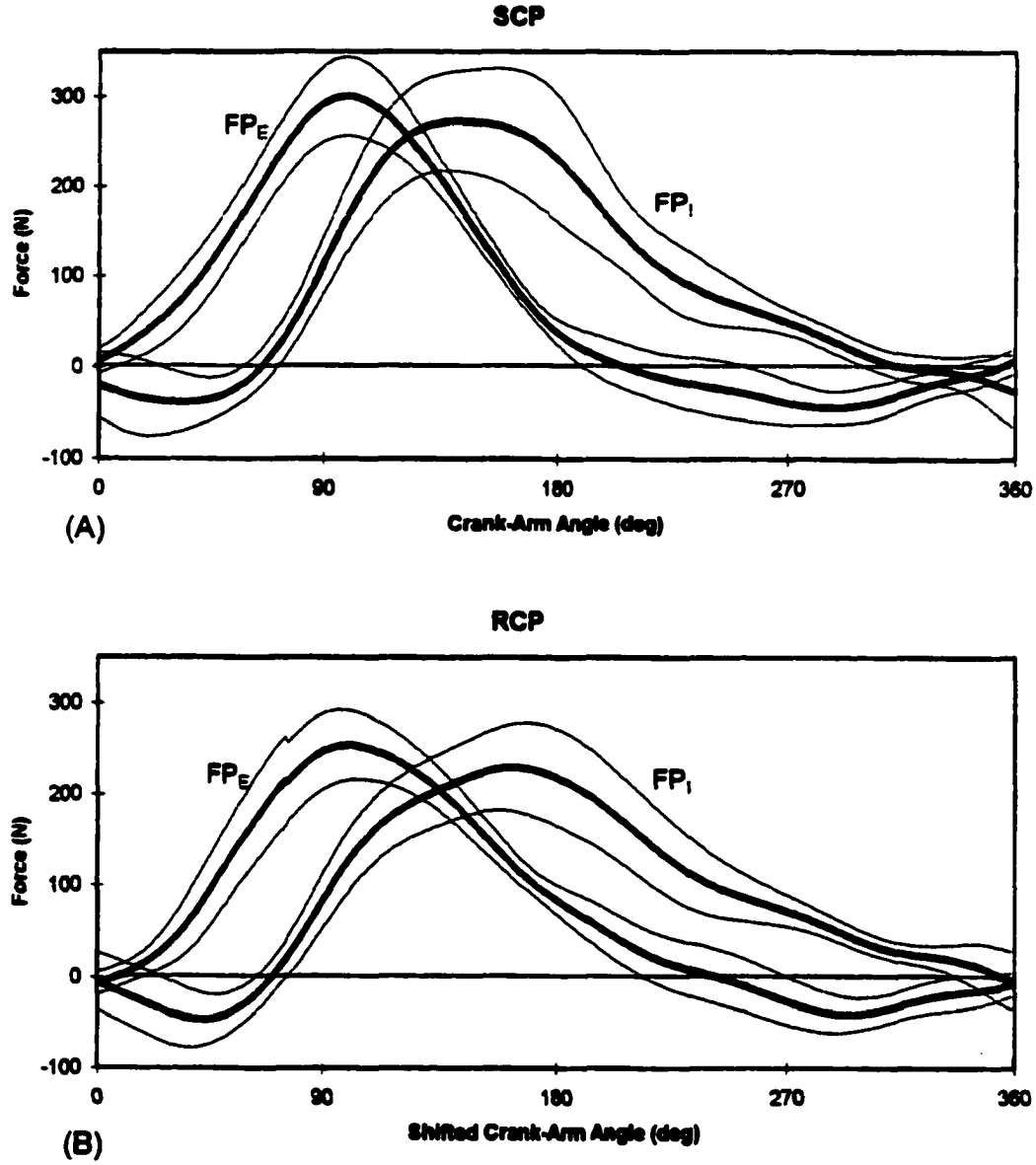

Figure 5.4: Mean effective (FP_E) and ineffective (FP_I) components of pedal force (± 1 standard deviation) while cycling at 90 rpm and 250 W (125 W/pedal) for both the SCP (A) and RCP (B). Crank-arm angles in the RCP are shifted by the 76° difference in HOA between the two cycling positions.

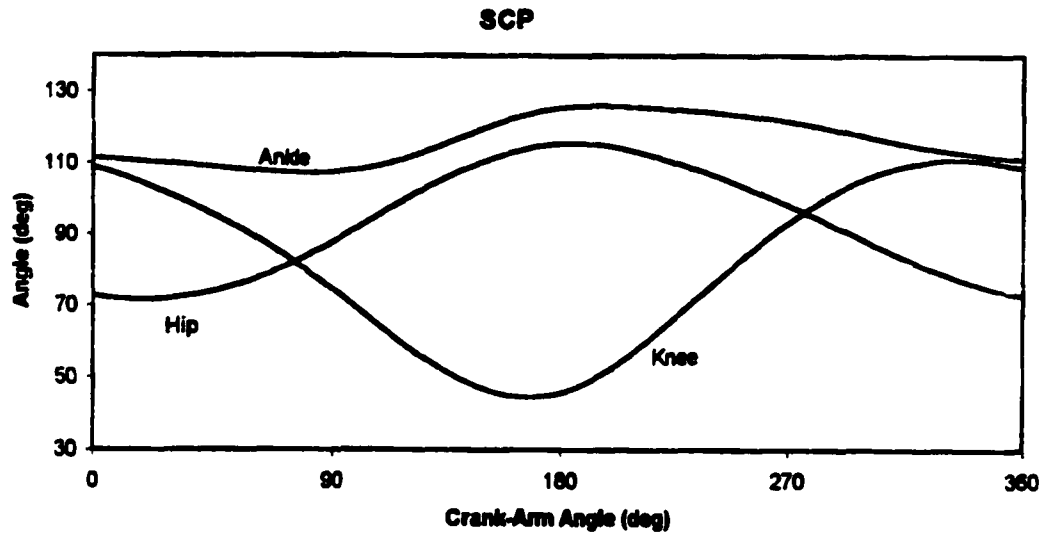

(A)

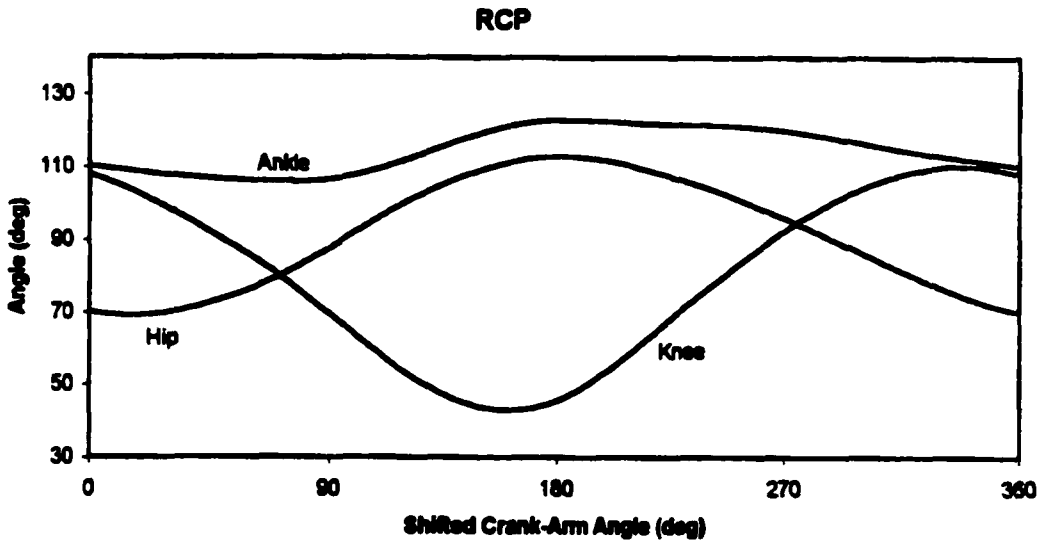

(B)

Figure 5.5: Mean lower-extremity joint angles for both the SCP (A) and RCP (B). Ankle and hip angles are the included joint angles while the knee angle is the anatomical joint angle. Crank-arm angles in the RCP are shifted by the 76° difference in HOA between the two cycling positions.

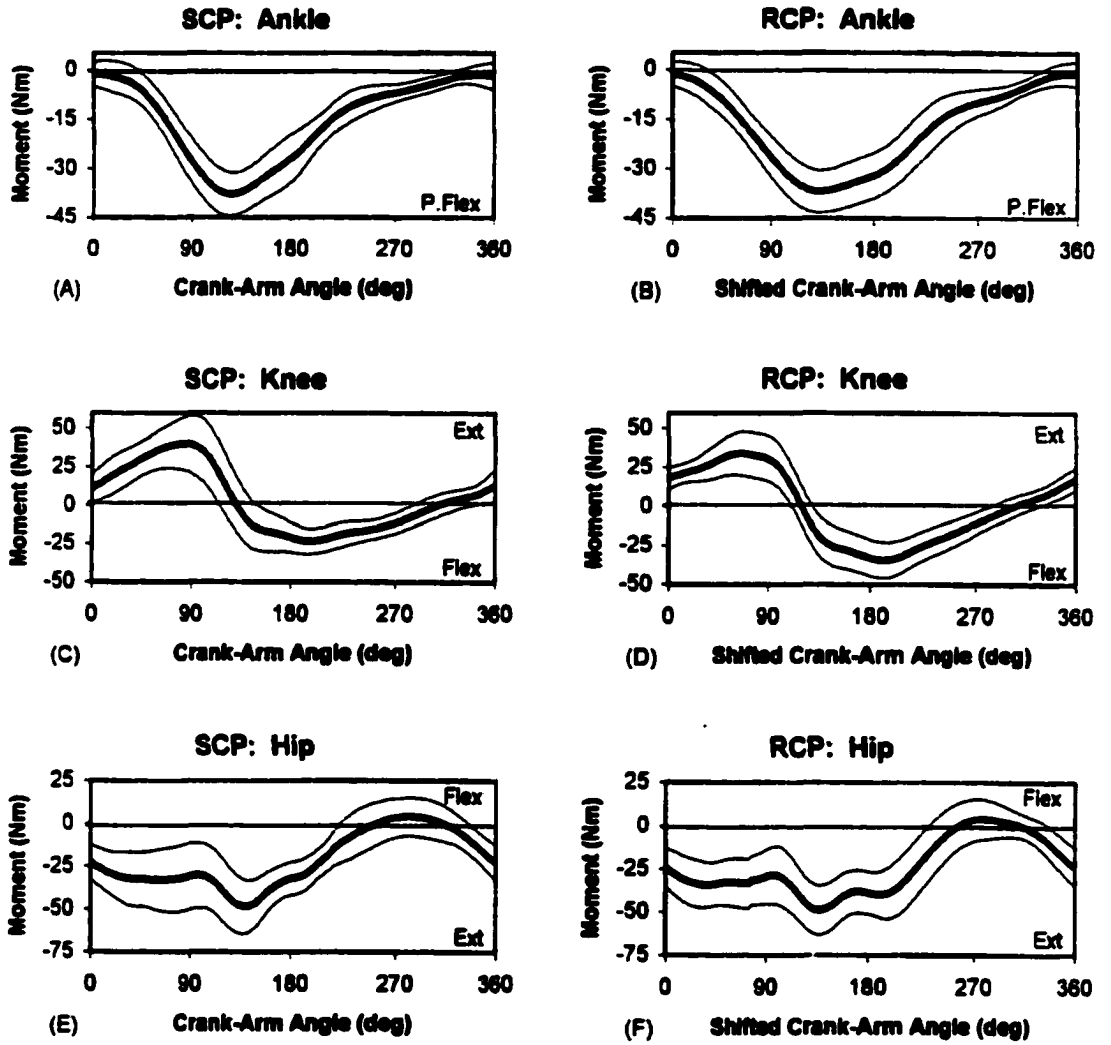

Figure 5.6: Mean generalized muscle moment profiles (± 1 standard deviation) for the ankle (A, B), knee (C, D), and hip (E, F) for the SCP and RCP, respectively. Crank-arm angles in the RCP are shifted by the 76° difference in HOA between the two cycling positions.

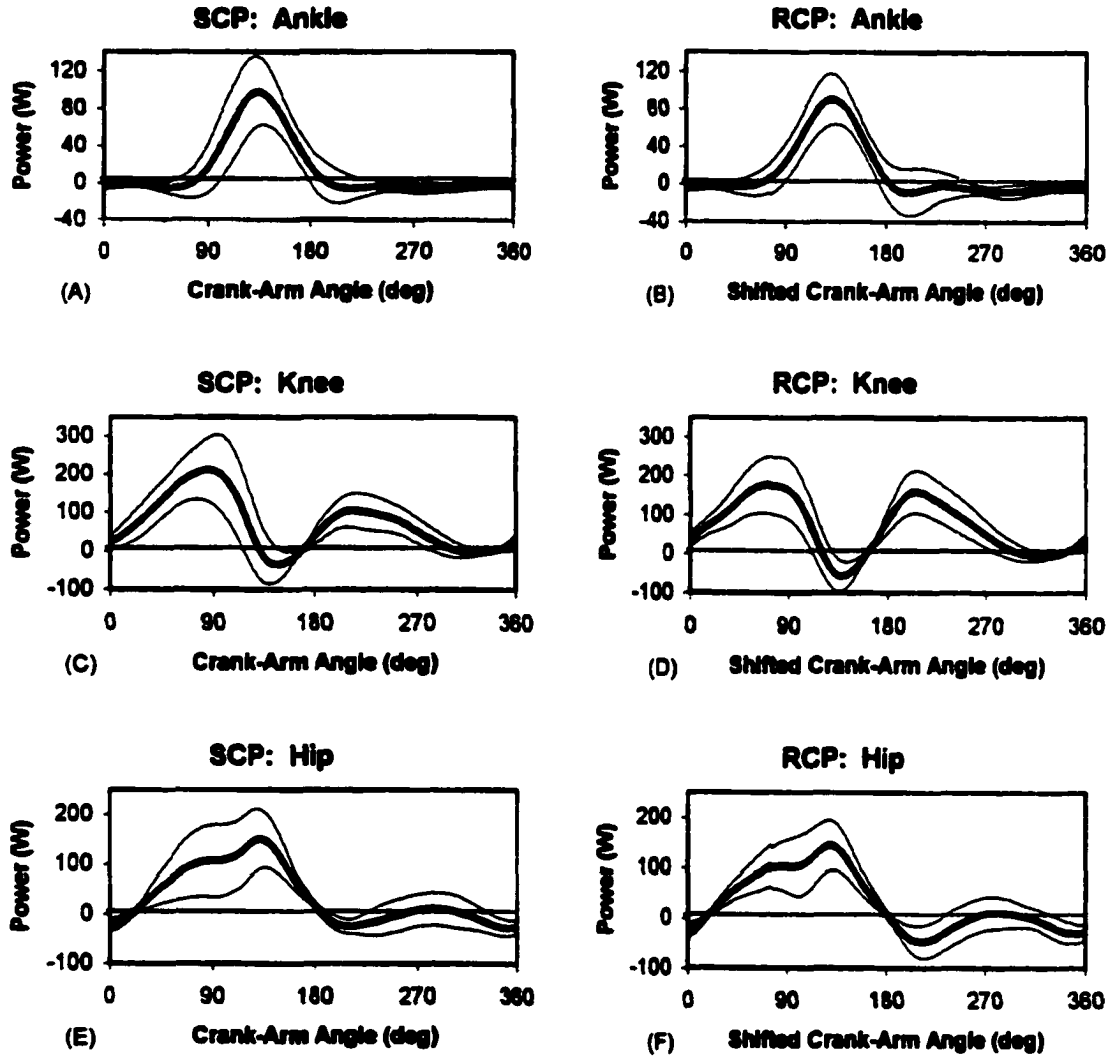

Figure 5.7: Mean generalized muscle power profiles (± 1 standard deviation) for the ankle (A, B), knee (C, D), and hip (E, F) for the SCP and RCP, respectively. Crank-arm angles in the RCP are shifted by the 76° difference in HOA between the two cycling positions.

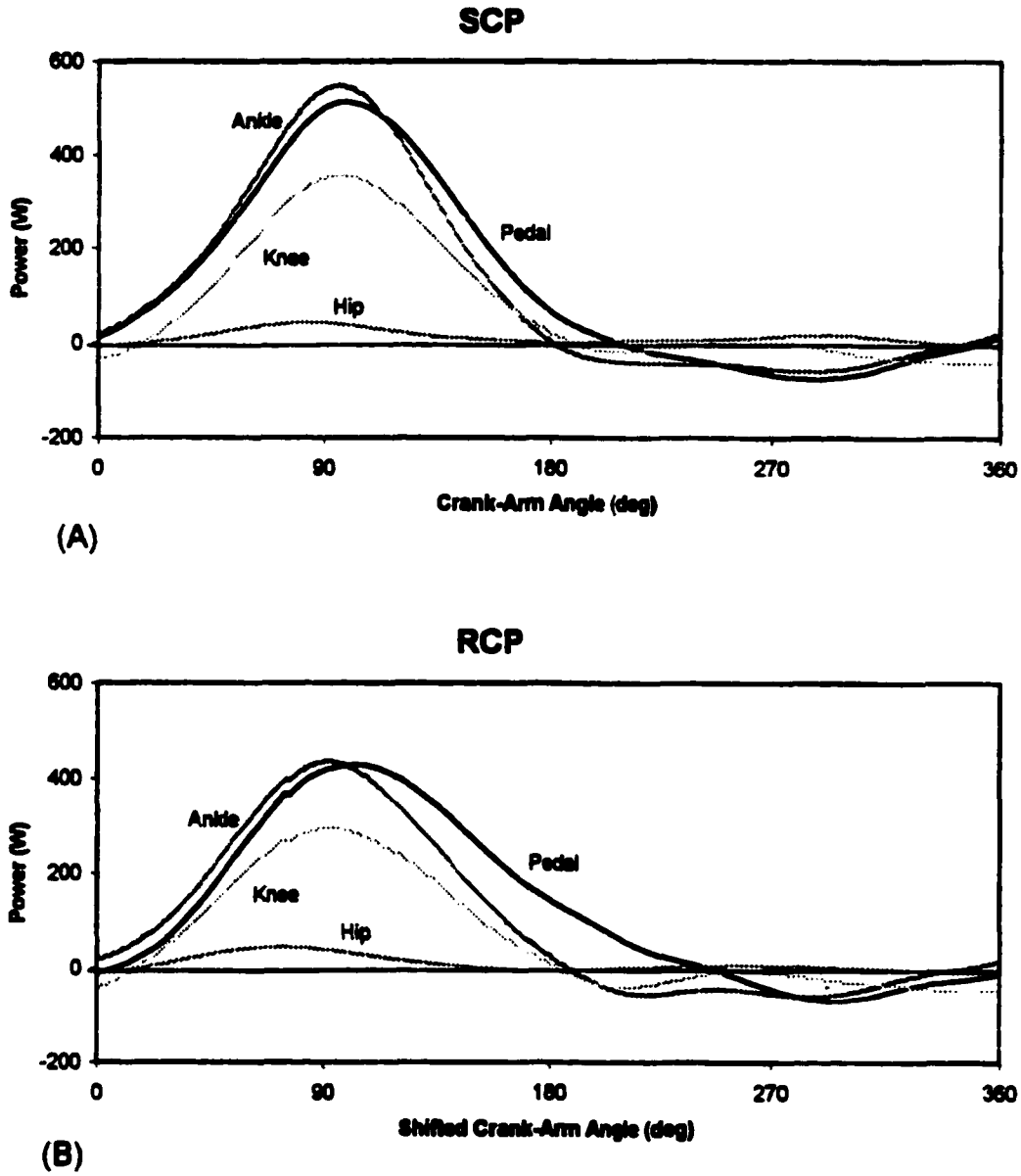

Figure 5.8: Mean joint reaction force powers describing energy flow between the pelvis and thigh (Hip), thigh and shank (Knee), shank and foot (Ankle), and foot and bicycle pedal (Pedal) for the SCP (A) and RCP (B). Crank-arm angles in the RCP are shifted by the 76° difference in HOA between the two cycling positions.